



**Universiteit
Leiden**
The Netherlands

Raman spectroscopy in bladder cancer diagnosis

Stomp-Agenant, M.

Citation

Stomp-Agenant, M. (2023, October 4). *Raman spectroscopy in bladder cancer diagnosis*. Retrieved from <https://hdl.handle.net/1887/3642844>

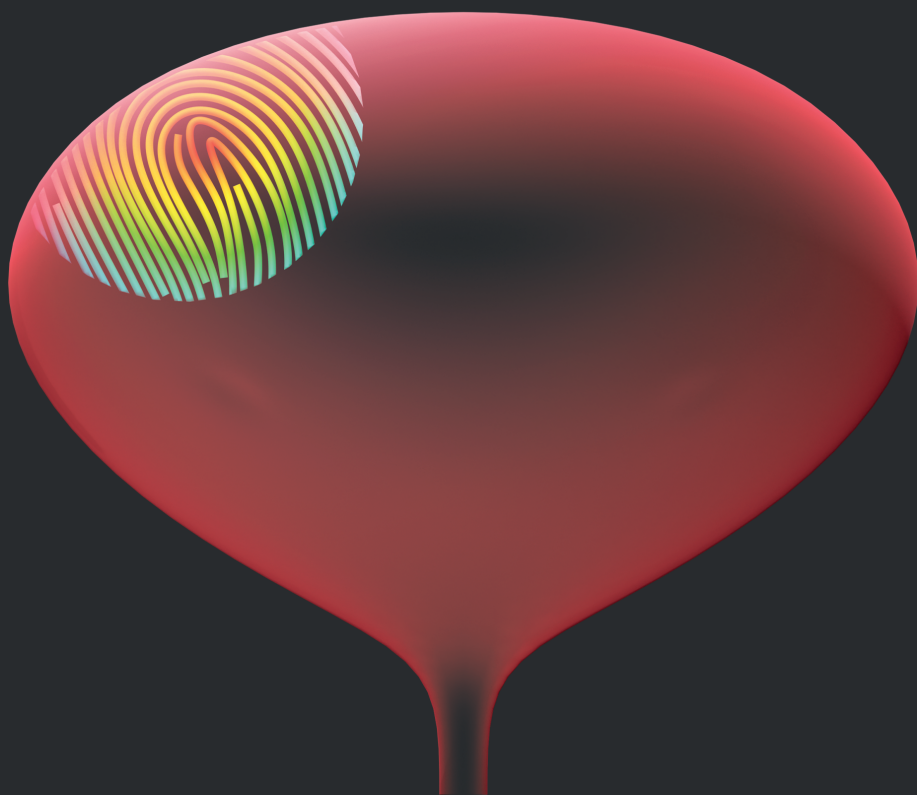
Version: Publisher's Version

License: [Licence agreement concerning inclusion of doctoral thesis in the Institutional Repository of the University of Leiden](#)

Downloaded from: <https://hdl.handle.net/1887/3642844>

Note: To cite this publication please use the final published version (if applicable).

RAMAN SPECTROSCOPY IN BLADDER CANCER DIAGNOSIS



MICHELLE STOMP-AGENANT

Raman Spectroscopy in Bladder Cancer Diagnosis

Michelle Stomp-Agenant

Financial support for the publication of this thesis was kindly provided by Chipsoft, Coloplast, Eurocept Homecare, KARL STORZ Endoscopie Nederland B.V., Mayumana, MemidisPharma, Reinier de Graaf Gasthuis, St. Antonius ziekenhuis, Team Westland en de Universiteits Bibliotheek Leiden (Alphabetically)

ISBN: 978-94-6473-193-4
Cover design: Wouter Stomp
Layout and design: Marilou Maes | persoonlijkproefschrift.nl
Printed by: Ipskamp Printing | proefschriften.net

Copyright 2023 M. Stomp-Agenant, Leiden, The Netherlands. All rights reserved. No part of this thesis may be reproduced or transmitted in any form, by any means, without prior written permission of the author

Raman Spectroscopy in Bladder Cancer Diagnosis

PROEFSCHRIFT

ter verkrijging van
de graad van doctor aan de Universiteit Leiden,
op gezag van rector magnificus prof.dr.ir. H. Bijl,
volgens besluit van het college voor promoties
te verdedigen op woensdag 4 oktober 2023
klokke 15:00 uur

door

Michelle Stomp-Agenant

Geboren te Colombo (Sri Lanka)

in 1982

Promotor

Prof.dr. R.C.M. Pelger

Co-promotor

Dr.Ir. C.F.P van Swol

Leden promotiecommissie

Prof.dr. B.P.F. Lelieveldt

Prof.dr. N. Stone (University of Exeter)

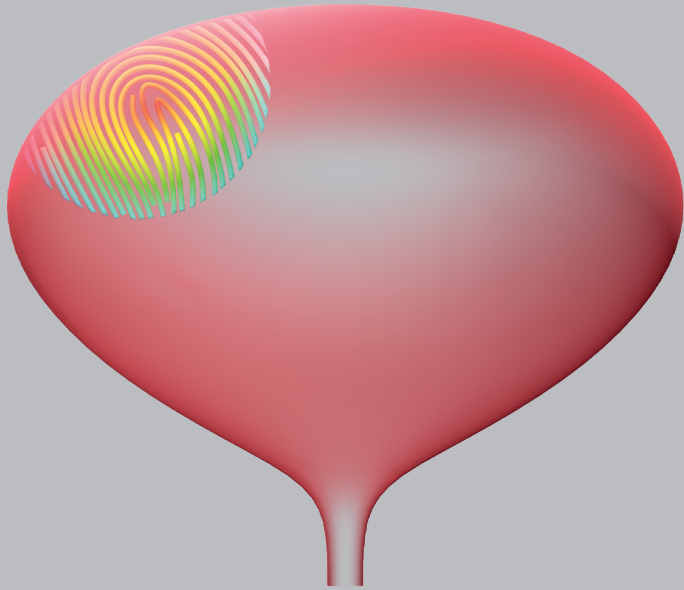
Dr. C.A. Goossens-Laan (Alrijne ziekenhuis)

Prof.dr. V.T.H.B.M. Smit

The research described in this thesis was carried out at the Urology and Clinical Physics departments of the St. Antonius Hospital and University Medical Centre Utrecht and the Urology department of the Leiden University Medical Centre.

CONTENTS

Chapter 1	General introduction and outline of this thesis	7
Chapter 2	Clinical superficial Raman probe aimed for epithelial tumor detection: Phantom model results <i>Biomed Opt Express. 2014</i>	31
Chapter 3	In vivo Raman spectroscopy for bladder cancer detection using a superficial Raman probe compared to a nonsuperficial Raman probe <i>J Biophotonics. 2022</i>	51
Chapter 4	Raman spectroscopy in the evaluation of tissue surrounding malignancy in radical cystectomy specimens <i>Submitted: Biomedical Optics Express</i>	69
Chapter 5	Real-time bladder lesion registration and navigation: a phantom study <i>PLoS One. 2013</i>	87
Chapter 6	Summary and general conclusion	111
	Samenvatting en algemene conclusie	119
Appendices	List of abbreviations	132
	List of publications	133
	Dankwoord	135
	Curriculum Vitae	137



CHAPTER 1

GENERAL INTRODUCTION AND OUTLINE OF THIS THESIS

GENERAL INTRODUCTION

Bladder cancer

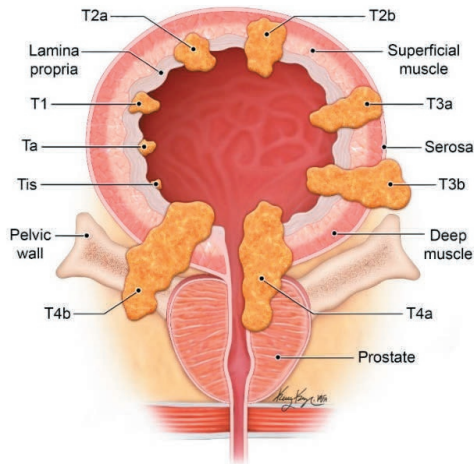
Bladder cancer is the ninth most frequently diagnosed malignancy worldwide. It mostly presents itself with gross painless hematuria. Ninety percent of bladder cancers are Urothelial Carcinomas (UC) [1–3]. Stage and grade of the tumor are important prognostic factors for recurrence, progression and survival. Therefore, treatment is adapted to these diagnostic parameters (figure 1 and 2). Differences exist between the diagnosis and treatment of non-muscle-invasive bladder cancer (NMIBC) which consist of $\leq T1$ tumors compared to muscle-invasive bladder cancer (MIBC) that consist of tumors $>T1$ [4,5]. This is described below and depicted in table 1 and figure 1.

Non-Muscle Invasive Bladder Carcinoma (NMIBC)

Most bladder tumors, 75-80% are detected while being NMIBC. These tumors are limited to the urothelial tissue and/or lamina propria, staged in Ta/CIS and T1 tumors, respectively. NMIBC is treated by a transurethral resection of a bladder tumor (TURBT). Additional chemo- or immunotherapeutic intravesical instillations are often administered to reduce recurrences and progression [8]. One single postoperative bladder chemo instillation will reduce the 5 year risk of recurrence with 13% [9]. In addition, series of intravesical chemo- or immunotherapy also reduce recurrence risks of NMIBC [10]. A 38% reduction in one year was found using repeat chemotherapeutic installations compared to TURBT alone [11]. For repeat immunotherapeutic instillations, a reduction of 27% in the odds of progression on BCG was found compared to no intravesical therapy [12]. Follow up of NMIBC patients is based on cystoscopy and, in high-grade cases, cytology.

NMIBC is known for its high recurrence and progression rates of 15-70% and 7-40%, respectively [13,14]. This results in that bladder cancer is one of the most expensive cancers to manage, due to its consequent need for surveillance and repeat treatment [15,16]. Even among patients whose cancer does not progress, recurrence leads to patient-centered detriments, including loss of income, a decrease in (urinary) quality of life from resections and intravesical therapies, and anxiety related to a patient's cancer outcomes [17]. Therefore, early recognition and accurate treatment is desired to prevent recurrence and progression.

Current diagnostic methods to detect NMIBC are office white light cystoscopy (WLC) and/or urine cytology. The tumor diagnosis and stage is based on pathological examination of the resected tissue after transurethral resection of a bladder tumor (TURBT) which also makes use of WLC. The pathologist determines the T-stage and the grade of the tumor. To enable correct treatment of NMIBC, cytology and WLC should have high accuracies in NMIBC detection.



TNM classification of urinary bladder cancer

T: Primary tumor

Tx	Primary tumor cannot be assessed
T0	No evidence of primary tumor
Ta	Non-invasive papillary carcinoma
Tis	Carcinoma <i>in situ</i> : 'flat' tumor
T1	Tumor invades subepithelial connective tissue
T2	Tumor invades muscle
	T2a Tumor invades superficial muscle (inner half)
	T2b Tumor invades deep muscle (outer half)
T3	Tumor invades perivesical tissue
	T3a Microscopically
	T3b Macroscopically
T4	Tumor invades any of the following: prostate stroma, uterus, vagina pelvic wall, abdominal wall
	T4a Tumor invades prostate stroma, seminal vesicle uterus or vagina
	T4b Tumor invades pelvic or abdominal wall

N: Lymph nodes

Nx	Regional lymph nodes cannot be assessed
N0	No regional lymph node metastasis
N1	Metastasis in a single lymph node in the true pelvis (hypogastric, obturator, external iliac or presacral)
N2	Metastasis in multiple lymph nodes in the true pelvis (hypogastric, obturator, external iliac or presacral)
N3	Metastasis in common iliac lymph node(s)

M: Distant metastasis

Mx	Distant metastasis cannot be assessed
M0	No distant metastasis
M1	Metastasis
	M1a Non-regional lymph nodes
	M1b Other distant lymph nodes

Figure 1. TNM classification of urinary bladder cancer. Subepithelial connective tissue is referred to be the lamina propria [4,6]. (Right part of the figure is reproduced with permission from MDPI)



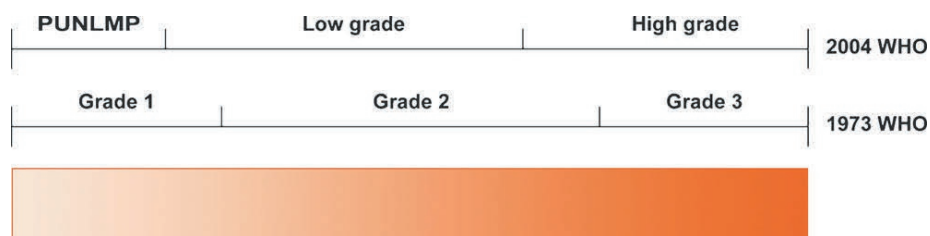


Figure 2. The grading stratification according to WHO 1973 and 2004/2016 classification [4,7]. (Figure reproduced with permission from Elsevier)

Although urine cytology is non-invasive and easily applicable, it has a limited overall specificity and, for low grade tumors, also a limited sensitivity (16%) [18,19]. Therefore, to improve early detection of bladder cancer, urine constituents are widely being evaluated as “liquid biopsy”, e.g. urinary biomarkers. Until now, the developed/evaluated biomarkers show limited sensitivity to detect low-grade UC [20,21]. Therefore, multiple efforts have been made to improve detection of bladder cancer cells in urine.

The other detection tool, WLC (office based and during TURBT) is invasive, unpleasant for the patient and expensive. Although widely used, WLC also has several other shortcomings. First, nonpapillary bladder cancers such as carcinoma in situ (CIS) may be difficult to visualize or differentiate from inflammation [22]. Second, smaller or satellite tumors may be missed. Third, with decreased vision due to hematuria, bladder cancer may be resected incompletely and residuals occur instead of ‘recurrences’. Incomplete resection may also result in under-staging [13,23]. Taken together, these disadvantages could lead to high recurrence rates.

Therefore, different techniques have been implemented clinically to increase the accuracy of WLC [13]. By adding narrow band imaging (NBI) or photodynamic diagnosis (PDD) to WLC, the sensitivity of bladder cancer detection is improved from 67% to 98% and 71% to 92%, respectively compared to WLC alone [24–26]. Other techniques that could reduce the risk of recurrences are under development, e.g. optical coherence tomography, fluorescence diagnostics, vibrational spectroscopy (e.g. Raman spectroscopy) and other optical methods. In trials, these techniques are being used for tissue evaluation, and referred to as “non-invasive optical biopsies” ex vivo and in vivo [26–32].

Muscle Invasive Bladder Carcinoma (MIBC)

When progression occurs, the tumor becomes MIBC, staged as $\geq T2$ tumors. MIBC can be local (only the detrusor muscle, T2), locally advanced (including T3-T4 tumors with

or without positive pelvic lymph nodes) or metastasized to other organs (Figure 1) [3]. Diagnosis is based on the pathologic evaluation of the resected tissue by TURBT. The maximal detectable T stage is T2 as no biopsies are taken deeper than the detrusor muscle. T3 or 4 can be detected on imaging or after cystectomy.

An FDG-PET or thoraco-abdominal CT scan could detect (locoregional) metastases and involvement of adjacent organs. If no (locoregional) metastases are present, cystectomy and a pelvic lymph node dissection is the gold standard therapy. The tissue is afterwards pathologically evaluated. When patients have clinically T2-T4 tumor without positive pelvic lymph nodes and metastasis, neoadjuvant chemotherapy (NAC) could be administered. However, the overall survival rate only improves with 5-8% after 5 years.

If the tumor is pathologically staged as T3/4 and/or lymph nodes are positive on resection while negative on imaging, adjuvant chemotherapy could be administered. [4,33]

The advantage of NAC compared to adjuvant chemotherapy is that the therapy is delivered at the earliest time point when the burden of micro-metastatic disease is expected to be low. There is a potential reflection of in vivo chemosensitivity and the tolerability and patient compliance is expected to be better pre-cystectomy. However, patients that do not respond to chemotherapy have a delay in surgical treatment and the cancer might progress. Therefore, efforts are made to develop biomarkers that will predict chemosensitivity and also markers to detect micro-metastasis. In several research papers "liquid biopsies", e.g. serum and urine biomarkers are being evaluated to enable early micro-metastatic detection [34].

Raman spectroscopy is a technique that determines the biochemical composition of the substance under study and therefore could be implemented for multiple purposes to improve bladder cancer diagnosis.

Raman spectroscopy

Raman spectroscopy is based on the Raman effect, which was discovered by Sir C.V. Raman in 1928 [35]. During a trip from India to Britain, he was interested in the blue color of the sea which led to a series of experiments on the diffraction of light which were published in Nature [36]. Until then, it was believed that the blue color of the sea was due to reflection of the sky and to absorption of the light by the particles suspended in the water. However, further research on the scattering of light led to the discovery of the Raman effect.



The principles of light diagnostics and the Raman effect are explained below. Light consists of incident photons. These photons can be absorbed by, scattered from, and/or pass through material without interaction. A molecule can be in its ground state (lowest energy level) or in an excited state (higher energy level than its ground state). If the energy of the incident photon matches the energy gap between the ground state and an excited state of a molecule, the photon will most likely be absorbed. Consequently, the molecule will be promoted to the excited state. From there, the system can relax non-radiatively and eventually fluorescence occurs, as is illustrated in figure 3. When the energy of the incident level does not match the energy gap between the ground state and the excited state of the molecule, scattering can occur. In this process, the incident photon distorts the electron clouds of the molecules. Two types of scattering exist in the visible-light and near-infrared spectral range: Rayleigh and Raman scattering. The more intense form, Rayleigh scattering, occurs when only the electron clouds are distorted. Because no energy exchange occurs, this is an elastic process. In contrast, if energy is transferred due to a change in polarizability of a molecule and its electron clouds according to its vibration, either from the photon to the molecule or vice versa, this process is called inelastic and referred to as Raman scattering [37]. Thus, Raman spectroscopy is a vibrational spectroscopy that characterizes molecular vibrations and rotations. These vibrations are based on the individual atom movement relative to each other, within the molecule. The set of vibrations is highly dependent on the exact structure of the molecule, often referred to as the “chemical fingerprint” of a molecule [37]. Raman scattering is a relatively rare phenomenon and occurs approximately in only one in every $10^6 - 10^8$ scattered photons [38,39].

Depending on the direction of energy transfer between the photon and the molecule, Raman scattering can be further categorized into two subtypes: Stokes and anti-Stokes. Stokes scattering takes place when the molecule receives energy from the incident photon leading to a lower energy state of the scattered photons compared to the incident photons and a longer wavelength. In contrast, anti-Stokes Raman scattering occurs when a molecule releases energy upon interaction with the incident photon and subsequently alters to a lower energy state. This occurs when a molecule was already in an excited state due to thermal perturbation or prior external excitation. In this case, the scattered photons are in a higher energy state than the incident photons and a shorter wavelength. Because at room temperature most molecules are in the ground state, Stokes scattering typically dominates. Stokes scattering is therefore commonly recorded for Raman spectroscopy, unless special experimental conditions are arranged.

The Raman effect is observed as Raman band shifts of the energy difference between the incident and scattered photons. This energy difference is a color change of the

photon and can be expressed in wavelengths in nanometers. In Raman spectroscopy, the reciprocal of the wavelength is used; wavenumbers (cm^{-1}). Figure 3 illustrates the Rayleigh, Stokes, and anti-Stokes scattering processes [38,39]

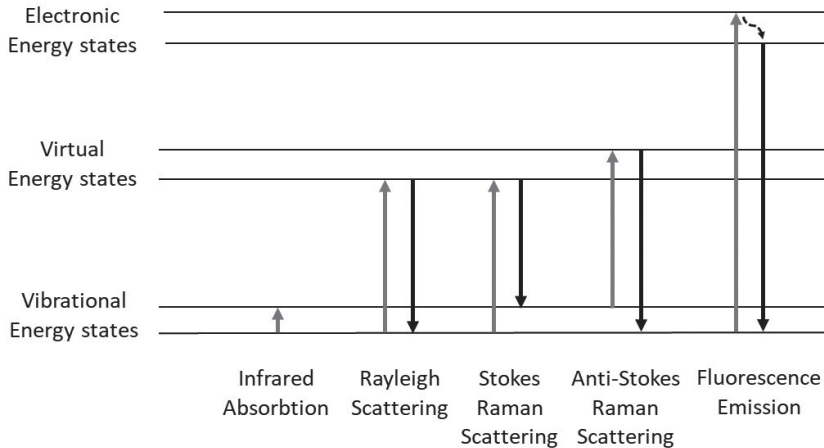


Figure 3. Molecular energy levels and Raman effect. In infrared absorption the energy of the photon matches the energy-gap between the ground state and excited state of the molecule and the small vibrational energy is absorbed. Rayleigh scattering is common, in this process the photon changes its direction but has no energy transfer or effect on the molecule. In the process of Stokes Raman Scattering there is an energy transfer from the photon to the molecule that results in excitation of vibrations or rotations of the molecule and a change in direction of the photon leading to a higher wavelength. This process is very rare. Anti-Stokes Raman Scattering is an extremely rare process, in which the energy transfer is from the molecule to the photon, resulting in an de-excitation of pre-excited vibrations or rotations and an change in direction of the photon leading to a shorter wavelength. In fluorescence emission, the molecule in its excited state relaxes non-radiatively between sublevels in its singlet excited state, after which it relaxes through fluorescence to its singlet ground state.

To implement Raman spectroscopy for biochemical detection purposes, a monochromatic laser light is used as illumination source (figure 4). Subsequently, after interaction of the photon with a specific molecular bond, the vibrational mode of the molecular bond changes, resulting in an altered energy level of the molecular bond. As a result, the wavelength of the photons is altered and when collected, this can be detected as Raman shift. This shift is specific for that specific molecular bond. Photons interacting with different biochemical bonds within the illuminated tissue undergo different Raman shifts. Together these can be displayed as a spectrum on a Raman shift axis as a *Raman spectrum*. In this way, a Raman spectrum is a direct representation of the molecular composition of the material under study, a ‘fingerprint’ of the material, thereby helping to understand its properties. Hence, Raman spectroscopy is a very specific technique to determine the biochemical components of its measured substrate.

Art historians have utilized Raman spectroscopy and Raman Microspectroscopy (RM) techniques for nondestructive characterization of archaeological artefacts [40]. But, it has also been used for exploration and characterization of the lunar surface, showing its wide use [41]. In the last two decades Raman spectroscopy also has attracted attention in the biological and clinical field. Within a molecularly complicated biological system, like a cell or tissue, Raman spectroscopy carries intrinsic details and information of the materials present and its biochemical conditions [42–44]. Therefore, this technique could be used to obtain a non-invasive optical biopsy, for example in (pre) cancer detection in various body organs [35,38,44–56]. The potential advantage of Raman spectroscopy that it is a non-invasive nondestructive technique which can be used in real-time and does not require staining or labelling [57–59].

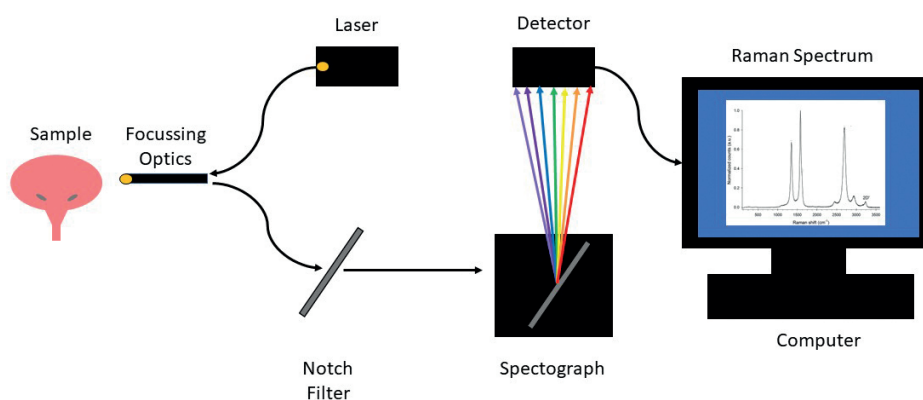


Figure 4. The incident laser irradiates the sample via focusing optics, in this case a probe. The Raman scattered photons are collected in the probe and sent through a notch filter to allow passing of the Raman signal and to block the laser line. The photons are dispersed by a diffraction grating in a spectrometer and sent to a detector. The signal from detector can be visualized as a Raman spectrum on a computer.

One disadvantage of Raman spectroscopy is its low signal intensity. To improve signal intensities of Raman spectroscopy, enhancement methods are being evaluated such as Coherent anti-Stokes Raman spectroscopy (CARS) and Surface-enhanced Raman spectroscopy (SERS) [38,60,61]. Modulated Raman spectroscopy (MRS) is being developed to reduce the fluorescent background of Raman spectroscopy [62].

Raman spectroscopy in bladder cancer diagnosis

Raman spectroscopy is a vibrational spectroscopic technique that has been explored in bladder cancer diagnosis for multiple purposes since 1995 [63]. One of the most important features of Raman spectroscopy is the ability to provide quantitative molecular information that can be translated into an objective diagnosis. This is opposed to the

subjective interpretation in the current gold standard: histopathology. The latter is prone to high inter-observer variability [64–66]. Raman spectroscopy is more objective, therefore this highly specific technique may be ideal for clinical use.

Raman spectroscopy was evaluated as “optical tissue biopsy” in the evaluation of bladder tissue *ex vivo* on TURBT biopsies and *in vivo* during TURBT. This instant optical biopsy generates a direct available diagnosis as opposed to pathological evaluation of the tissue that takes multiple days. Another advantage of such a technique is that no interobserver variability occurs. When this technique is combined with WLC, the specificity of tumor detection may improve and unnecessary biopsies of benign tissues could be omitted. Also, surgical margins might be evaluated with a higher specificity. Raman spectroscopy was also evaluated on liquids such as urine and serum, referred to as “optical liquid biopsies”. To reduce the amount of cystoscopies, Raman spectroscopy could be used to evaluate urine (constituents). Several studies evaluated detection of UC in (artificial) urine using Raman spectroscopy. This could enable early bladder cancer detection and this highly specific technique may reduce the amount of follow-up cystoscopies [43,62,63,67–77]. Also, two papers evaluated detection of bladder cancer in serum and subclassification of MIBC and NMIBC to reduce the amount of cystoscopies and reduce the delay of curative therapy [78,79].

Two systematic reviews and meta-analyses of Raman spectroscopy in bladder cancer diagnosis have been published [80,81]. In this introduction, an overview of the clinical studies on the use of Raman spectroscopy in bladder cancer are being presented and discussed. The studies of Raman spectroscopy on tissue (optical tissue biopsies) and on Raman spectroscopy on fluids such as urine and serum (optical liquid biopsies) will be presented and discussed separately.

Optical tissue biopsies

We found 15 studies of Raman spectroscopy on bladder tissue including *ex vivo* and *in vivo* studies (Table 1). The major goal in these studies is improving the sensitivity and specificity of UC detection to enable an optical non-invasive quick diagnosis.



Table 1. Overview of bladder tissue evaluation papers using Raman spectroscopy.

Publication	Raman spectroscopy	Spectra/Biopsy number	Classification	Sensitivity (%)	Specificity (%)	Accuracy (%)
Crow et al. 2004 [57]	Regular	1525/75	Normal/cystitis/UC	90-95	95-98	92
Crow et al. 2005 [82]	Regular	220/29	Normal/UC	79-89	79-98	84
Prieto et al. 2005 [83]	Kerr-Gated	NA	Normal	NA	NA	NA
Koljenovic et al. 2005 [84]	High Wavenumber – map	6599/2	Normal	NA	NA	NA
De Jong et al. 2006 [85]	Regular - map	90/15	Normal/UC	94	92	93
Stone et al. 2007 [59]	Regular	1445/73	Normal/cystitis/CIS/UC LG/UC HG	NA	NA	NA
Grimbergen et al. 2009 [86]	Regular (with and without ALA)	2002/130	Normal/UC	100	80.8	NA
Draga et al. 2010 [87]	Regular (with and without ALA/ HAL)	38 patients (>76 spectra)	Normal/UC	85	79	NA
Barman et al. 2012 [44]	Regular (confocal)	140/28	Normal/UC	85.7	100	92.9
Chen et al. 2018 [42]	Regular	262/32	Normal/UC LG/UC HG	88.5-97.5	95.1-98	93.1
Cordero et al. 2019 [88]	Regular - map	NA/48	Normal/UC LG/UC HG	92	93	92
Baria et al. 2019 [89]	Regular	NA/50	Normal/UC UC LG/UC HG Ta/T1/T2	95 NA	87 NA	95 85
Placzek et al. 2020 [90]	Regular	NA/119	Normal/UC UC LG/UC HG	95 81	88 68	92 77
Morselli et al. 2021 [91]	Regular	NA/169	Normal/UC UC LG/UC HG	72 65	77 73	77 71
Stomp et al. 2022 [92]	Regular	156/156	Normal/UC	90	85	95 (AUROCC)

ALA = 5-AminoLevulinic Acid; HAL = HexAminoLevulinic acid; NA = Not Available

Biochemical composition of bladder tumors

To gain insight in the biochemical composition of bladder tumors, different studies were performed. In 2007 Stone et al. evaluated bladder biopsies, categorized in; normal, cystitis, CIS, UC low-grade (LG) and high-grade (HG). An increased DNA content was found and decreased collagen content as the tissue progresses from normal to malignant [59]. De Jong et al. and Omberg et al. evaluated the biochemical basis of normal compared to UC [85,93]. In both studies, the ratio of total collagen content and non-collagen content was higher in non-tumor tissue. Also, tumorous tissue was characterized by higher lipid, nucleic acid, and protein content and glycogen expression compared to normal tissue [85].

Raman classification: benign versus malignant

These findings are the basis of the Raman classification feasibility. Four studies evaluated the Raman classification of benign versus malignant tissue. Sensitivities of 72%-100% (mean 89%), specificities of 77%-100% (mean 86%) and accuracies of 77%-92% (mean 90%) were reached [82,89–91]. Raman spectroscopy combined with other methods, such as Optical Coherence Tomography (OCT), fluorescence spectroscopy and reflectance spectroscopy, led to increased accuracies [90,91]. These results suggest that Raman spectroscopy can be a diagnostic tool with high potential for bladder cancer detection and evaluation. However, Raman spectroscopy has a limited field of view. Therefore, screening the entire bladder with Raman spectroscopy is too time consuming and its measurements must be targeted. Visually suspicious lesions could be detected using WLC with or without PDD or NBI. Raman spectroscopy could improve the specificity of these highly sensitive techniques that lack specificity [94]. Grimbergen et al. found that when the classification algorithm was fed with spectra of bladder tissue exposed to 5-ALA, classification of normal versus UC was still high for bladder biopsies exposed to 5-ALA. Therefore, Raman spectroscopy is feasible when using PDD and is particularly attractive as complementary diagnostic tool for real-time guidance during TURBT [86].

Raman classification ex vivo: bladder cancer grading and staging

Besides malignancy detection, the ability of direct noninvasive UC grading during TURBT could enable direct customized treatment without delay and with a higher effectivity. Two groups classified benign, LG and HG UC and reached accuracies of 92-93% [23,88]. When Raman spectroscopy is enabling direct differentiation between LG and HG UC, the appropriate postoperative management could be applied. For example, a chemotherapeutic bladder instillation could be given to the appropriate patients and reduce the recurrence risk while limiting adverse-effects in patients that would not benefit from such an instillation.



The second clinical tumor parameter to determine its correct treatment, is staging. Prieto et al. obtained spectra of different depths that would enable staging of bladder tumors in future [83]. Baria et al. was the only group to evaluate UC staging and found accuracies of 84-98% [89].

Besides an instant optical biopsy including a grade and stage during TURBT, per-operative Raman spectroscopy could also have a role in evaluation of the lateral margins or base of the resection plane to reduce the need for re-TURBT, which is commonly required in regular diagnostics. However, the feasibility of measurements at the margins or base of resection is questioned, since cauterization effects may cause problematic artefacts. Future research will be required to evaluate this.

Raman signal improvement in bladder cancer

To increase the Raman signal and improve its classification, several ex vivo modifications to Raman spectroscopy have been proposed. Koljenovic et al. used high wavenumbers only, to limit the Raman signal from the probe's fused silica. They concluded that high wavenumber Raman spectra contain sufficient information for tissue classification [84].

Barman et al. showed that a confocal probe enables significant enhancement of diagnostic specificity by suppressing spectral information from deeper tissue layers beyond the region of interest [44]. A confocal probe would therefore improve tumor grading.

In vivo applicability of Raman spectroscopy has been demonstrated in other fields of research, e.g. the evaluation of intraoperative margins in partial mastectomy [95], characterization of atherosclerotic plaques in vascular surgery [35] and during colonoscopy [53].

Raman bladder cancer classification in vivo

For in vivo measurements of the bladder, small flexible fiber-optic probes compatible with the working channel of a rigid or flexible cystoscope have been developed. For many years the application has been hampered by many technical issues. Two papers have been published using in vivo Raman measurements of bladder cancer and reached similar results compared to the ex vivo studies [87,92].

Raman future perspectives in UC

The ultimate goal is that Raman spectroscopy could be available in the office, while performing WLC. Direct grading and staging would enable direct treatment, such as outpatient clinic fulguration or electrocoagulation which are applied more frequently

currently especially for recurrent LG UC. One of the drawbacks of these treatments is that no pathology specimen is obtained. Consequently, the urologist has to estimate tumor stage and grade and has to ensure that progression has not occurred. Since this estimation is often inaccurate, a pathologic diagnosis before fulguration is desirable. Raman measurements of these tumors might provide this diagnosis so that office based fulguration may become a safer treatment modality. Nevertheless, technical issues should still be overcome, because no Raman probe compatible with a flexible cystoscope is yet available.

Optical liquid biopsies

Urinalysis

Bladder cancer has a high recurrence rate and is in need for continued surveillance and repeat treatment. When tumor cells can be detected in urine with a high accuracy, then (follow-up) cystoscopies could be omitted. Raman spectroscopy on urine cytology or supernatant has been tested and could be a valuable tool to improve the sensitivity of non-invasive bladder cancer (recurrence) detection. In Table 2, trials are presented that evaluated Raman spectroscopy on urothelial cells or on biomarkers from voided or artificial urine as a 'liquid biopsy', to detect UC [3].

Different forms of Raman spectroscopy were examined on urine (cytology and supernatant) and on cells from different cell lines, including regular Raman spectroscopy, RM, MRS, SERS and Raman Molecular Imaging (RMI). Due to the larger sample size and testing on biological fluids (urine supernatant or sediment) instead of cell lines, the articles by Shapiro, Cui and Hu et al. provide most information about the Raman spectroscopic detection of bladder cancer in urine [67,75,76]. These groups also provide specific Raman bands of interest for discrimination between benign and malignant urine, however none of them found a single band or a specific set of bands on which a classifier could be based for a sensitive bladder cancer detection.

In discriminating samples containing UC from benign, sensitivities of 82.4%-100% (mean 96.5%), specificities of 79.5%-100% (mean 92.4%) and accuracies of 80.4%-100% (mean 93.3%) were reached [43,62,67–77]. Also, LG UC could be discriminated from HG UC using MRS which limits the fluorescent background, with a maximal accuracy of 99.4% [77].



Table 2. Overview of liquid biopsy papers using Raman spectroscopy.

Publication	Raman spectroscopy	Samples (n) / kind	Classification	Sensitivity (%)	Specificity (%)	Accuracy (%)
Shapiro et al. 2011 [67]	RMI (5 cells)	340 / Urine cytology	Normal / UC Normal / HG UC Normal / LG UC / HG UC	92 100 95	91 NA 90.5	NA NA NA
Canetta et al. 2011 [68]	MRS	80 / cell lines (artificial urine)	Normal / UC	98	95	NA
Praveen et al. 2013 [69]	MRS	NA / cell lines	Normal / UC	100	100	100
Canetta et al. 2014 [43]	MRS	80 / cell lines (artificial urine)	Normal / UC	98	95	NA
De Luca et al. 2015 [62]	MRS	NA / cell lines	Normal / UC	98	96	NA
Li et al. 2015 [78]	SERS	91 / blood	Normal / UC	90.9	100	NA
Yosef et al. 2017 [70]	RM	20 / Urine cytology	Normal / HG UC	100	100	100
Kraus et al. 2017 [72]	RM	20 / Urine cytology	Normal / HG UC	NA	NA	89-90
Kraus et al. 2018 [71]	RM	20 / Urine cytology	Normal / HG UC	NA	NA	88-99
Pallaoro et al. 2018 [73]	SERS	10 / urine cytology	Normal / UC (Canine)	100	83	NA
Huttanus et al. 2019 [74]	Regular (Remetrix™)	24 / urine	Normal / UC	82.4	79.5	80.4
Chen et al. 2019 [79]	SERS	90 / blood 59 / blood	Normal / UC NMIBC / MIBC	98.3 90.6	96.7 96.3	97.8 93.2
Cui et al. 2020 [75]	SERS (silver)	158 / urine supernatant	Normal / UC / PC	NA	NA	89-91.9
Hu et al. 2021 [76]	SERS (silver)	248 / urine cytology & supernatant 168 167	Normal / UC Normal / LG UC Normal / HG UC	NA 97.53 95.00-100	NA 90.80 93.10-97.7	99.3-99.7 99.5 NA
O'Dwyer et al. 2021 [77]	MRS (ThinPrep)	2 / cell lines	LG UC / HG UC	95.2-99.5	96.6-99.6	96.0-99.4

RM = Raman Molecular Imaging; MRS = Modulated Raman spectroscopy; RM = Raman Microspectroscopy; SERS = Surface Enhanced Raman spectroscopy; UC= Urothelial Carcinoma; LG = Low-Grade; HG = High-Grade; PC=Prostate Carcinoma, NA= Not Available

Thus, Raman spectroscopy urinalysis already has shown an advantage compared to regular pathologic urine cytology in its sensitivity and accuracy. Huttanus et al. developed Ramematrix as chemometric urinalysis for bladder cancer screening and performed a proof-of concept study [74] and 'O Dwyer et al. provide a freely available automated process of nuclear targeting and using different classifiers and the open source Micro-Manager platform [77].

There are many advantages of Raman spectroscopy on urine; It is a label free technique and sample collection is noninvasive as opposed to serum. Raman spectroscopy requires minimal sample preparation and chemical composition data is returned in near/real time. Another advantage of Raman spectroscopy is that there is minimal interference from water, as opposed to infrared methods and scanning through glass is possible. This technique is nondestructive to the sample and can easily be scaled for larger number of samples (through automation) [74]. Thus Raman spectroscopy is promising, however there are obstacles in the development of clinical Raman applications. The strong fluorescence background could (partly) obscure the weak Raman signals, making detection of useful spectra difficult and limit the diagnostic accuracy and sensitivity of clinical Raman measurements [62]. An obstacle for clinical application Raman Microscopic Imaging for bladder cancer diagnosis is the need for specialized, expensive equipment and training of laboratory personnel [67]. Raman spectroscopy has yet a limited reproducibility due to its weak signal, research with low sampling sizes and clinical preparation and system setup [77]. Although the results of Raman spectroscopy urinalysis are promising, there are still plenty of obstacles before this may become a standardized analytical tool that can be used clinically.

Blood serum analysis

UC could possibly also be detected in blood serum samples. Taking a blood sample is much less invasive than performing a TURBT which is an invasive procedure with the possibility of complications e.g infection or perforation of the bladder wall. Therefore, two groups tested (SE)RS on blood samples as serum liquid biopsies. Sensitivities of 90.9% - 98.3% and specificities of 96.7% - 100% were reached [78,79].

It is important to differentiate NMIBC from MIBC because in the first case, only the tumor itself needs to be treated by resection, while in the latter case, the entire bladder requires treatment (cystectomy or trimodality treatment). Currently, only pathological evaluation after TURBT enables differentiation between these two, and more research focusses on less invasive diagnostic tools to differentiate NMIBC from MIBC. The hypothesis of one group in case of MIBC is, that tumor cells could be detected in blood serum samples. Therefore, they evaluated blood serum and discriminated NMIBC from



MIBC using SERS. The sensitivity, specificity and accuracy were 90.6%, 96.3% and 93.2%, respectively [79]. These are promising results which possibly could also be translated into the setting of detecting metastasis in blood serum using Raman spectroscopy before, or in the follow-up after treatment of MIBC.

In my opinion, it would be more logical to search for Raman characteristics in serum of metastasized bladder tumor patients. Cancer cells are spreading through the lymphatic system and through serum, thus when the tumor is metastasizing we might detect these characteristics in serum. We are still searching for methods to detect micro-metastasis in bladder cancer, because these patients would have more benefit from neo-adjuvant chemotherapy (NAC) as opposed to patients that do not have micro-metastasis. When no micro-metastasis are present, NAC can be omitted and surgical delay is eliminated. This is most important because the NAC has many side-effects that lead to increased morbidity and the overall survival improves only 5-8% at five years [33].

OUTLINE OF THIS THESIS

Chapter 2 compares two fibre optic Raman probes in a phantom model. The superficial probe is compared to a non-superficial probe regarding depth-response function and signal-to-noise ratio. In Chapter 3 Raman Spectroscopic measurements are taken in vivo using the superficial Raman probe, of UC and benign tissue and each location is pathologically analyzed. Chapter 4 evaluates spatial tissue analysis using Raman spectroscopy and histopathology of three cystectomy specimen. Raman spectroscopy might be used to follow up specific lesions in time. To enable re-assessment of specific locations in the bladder using Raman spectroscopy, a bladder navigation tool was developed, as spin-off of the Raman spectroscopy research. In this study bladder lesions were 3D registered. Using a cystoscope, navigation to that lesion was performed (without using the camera) in a phantom model in Chapter 5. A general discussion is presented and a summary is given in Chapter 6.

REFERENCES

- 1 Antoni S, Ferlay J, Soerjomataram I, Znaor A, Jemal A, Bray F. Bladder Cancer Incidence and Mortality: A Global Overview and Recent Trends. *Eur Urol.* 2017;71(1):96–108.
- 2 Cumberbatch MGK, Jubber I, Black PC, Esperto F, Figueroa JD, Kamat AM, et al. Epidemiology of Bladder Cancer: A Systematic Review and Contemporary Update of Risk Factors in 2018. *Eur Urol.* 2018 Dec;74(6):784–95.
- 3 Bladder cancer: diagnosis and management of bladder cancer: © NICE (2015) Bladder cancer: diagnosis and management of bladder cancer. *BJU Int.* 2017 Dec;120(6):755–65.
- 4 Babjuk M, Burger M, Comperat E, Gontero P, Liedberg F. EAU guidelines on Non-muscle-invasive Bladder Cancer (TaT1 and CIS). 2021 Apr Available from: <https://uroweb.org/wp-content/uploads/EAU-Guidelines-on-Non-muscle-invasive-Bladder-Cancer-TaT1-2021V2.pdf>
- 5 Witjes JA, Compérat E, Cowan NC, De Santis M, Gakis G, Lebreton T, et al. EAU Guidelines on Muscle-invasive and Metastatic Bladder Cancer: Summary of the 2013 Guidelines. *Eur Urol.* 2014 Apr;65(4):778–92.
- 6 Wong VK, Ganeshan D, Jensen CT, Devine CE. Imaging and Management of Bladder Cancer. *Cancers.* 2021 Jan;13(6):1396.
- 7 MacLennan GT, Kirkali Z, Cheng L. Histologic grading of noninvasive papillary urothelial neoplasms. *Eur Urol.* 2007 Apr;51(4):889–97; discussion 897-898.
- 8 Sylvester RJ, Brausi M, Kirkels W, Hoelt W, Calais da Silva F, Powel P, et al. Long-term efficacy results of EORTC genito-urinary group randomized phase 3 study 30911 comparing intravesical instillations of epirubicin, bacillus Calmette Guérin, and bacillus Calmette Guérin plus ioniazid in patients with intermediate- and high-risk stage TaT1 urothelial carcinoma of the bladder. *Eur Urol.* 2010 May; 57(5):766-73.
- 9 Sylvester RJ, Oosterlinck W, Holmang S, Sydes MR, Birtle A, Gudjonsson S, et al. Systematic Review and Individual Patient Data Meta-analysis of Randomized Trials Comparing a Single Immediate Instillation of Chemotherapy After Transurethral Resection with Transurethral Resection Alone in Patients with Stage pTa–pT1 Urothelial Carcinoma of the Bladder: Which Patients Benefit from the Instillation? *Eur Urol.* 2016 Feb;69(2):231–44.
- 10 Chou R, Selph S, Buckley DI, Fu R, Griffin JC, Grusing S, et al. Intravesical Therapy for the Treatment of Nonmuscle Invasive Bladder Cancer: A Systematic Review and Meta-Analysis. *J Urol.* 2017 May;197(5):1189–99.
- 11 Huncharek M, McGarry R, Kupelnick B. Impact of intravesical chemotherapy on recurrence rate of recurrent superficial transitional cell carcinoma of the bladder: results of a meta-analysis. *Anticancer Res.* 2001 Feb;21(1B):765–9.
- 12 Sylvester RJ, van der MEIJDEN APM, Lamm DL. Intravesical bacillus Calmette-Guérin reduces the risk of progression in patients with superficial bladder cancer: a meta-analysis of the published results of randomized clinical trials. *J Urol.* 2002 Nov;168(5):1964–70.



- 13 Brausi M, Collette L, Kurth K, van der Meijden AP, Oosterlinck W, Witjes JA, et al. Variability in the recurrence rate at first follow-up cystoscopy after TUR in stage Ta T1 transitional cell carcinoma of the bladder: a combined analysis of seven EORTC studies. *Eur Urol.* 2002 May;41(5):523–31.
- 14 Sylvester RJ, van der Meijden APM, Oosterlinck W, Witjes JA, Bouffouix C, Denis L, et al. Predicting recurrence and progression in individual patients with stage Ta T1 bladder cancer using EORTC risk tables: a combined analysis of 2596 patients from seven EORTC trials. *Eur Urol.* 2006 Mar;49(3):466–465; discussion 475–477.
- 15 Botteman MF, Pashos CL, Redaelli A, Laskin B, Hauser R. The health economics of bladder cancer. *PharmacoEconomics.* 2003 Dec;21(18):1315–30.
- 16 Sangar VK, Ragavan N, Matanhelia SS, Watson MW, Blades RA. The economic consequences of prostate and bladder cancer in the UK. *BJU Int.* 2005 Jan;95(1):59–63.
- 17 Gore JL, Wright JL. Can We Prevent Bladder Cancer Recurrences? *Eur Urol.* 2019 Apr;75(4):602–3.
- 18 Yafi FA, Brimo F, Steinberg J, Aprikian AG, Tanguay S, Kassouf W. Prospective analysis of sensitivity and specificity of urinary cytology and other urinary biomarkers for bladder cancer. *Urol Oncol Semin Orig Investig.* 2015 Feb;33(2):66.e25–66.e31.
- 19 Talwar R, Sinha T, Karan SC, Doddamani D, Sandhu A, Sethi GS, et al. Voided Urinary Cytology in Bladder Cancer: Is It Time to Review the Indications? *Urology.* 2007 Aug;70(2):267–71.
- 20 Bansal N, Gupta A, Sankhwar SN, Mahdi AA. Low- and high-grade bladder cancer appraisal via serum-based proteomics approach. *Clin Chim Acta Int J Clin Chem.* 2014 Sep;436:97–103.
- 21 Vrooman OPJ, Witjes JA. Urinary Markers in Bladder Cancer. *Eur Urol.* 2008 May;53(5):909–16.
- 22 Witjes JA. Bladder Carcinoma in Situ in 2003: State of the Art. *Eur Urol.* 2004 Feb;45(2):142–6.
- 23 Cheng L, Neumann RM, Weaver AL, Cheville JC, Leibovich BC, Ramnani DM, et al. Grading and staging of bladder carcinoma in transurethral resection specimens. Correlation with 105 matched cystectomy specimens. *Am J Clin Pathol.* 2000 Feb;113(2):275–9.
- 24 Mowatt G, Zhu S, Kilonzo M, Boachie C, Fraser C, Griffiths TRL, et al. Systematic review of the clinical effectiveness and cost-effectiveness of photodynamic diagnosis and urine biomarkers (FISH, ImmunoCyt, NMP22) and cytology for the detection and follow-up of bladder cancer. *Health Technol Assess Winch Engl.* 2010 Jan;14(4):1–331, iii–iv.
- 25 Ye Z, Hu J, Song X, Li F, Zhao X, Chen S, et al. A comparison of NBI and WLI cystoscopy in detecting non-muscle-invasive bladder cancer: A prospective, randomized and multi-center study. *Sci Rep.* 2015 Jun;5(1):10905.
- 26 Bochenek K, Aebischer D, Międzybrodzka A, Cieślak G, Kawczyk-Krupka A. Methods for bladder cancer diagnosis - The role of autofluorescence and photodynamic diagnosis. *Photodiagnosis Photodyn Ther.* 2019 Sep;27:141–8.
- 27 Liu J-J, Droller MJ, Liao JC. New optical imaging technologies for bladder cancer: considerations and perspectives. *J Urol.* 2012 Aug;188(2):361–8.
- 28 Lee CSD, Yoon CY, Witjes JA. The past, present and future of cystoscopy: the fusion of cystoscopy and novel imaging technology. *BJU Int.* 2008 Nov;102(9 Pt B):1228–33.

- 29 Liem EI, de Reijke TM. Can we improve transurethral resection of the bladder tumour for nonmuscle invasive bladder cancer? *Curr Opin Urol*. 2017;27(2):149–55.
- 30 Lopez A, Liao JC. Emerging endoscopic imaging technologies for bladder cancer detection. *Curr Urol Rep*. 2014 May;15(5):406.
- 31 von Rundstedt F-C, Lerner SP. New imaging techniques for nonmuscle invasive bladder cancer. *Curr Opin Urol*. 2014 Sep;24(5):532–9.
- 32 Patel P, Bryan RT, Wallace DMA. Emerging endoscopic and photodynamic techniques for bladder cancer detection and surveillance. *ScientificWorldJournal*. 2011;11:2550–8.
- 33 EAU Guidelines on MIBC - DISEASE MANAGEMENT - Uroweb [Internet]. Uroweb - Eur Assoc Urol. [cited 2022 Aug 17]. Available from: <https://uroweb.org/guidelines/muscle-invasive-and-metastatic-bladder-cancer/chapter/disease-management>
- 34 Nandagopal L, Sonpavde G. Circulating Biomarkers in Bladder Cancer. *Bladder Cancer Amst Neth*. 2(4):369–79.
- 35 Rao AR, Hanchanale V, Javle P, Karim O, Motiwala H. Spectroscopic view of life and work of the Nobel Laureate Sir C.V. Raman. *J Endourol*. 2007 Jan;21(1):8–11.
- 36 Raman CV, Krishnan KS. A New Type of Secondary Radiation. *Nature*. 1928 Mar;121(3048):501–2.
- 37 The Raman Effect: A Unified Treatment of the Theory of Raman Scattering by Molecules | Wiley [Internet]. Wiley.com. [cited 2023 May 6]. Available from: <https://www.wiley.com/en-us/The+Raman+Effect%3A+A+Unified+Treatment+of+the+Theory+of+Raman+Scattering+by+Molecules-p-9780471490289>
- 38 Tu Q, Chang C. Diagnostic applications of Raman spectroscopy. *Nanomedicine Nanotechnol Biol Med*. 2012 Jul;8(5):545–58.
- 39 Raman spectroscopy. Wikipedia. 2023 Feb [cited 2023 Feb 15]. Available from: https://en.wikipedia.org/w/index.php?title=Raman_spectroscopy&oldid=1138663591
- 40 Edwards HGM. Probing history with Raman spectroscopy. *The Analyst*. 2004 Oct;129(10):870–9.
- 41 Manigand Potin S, Manigand S, Turenne N, Sidhu S, Connell S, Applin D, et al. Raman spectroscopy investigation of lunar surface endmembers and analogues. 2021 Sep;EP-SC2021-97.
- 42 Chen H, Li X, Broderick N, Liu Y, Zhou Y, Han J, et al. Identification and characterization of bladder cancer by low-resolution fiber-optic Raman spectroscopy. *J Biophotonics*. 2018 Sep;11(9):e201800016.
- 43 Canetta E, Riches A, Borger E, Herrington S, Dholakia K, Adya AK. Discrimination of bladder cancer cells from normal urothelial cells with high specificity and sensitivity: combined application of atomic force microscopy and modulated Raman spectroscopy. *Acta Biomater*. 2014 May;10(5):2043–55.
- 44 Barman I, Dingari NC, Singh GP, Kumar R, Lang S, Nabi G. Selective sampling using confocal Raman spectroscopy provides enhanced specificity for urinary bladder cancer diagnosis. *Anal Bioanal Chem*. 2012 Dec;404(10):3091–9.
- 45 Cauberg Evelyne CC, de la Rosette JJMCH, de Reijke TM. Emerging optical techniques in advanced cystoscopy for bladder cancer diagnosis: A review of the current literature. *Indian J Urol IJU J Urol Soc India*. 2011 Apr;27(2):245–51.
- 46 Kong K, Kendall C, Stone N, Notingher I. Raman spectroscopy for medical diagnostics--From in-vitro biofluid assays to in-vivo cancer detection. *Adv Drug Deliv Rev*. 2015 Jul;89:121–34.



- 47 Kallaway C, Almond LM, Barr H, Wood J, Hutchings J, Kendall C, et al. Advances in the clinical application of Raman spectroscopy for cancer diagnostics. *Photodiagnosis Photodyn Ther*. 2013 Sep;10(3):207–19.
- 48 Lui H, Zhao J, McLean D, Zeng H. Real-time Raman spectroscopy for in vivo skin cancer diagnosis. *Cancer Res*. 2012 May;72(10):2491–500.
- 49 Huang Z, McWilliams A, Lui H, McLean DI, Lam S, Zeng H. Near-infrared Raman spectroscopy for optical diagnosis of lung cancer. *Int J Cancer*. 2003 Dec;107(6):1047–52.
- 50 Teh SK, Zheng W, Ho KY, Teh M, Yeoh KG, Huang Z. Diagnostic potential of near-infrared Raman spectroscopy in the stomach: differentiating dysplasia from normal tissue. *Br J Cancer*. 2008 Jan;98(2):457–65.
- 51 Ashok PC, Praveen BB, Bellini N, Riches A, Dholakia K, Herrington CS. Multi-modal approach using Raman spectroscopy and optical coherence tomography for the discrimination of colonic adenocarcinoma from normal colon. *Biomed Opt Express*. 2013;4(10):2179–86.
- 52 Bergholt MS, Zheng W, Lin K, Ho KY, Teh M, Yeoh KG, et al. In vivo diagnosis of gastric cancer using Raman endoscopy and ant colony optimization techniques. *Int J Cancer*. 2011 Jun;128(11):2673–80.
- 53 Molckovsky A, Song L-MWK, Shim MG, Marcon NE, Wilson BC. Diagnostic potential of near-infrared Raman spectroscopy in the colon: differentiating adenomatous from hyperplastic polyps. *Gastrointest Endosc*. 2003 Mar;57(3):396–402.
- 54 Shim MG, Wilson BC, Marple E, Wach M. Study of Fiber-Optic Probes for in vivo Medical Raman spectroscopy. *Appl Spectrosc*. 1999 Jun;53(6):619–27.
- 55 Kanter EM, Vargis E, Majumder S, Keller MD, Woeste E, Rao GG, et al. Application of Raman spectroscopy for cervical dysplasia diagnosis. *J Biophotonics*. 2009 Feb;2(1–2):81–90.
- 56 Stone N, Kendall C, Smith J, Crow P, Barr H. Raman spectroscopy for identification of epithelial cancers. *Faraday Discuss*. 2004;126:141–57; discussion 169–183.
- 57 Crow P, Uff JS, Farmer JA, Wright MP, Stone N. The use of Raman spectroscopy to identify and characterize transitional cell carcinoma in vitro. *BJU Int*. 2004 Jun;93(9):1232–6.
- 58 Crow P, Stone N, Kendall CA, Persad RA, Wright MPJ. Optical diagnostics in urology: current applications and future prospects. *BJU Int*. 2003 Sep;92(4):400–7.
- 59 Stone N, Hart Prieto MC, Crow P, Uff J, Ritchie AW. The use of Raman spectroscopy to provide an estimation of the gross biochemistry associated with urological pathologies. *Anal Bioanal Chem*. 2007 Mar;387(5):1657–68.
- 60 Kong KV, Leong WK, Lam Z, Gong T, Goh D, Lau WKO, et al. A rapid and label-free SERS detection method for biomarkers in clinical biofluids. *Small Weinh Bergstr Ger*. 2014 Dec;10(24):5030–4.
- 61 Krafft C, Dietzek B, Popp J. Raman and CARS microspectroscopy of cells and tissues. *The Analyst*. 2009 Jun;134(6):1046–57.
- 62 De Luca AC, Dholakia K, Mazilu M. Modulated Raman spectroscopy for Enhanced Cancer Diagnosis at the Cellular Level. *Sensors*. 2015 Jun;15(6):13680–704.
- 63 Feld MS, Manoharan R, Salenius J, Orenstein-Carndona J, Roemer TJ, Brennan III JF, et al. Detection and characterization of human tissue lesions with near-infrared Raman spectroscopy. In: Lakowicz JR, editor. San Jose, CA; 1995; pp 99–104.

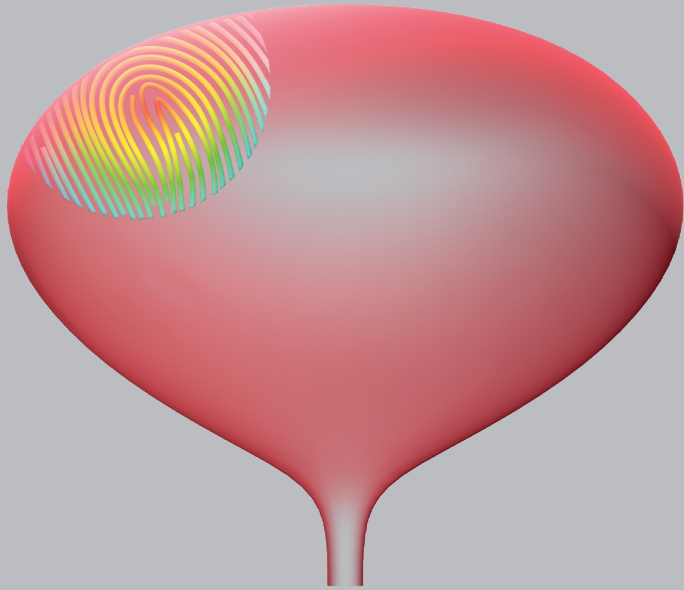
- 64 May M, Brookman-Amisshah S, Roigas J, Hartmann A, Störkel S, Kristiansen G, et al. Prognostic accuracy of individual uropathologists in noninvasive urinary bladder carcinoma: a multicentre study comparing the 1973 and 2004 World Health Organisation classifications. *Eur Urol*. 2010 May;57(5):850–8.
- 65 Van Rhijn BWG, Van Der Kwast TH, Kakiashvili DM, Fleshner NE, Van Der Aa MNM, Alkhateeb S, et al. Pathological stage review is indicated in primary pT1 bladder cancer. *BJU Int*. 2010;106(2):206–11.
- 66 Compérat E, Egevad L, Lopez-Beltran A, Camparo P, Algaba F, Amin M, et al. An interobserver reproducibility study on invasiveness of bladder cancer using virtual microscopy and heatmaps. *Histopathology*. 2013;63(6):756–66.
- 67 Shapiro A, Gofrit ON, Pizov G, Cohen JK, Maier J. Raman molecular imaging: a novel spectroscopic technique for diagnosis of bladder cancer in urine specimens. *Eur Urol*. 2011 Jan;59(1):106–12.
- 68 Canetta E, Mazilu M, De Luca AC, Caruthers AE, Dholakia K, Neilson S, et al. Modulated Raman spectroscopy for enhanced identification of bladder tumor cells in urine samples. *J Biomed Opt*. 2011 Mar;16(3):037002.
- 69 Praveen BB, Mazilu M, Marchington RF, Herrington CS, Riches A, Dholakia K. Optimisation of wavelength modulated Raman spectroscopy: towards high throughput cell screening. *PLoS One*. 2013;8(6):e67211.
- 70 Yosef HK, Krauß SD, Lechtonen T, Jütte H, Tannapfel A, Käßlerlein HU, et al. Noninvasive Diagnosis of High-Grade Urothelial Carcinoma in Urine by Raman Spectral Imaging. *Anal Chem*. 2017 Jun;89(12):6893–9.
- 71 Krauß SD, Roy R, Yosef HK, Lechtonen T, El-Mashtoly SF, Gerwert K, et al. Hierarchical deep convolutional neural networks combine spectral and spatial information for highly accurate Raman-microscopy-based cytopathology. *J Biophotonics*. 2018 Oct;11(10):e201800022.
- 72 Krauß SD, Yosef HK, Lechtonen T, Jütte H, Tannapfel A, Käßlerlein HU, et al. Integrating spatial, morphological, and textural information for improved cell type differentiation using Raman microscopy. *J Chemom*. 2018;32(1):e2973.
- 73 Pallaoro A, Mirsafavi RY, Culp WTN, Braun GB, Meinhart CD, Moskovits M. Screening for canine transitional cell carcinoma (TCC) by SERS-based quantitative urine cytology. *Nanomedicine Nanotechnol Biol Med*. 2018 Jun;14(4):1279–87.
- 74 Huttanus HM, Vu T, Guruli G, Tracey A, Carswell W, Said N, et al. Raman chemometric urinalysis (Rametrix) as a screen for bladder cancer. *PLoS One*. 2020;15(8):e0237070.
- 75 Cui X, Liu T, Xu X, Zhao Z, Tian Y, Zhao Y, et al. Label-free detection of multiple genitourinary cancers from urine by surface-enhanced Raman spectroscopy. *Spectrochim Acta A Mol Biomol Spectrosc*. 2020 Oct;240:118543.
- 76 Hu D, Xu X, Zhao Z, Li C, Tian Y, Liu Q, et al. Detecting urine metabolites of bladder cancer by surface-enhanced Raman spectroscopy. *Spectrochim Acta A Mol Biomol Spectrosc*. 2021 Feb;247:119108.
- 77 O'Dwyer K, Domijan K, Dignam A, Butler M, Hennelly BM. Automated Raman Micro-Spectroscopy of Epithelial Cell Nuclei for High-Throughput Classification. *Cancers*. 2021 Sep;13(19):4767.
- 78 Li S, Li L, Zeng Q, Zhang Y, Guo Z, Liu Z, et al. Characterization and noninvasive diagnosis of bladder cancer with serum surface enhanced Raman spectroscopy and genetic algorithms. *Sci Rep*. 2015 May;5:9582.



- 79 Chen S, Zhu S, Cui X, Xu W, Kong C, Zhang Z, et al. Identifying non-muscle-invasive and muscle-invasive bladder cancer based on blood serum surface-enhanced Raman spectroscopy. *Biomed Opt Express*. 2019 Jul;10(7):3533–44.
- 80 Kim DK, Kim YH, Lee HY, Lee S, Doo SW, Yang WJ, et al. Diagnostic accuracy of Raman spectroscopy for the diagnosis of bladder cancer: A systematic review and meta-analysis. *J Cancer Res Ther*. 2021 Jun;17(2):426–33.
- 81 Jin H, Lin T, Han P, Yao Y, Zheng D, Hao J, et al. Efficacy of Raman spectroscopy in the diagnosis of bladder cancer: A systematic review and meta-analysis. *Medicine (Baltimore)*. 2019 Nov;98(47):e18066.
- 82 Crow P, Molckovsky A, Stone N, Uff J, Wilson B, WongKeeSong L-M. Assessment of fiberoptic near-infrared raman spectroscopy for diagnosis of bladder and prostate cancer. *Urology*. 2005 Jun;65(6):1126–30.
- 83 Prieto MCH, Matousek P, Towrie M, Parker AW, Wright M, Ritchie AW, et al. Use of picosecond Kerr-gated Raman spectroscopy to suppress signals from both surface and deep layers in bladder and prostate tissue. *J Biomed Opt*. 2005 Aug;10(4):44006.
- 84 Koljenović S, Bakker Schut TC, Wolthuis R, de Jong B, Santos L, Caspers PJ, et al. Tissue characterization using high wave number Raman spectroscopy. *J Biomed Opt*. 2005 Jun;10(3):031116.
- 85 de Jong BWD, Schut TCB, Maquelin K, van der Kwast T, Bangma CH, Kok D-J, et al. Discrimination between nontumor bladder tissue and tumor by Raman spectroscopy. *Anal Chem*. 2006 Nov;78(22):7761–9.
- 86 Grimbergen MCM, van Swol CFP, van Moorselaar RJA, Uff J, Mahadevan-Jansen A, Stone N. Raman spectroscopy of bladder tissue in the presence of 5-aminolevulinic acid. *J Photochem Photobiol B*. 2009 Jun;95(3):170–6.
- 87 Draga ROP, Grimbergen MCM, Vijverberg PLM, van Swol CFP, Jonges TGN, Kummer JA, et al. In vivo bladder cancer diagnosis by high-volume Raman spectroscopy. *Anal Chem*. 2010 Jul;82(14):5993–9.
- 88 Cordero E, Rüger J, Marti D, Mondol AS, Hasselager T, Mogensen K, et al. Bladder tissue characterization using probe-based Raman spectroscopy: Evaluation of tissue heterogeneity and influence on the model prediction. *J Biophotonics*. 2020 Feb;13(2):e201960025.
- 89 Baria E, Morselli S, Anand S, Fantechi R, Nesi G, Gacci M, et al. Label-free grading and staging of urothelial carcinoma through multimodal fibre-probe spectroscopy. *J Biophotonics*. 2019 Nov;12(11):e201900087.
- 90 Placzek F, Bautista EC, Kretschmer S, Wurster LM, Knorr F, González-Cerdas G, et al. Morpho-molecular ex vivo detection and grading of non-muscle-invasive bladder cancer using forward imaging probe based multimodal optical coherence tomography and Raman spectroscopy. *Analyst*. 2020 Feb;145(4):1445–56.
- 91 Morselli S, Baria E, Cicchi R, Liaci A, Sebastianelli A, Nesi G, et al. The feasibility of multimodal fiber optic spectroscopy analysis in bladder cancer detection, grading, and staging. *Urologia*. 2021 Nov;88(4):306–14.
- 92 Stomp-Agenant M, van Dijk T, R Onur A, Grimbergen M, van Melick H, Jonges T, et al. In vivo Raman spectroscopy for bladder cancer detection using a superficial Raman probe compared to a nonsuperficial Raman probe. *J Biophotonics*. 2022 Mar;e202100354.
- 93 Omberg KM, Osborn JC, Zhang SL, Freyer JP, Mourant JR, Schoonover JR. Raman spectroscopy and Factor Analysis of Tumorigenic and Non-Tumorigenic Cells. *Appl Spectrosc*. 2002 Jul;56(7):813–9.

- 94 Jocham D, Stepp H, Waidelich R. Photodynamic Diagnosis in Urology: State-of-the-Art. *Eur Urol.* 2008 Jun;53(6):1138–50.
- 95 Haka AS, Volynskaya Z, Gardecki JA, Nazemi J, Lyons J, Hicks D, et al. In vivo margin assessment during partial mastectomy breast surgery using raman spectroscopy. *Cancer Res.* 2006 Mar;66(6):3317–22.





CHAPTER 2

CLINICAL SUPERFICIAL RAMAN PROBE AIMED FOR EPITHELIAL TUMOR DETECTION: PHANTOM MODEL RESULTS

Agenant M
Grimbergen M
Draga R
Marple E
Bosch R
van Swol C

Biomed Opt Express. 2014 Mar 5(4):1203-16

ABSTRACT

A novel clinical Raman probe for sampling superficial tissue to improve in vivo detection of epithelial malignancies is compared to a non-superficial probe regarding depth response function and signal-to-noise ratio. Depth response measurements were performed in a phantom tissue model consisting of a polyethylene terephthalate disc in an 20%-Intralipid® solution. Sampling ranges of 0-200 and 0-300 μm were obtained for the superficial and non-superficial probe, respectively. The mean signal-to-noise ratio of the superficial probe increased by a factor of 2 compared with the non-superficial probe. This newly developed superficial Raman probe is expected to improve epithelial cancer detection in vivo.

INTRODUCTION

Raman spectroscopy is a highly specific optical technique that has been proven to non-invasively detect epithelial tissue malignancies. It uses molecular-specific inelastic scattering of photons to assess the molecular contents of biological tissue. Photons of monochromatic light (usually from a laser) interact with molecular bonds of biological tissue, which results in an energy shift of the incident photons. Different molecular bonds create different energy shifts that can be visualized as intensity peaks at specific wavenumbers. This allows to obtain information on the molecular composition of the studied tissue and may enable differential diagnosis of (pre-) malignancies in tissues [1–5].

To use Raman spectroscopy for cancer diagnosis it must be incorporated in the current diagnostic approach for suspicious lesions. Our group has special interest in urothelial cell carcinoma diagnosis which is currently based on visual inspection during white light endoscopy. After cystoscopic detection of a suspicious lesion in the outpatient clinic that lesion is endoscopically resected in the operating theater. The resected tissue is then analyzed by the pathologist to obtain the diagnosis. To use Raman spectroscopy in a clinical situation and improve the diagnostic accuracy of urothelial carcinoma, an endoscopic approach is required. Therefore, the Raman probe should have a sufficiently small diameter to allow passage through the endoscopic channel. Furthermore, as part of the clinical Raman system the Raman probe should also meet the requirements of the Medical Device Directive (MDD) as well as other clinical functional requirements. Industrial Raman probes with excellent specifications in the Raman domain are available; however, these are usually not suitable for clinical application because of their limiting factors e.g. the spot-size, sampling volume, acquisition time and the MDD requirements such as the biocompatibility. The biocompatibility demanded by the MDD entails the use of biocompatible materials and application of strict hospital hygiene requirements including (re)sterilization without damaging the Raman probe.

According to the clinical and functional requirements, the probe should be suitable for endoscopic use, as well as providing good signal quality, i.e. have a high signal-to-noise ratio (SNR). However, clinically, a collection time of longer than 5 s is not feasible as probe displacement during a measurement results in meaningless data. Furthermore, some materials used in probe designs (e.g. sapphire) might interfere more than others with the tissue Raman signal; use of such materials should (ideally) be avoided in a clinical probe design. Finally, the probe optics should be optimized to obtain an adequate clinical sampling range because epithelial carcinoma originate superficially (100-200 μm below the surface) on top of the underlying stromal tissue [6].

During the last 20 years, several groups have constructed probes that suffice with respect to most of the criteria [7–13]. Nevertheless, to our knowledge, a superficial Raman probe that complies with both the Medical Device Directive and the clinical/functional requirements is not yet available. Using gathered information from our previous clinical study with a non-superficial Raman probe [3], a more superficial probe has been designed to meet these requirements. This new probe was designed for a clinical trial in which our group investigates in vivo Raman spectroscopy for the diagnosis of bladder cancer. The probe is constructed of biocompatible materials that result in minimal interference with tissue Raman signals; it can be sterilized and its physical shape allows endoscopic application. At the same time it is designed to provide an ample SNR at clinically acceptable laser exposure and collection times. The aim of the present study is to compare the sampling range and SNR of the superficial Raman probe with those of a non-superficial probe [3] in a phantom tissue model.

MATERIALS AND METHODS

Raman system

For all measurements a portable Raman spectroscopy system was used as described by Draga et al. [3]. The system consists of a 785 nm diode laser (DFB-0785-1000, Sacher Lasertechnik, Marburg, Germany), a Raman probe (EmVision LLC, Loxahatchee, Florida, USA), a spectrograph (HoloSpec Imaging Spectrograph f/1.8i (HSG-785-LF), Kaiser Optical Systems, Ecully, France), a charge-coupled device camera (PIXIS 256 BRDD, Princeton Instruments, Trenton, New Jersey, USA) and a personal computer. The system has been approved for clinical research by the Dutch Health Care Inspectorate (IGZ) allowing a multicenter trial within the European Union.

Probe designs

For the present study, the newly developed clinical superficial Raman probe was compared with the non-superficial Raman probe which was used in an earlier clinical study by our group [3,13]. Both probes enable efficient excitation and collection of Raman excited light from a 785 nm laser; they are described below and illustrated in figure 1.

Non-superficial Raman probe

The non-superficial Raman probe is a standard bundle-style probe. It contains seven low hydroxyl (OH) content Raman collection fibers (300 μm core/0.22 NA) which are incorporated surrounding a central excitation fiber (400 μm core/0.22 NA). A small band pass filter is positioned in front of the delivery fiber and a donut-shaped long pass filter is positioned in front of the seven collection fibers, which rejects the laser light and passes the Raman signal from the sample. All parts of the probe are bound together with an

epoxy-based glue and placed inside a stainless steel needle tube, with an outer diameter of 2.1 mm. This allows easy passage through the channel of urological endoluminal scopes.

Superficial Raman probe

The design of the superficial Raman probe (EmVision LLC, Loxahatchee, USA) uses the same external dimensions as the above-mentioned non-superficial Raman probe; however, the seven collection fibers surround a stainless steel tube which (on the inside) has a central excitation fiber of a smaller diameter (200 μm core/0.22 NA). To enable sampling of superficial tissue layers, an overlap of the focus of the excitation beam and the collection region is created by incorporation of a unique two-component converging lens. This lens consists of a distal element (2-mm diameter) which is a 1-mm thick flat window of fused silica and a proximal element of a plano-convex sapphire lens (Fig. 1B.). The high refractive index of the lens bends the light sharply. This configuration allows overlap of the excitation and collection light at the sample without interference from the sapphire Raman signal and an approximate 0.5 mm surface diameter of the region sampled. The superficial Raman probe design is described in detail in its patent [14].

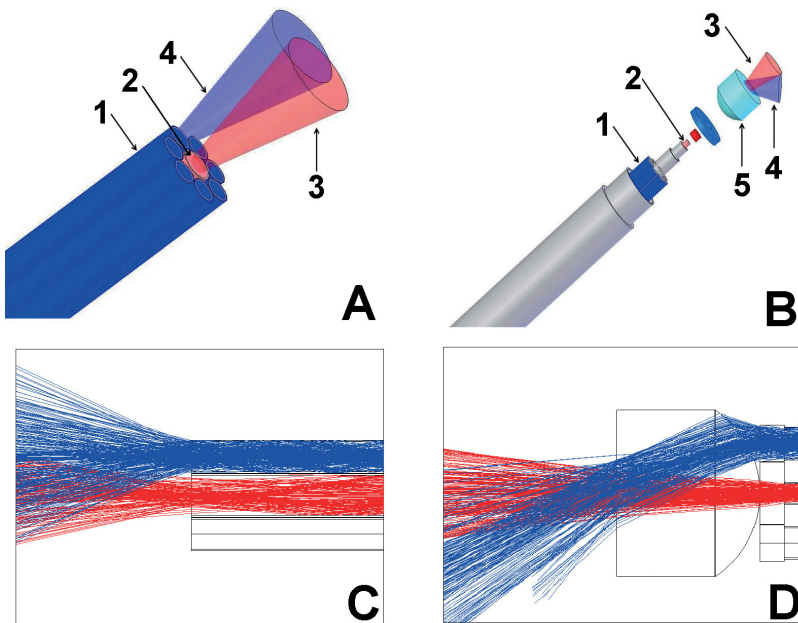


Figure 1. Top left (A) and right (B) are exploded views of the distal probe tip. The Raman laser excitation region and the direction of the Raman collection cone(s) create an overlap with the laser cone at the surface of the lens and is illustrated for the non-superficial Raman probe (A) and the superficial Raman probe (B) (1 = 7 times collection fibers, 2 = excitation fiber, 3 = Raman laser cone, 4 = Raman collection cone, 5 = two component front lens). Bottom left (C) and right (D) are Zemax ray traces of the non-superficial and the superficial Raman probe, respectively, using the refractive index of water, which is comparable to the 20%-Intralipid[®] that was used in the phantom tissue model. The Raman excitation light and only one collection fiber cone is illustrated; however, all the collection light is altered in the same way as this one.

Phantom tissue model and measurements

The phantom tissue model consists of two layers in order to determine the depth response function of the probes, referred to here as 'sampling depth' (figure 2). The top layer, with an adjustable thickness, consists of a 20%-Intralipid® solution that is widely used to simulate scattering of the 785 nm light of epithelial tissue [15–18]. A polyethylene terephthalate (PET) slide, 170- μm thick, was used as a sub layer to mimic the stromal tissue as this material has specific Raman peaks (e.g. 732.5 cm^{-1}). Accordingly, each Raman spectrum from the phantom tissue model contains signal from both layers (the top layer and the sub layer). Aluminum foil was used as shielding material to prevent the Raman signal from being acquired from the cup itself (figure 2A). In the model, by increasing the top layer thickness, the signal intensity of the sub layer decreases as the probe moves relatively further away from the sub layer (figure 2B). The sampling depth is defined as: the top layer thickness where the normalized signal intensity of the top layer meets the normalized signal intensity of the sub layer. To determine the specific top layer and sub layer Raman signal contributions in each spectrum, top layer-only and sub layer-only spectra were obtained, respectively, at a top layer thickness of 1.5 cm and directly on the sub layer with no top layer in between (without 20% Intralipid®). From these spectra a specific top layer peak (1439.5 cm^{-1}) with minimal signal interference of the sub layer material and a specific sub layer peak (732.5 cm^{-1}) with minimal signal interference of top layer material were determined. Sets of 10 Raman spectra (acquisition time of 500 ms) were taken at increasing top layer thicknesses from 0-1,500 μm , with incremental steps of 50 μm .

Spectral calibration was performed for each probe using a neon-argon lamp to calibrate the spectral dispersion of the detection system and acetaminophen to standardize the Raman shift axis. The spectra were processed for background fluorescence subtraction using a modified polyfit algorithm based on an iterative fitting procedure that converges the spectrum to its baseline [19]. Furthermore, each spectrum was normalized towards its mean spectral intensity to account for variations in absolute spectral intensity.

For all Raman spectra sets at each top layer thickness, the mean intensity of the top layer (1,439.5 cm^{-1}) and sub layer (732.5 cm^{-1}) peaks was obtained. Eventually, these mean top layer and sub layer peak intensities were normalized to their maximal intensity, to account for the difference in absolute top layer and sub layer peak intensity. The sampling depth was determined regarding at which top layer thickness the intensities of both peaks were equal.

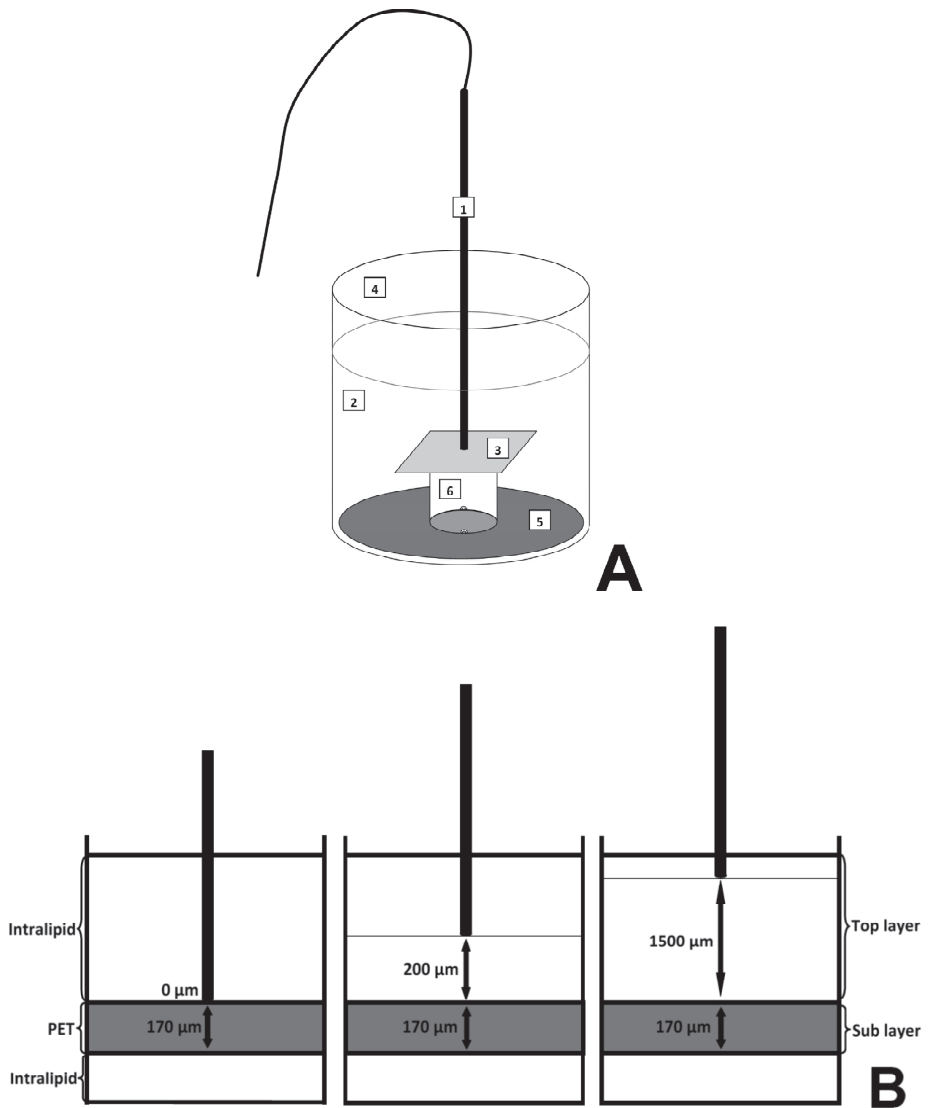


Figure 2. Top (A) shows a schematic depiction of the phantom tissue model based on two layers i.e. 20%-Intralipid® (top layer) and PET (sub layer). The Raman probe is vertically fixed perpendicular to the PET slide (1 = Raman probe, 2 = 20%-Intralipid®, 3 = PET slide, 4 = 30 cc cup, 5 = Aluminum foil, 6 = Hollow tube). Bottom (B) shows a schematic depiction of the probe volume in the phantom tissue model that mimics epithelial tissue (top layer) and its stromal tissue (sub layer) below. The top layer is variable in thickness as opposed to the sub layer which has a constant thickness of 170 μm. By increasing the top layer thickness, the specific top layer and sub layer contributions can be compared and the sample depth is determined at which top layer thickness both contributions are equal.

Signal-to-noise ratio comparison

To compare the spectral quality of the two probes one measurement set from the above sampling depth experiment of both probes was used, i.e. 10 spectra of each probe at a top layer thickness of 200 μm , which is similar to the urothelial tissue thickness. The mean SNR over the spectral range (SNR_{msr}) is used to assess the quality of the entire spectrum for both probes. The SNR_{msr} was determined by using the mean of two consecutive spectra and the standard deviation (SD) of the difference between those two consecutive spectra within the same set [20]. To identify the possible difference of Raman activity for both substances used in the sampling depth experiment, the SNR at the specific sub layer peak (732.5 wavenumbers) and at the top layer peak (1,439.5) was also determined from that SNR_{msr} spectrum.

RESULTS

General performance

In figure 3 the mean raw spectra of both probes without correction are depicted.

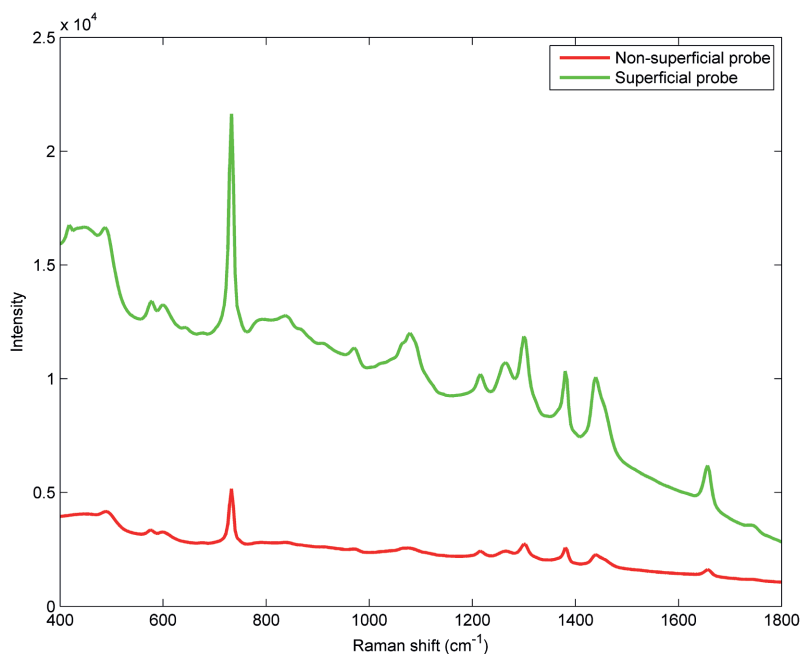


Figure 3. Mean raw Raman spectra of all measurements per probe, before correction.

Figure 4 shows the mean spectra of both probes after fluorescence subtraction to the baseline using the modified polyfit method [19].

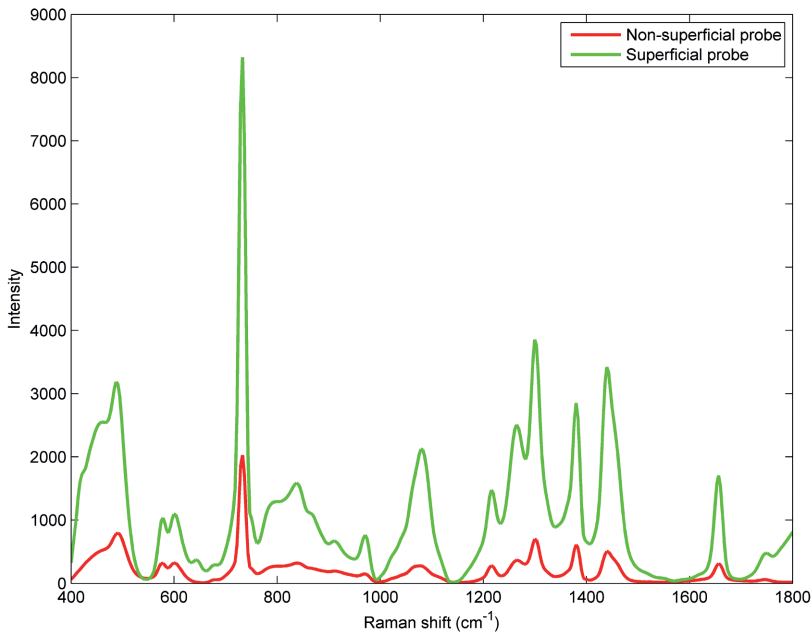


Figure 4. Mean Raman spectra of all measurements per probe after background fluorescence subtraction and noise smoothing.

Specific sub layer and top layer intensities

Mean spectra of the top layer-only and sub layer-only measurements show unique spectral peaks at $1,439.5 \text{ cm}^{-1}$ (top layer peak) and 732.5 cm^{-1} (sub layer peak). This is depicted in figure 5.

Sampling depth measurements

The mean peak intensities of the top layer ($1,439.5 \text{ cm}^{-1}$) and sub layer (732.5 cm^{-1}) after correction for excitation intensity were calculated at each incremental top layer thickness. To correct for the absolute intensity difference between both peaks, these intensities were normalized to their maximal intensity per probe (figure 6). The maximal intensity for the top layer and sub layer peaks were found at a $1,500 \mu\text{m}$ and a $0 \mu\text{m}$ top layer thickness, respectively. When the top layer thickness was increased, the top layer and sub layer peak intensities showed an increase and decrease, respectively. In figure 6, the intersection of these normalized top layer and sub layer peak intensities determines

the sampling depth for each probe. The sampling depth of the non-superficial Raman probe was approximately 300 μm and that of the superficial Raman probe approximately 200 μm .

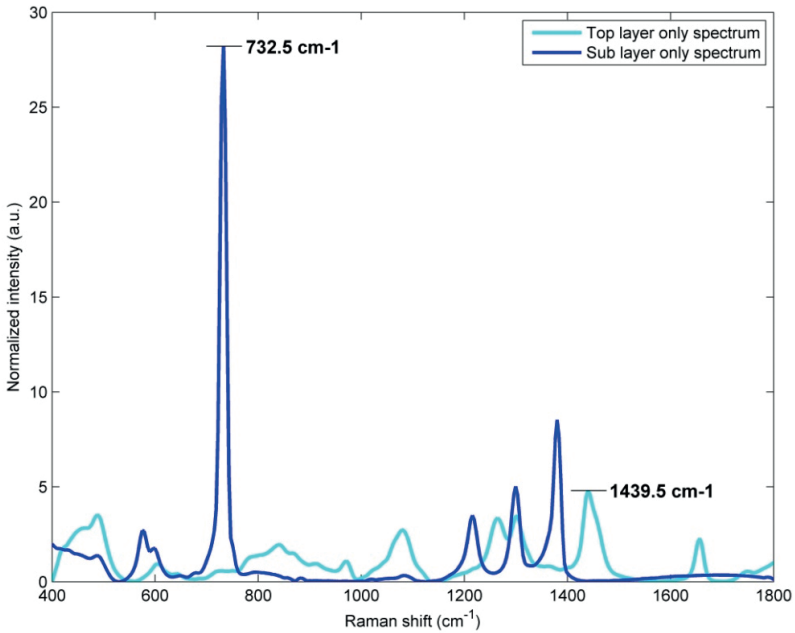


Figure 5. Mean Raman spectra after normalization to their mean intensity of top layer-only and sub layer-only measurements. The main peak of the top layer (light blue) was found at a wavenumber shift of 1,439.5 cm^{-1} and the main peak of the sub layer (dark blue) was found at 732.5 cm^{-1} .

Signal-to-noise ratio comparison

Table 1 presents the SNR_{msr} of both probes in the phantom tissue model with a top layer of 200 μm . The SNR_{msr} of the superficial Raman probe has increased by a factor of 2 compared with the non-superficial Raman probe. Similarly, at the specific sub and top layer peaks the SNR was also increased by a factor 2 for the superficial probe compared to the non-superficial probe.

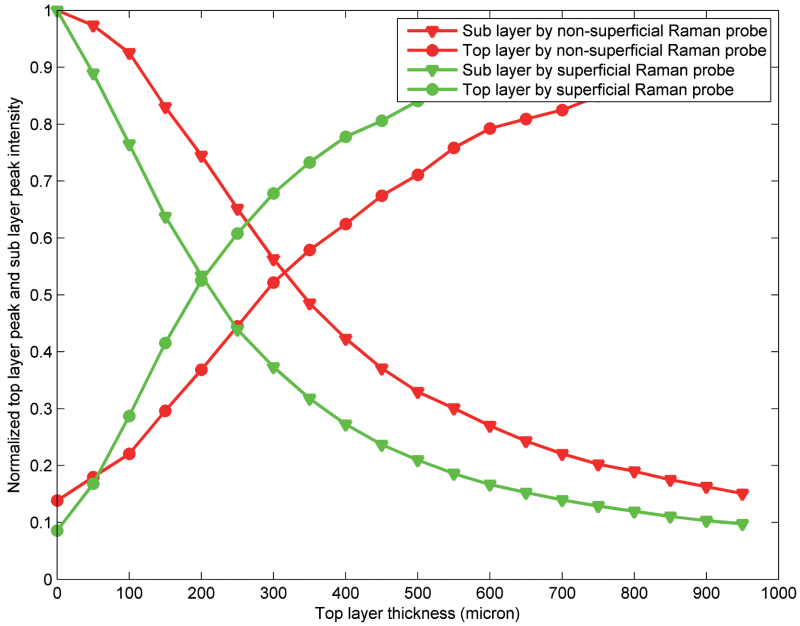


Figure 6. Raman peak intensities at $1,439.5\text{ cm}^{-1}$ and 732.5 cm^{-1} and (top layer and sub layer peak) as a function of top layer thickness in the phantom tissue model for the non-superficial and the superficial Raman probe with their standard deviation. The intersections of the non-superficial Raman probe and the superficial Raman probe at approximately $300\text{ }\mu\text{m}$ and $200\text{ }\mu\text{m}$, respectively, indicate that the sampling depth is closer to the distal probe tip for the superficial Raman probe.

Table 1. Signal-to-noise ratio over the mean spectral range (SNR_{msr}) measured in the phantom tissue model at $200\text{ }\mu\text{m}$ probe distance from the sub layer and specific SNR_{msr} of the sub layer and top layer peaks.

	Non-superficial Raman probe	Superficial Raman probe	Factor
SNR_{msr}	90.5	181.7	2.0
SNR_{msr} (sub layer peak 732.5 cm^{-1})	315.1	596.7	1.9
SNR_{msr} (top layer peak 1439.5 cm^{-1})	77.9	166.5	2.1

DISCUSSION

A clinical superficial Raman probe that meets the MDD and clinical/functional requirements is presented. The superficial Raman probe is constructed of biocompatible materials. Moreover, it has shown to withstand repeated (>15 for multiple probes) plasma (STERRAD®) sterilization (results not shown). Furthermore, the short collection time of 5 s (10 x 500 ms) minimizes probe movement during the measurement, while the probe's diameter of 2.1 mm allows endoscopic use as required for urothelial tissue diagnosis.

In this study, the sampling depth of the superficial Raman probe was compared with the non-superficial Raman probe in a phantom tissue model. In this model the intersection of the sub layer and top layer peak intensities indicate a sampling depth which allows comparison of the two probes. The optimal sampling range of the superficial probe is 0-200 μm and for the non-superficial probe 0-300 μm . The depth setting error was maximal 5 μm and the SD of the intensity at the intersection was 0.02 and 0.08 for the non-superficial and the superficial probe, respectively. The superficial probe more closely approximates the sampling range of the origination of urothelial carcinoma (100-200 μm from the surface). Accordingly, this probe should enable better urothelial cancer diagnosis because the Raman signal is mostly obtained from the urothelial cell layer and is less clouded by signal from its underlying stromal layer (figure 7). However, because this test was performed to compare the probes, these results cannot be used to indicate the exact sampling range in tissue because the model is a simplification of tissue composition. As opposed to tissue, the model contains materials with uniform consistency, and has a straight transition of materials and constant thicknesses. It also has different optical properties.

To determine the SNR, raw spectra without background subtraction and noise smoothing were used. The measurement sets with a top layer thickness of 200 μm for both probes were chosen for SNR determination, because this thickness is similar to the normal urothelial thickness overlying its stromal sub layer. Therefore, these measurement sets are most similar to the in vivo situation.

In general, the SNR_{msr} of the superficial probe is twice as high compared with the previously used non-superficial probe in the phantom tissue model with a top layer thickness of 200 μm . This is also the case for the specific top layer and sub layer peaks. Accordingly, to obtain the same signal quality, a clinical Raman measurement of 5 s with the new superficial probe would take up to 20 s with the old non-superficial probe, which is a clinical challenge. Furthermore, as the SNR does not linearly increase with

longer integration times, an even longer integration time than 20 s might be required to obtain the same signal quality.

These results allow to conclude that the SNR of the superficial probe is improved compared to the non-superficial probe. However, the absolute SNR_{msr} outcomes only allow comparison of the two probes; these data are not suitable for comparison with other SNR experiments because of the specific Raman contributions of the phantom tissue model substances (as described above).

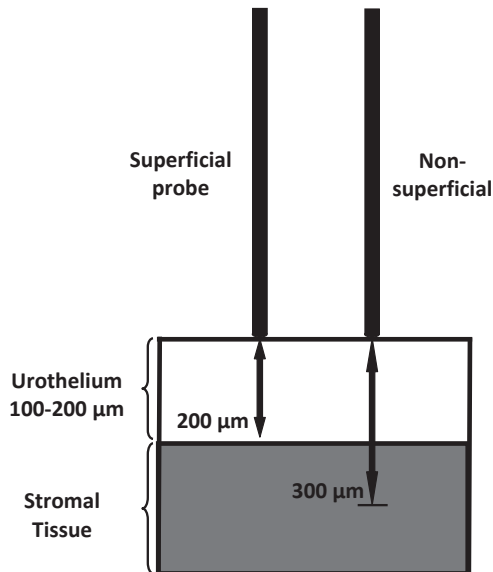


Figure 7. The sampling range of both Raman probes are illustrated in urothelial tissue. The superficial probe has a sampling range of approximately 0-200 μm , which is similar to the total urothelium thickness. The non-superficial Raman probe has a less pure urothelium signal, as the stromal tissue is part of the sampling range which was 0-300 μm . The stromal layer may blur the urothelial signal.

Since the mid-1990s several Raman probe designs have been developed for cancer diagnosis (table 2). Mahadevan-Janssen et al. were the first to construct a clinical probe in 1998; they also attempted to miniaturize this design to enable clinical endoscopic use [10]. Shim et al. constructed a miniature Raman probe which focuses on superficial layers using a beam steering technique with beveling of the collection fibers [13]. Their sampling range was 0-600 μm with a 10° beveled probe; however, this probe was not qualified for clinical use with respect to biocompatibility as required by the MDD. Furthermore in their probe design, the filters are placed approximately 3 cm from the distal end of the needle tube which limits flexible endoscopic application. Although,

Hattori et al. produced an endoscopic probe, the integration time of 50 s would not have been practical as probe movement might occur during urological endoscopy. Furthermore, with a focal depth of 10 mm the contribution of the stromal tissue signal might obscure the Raman signal of the thin urothelial cell layer where urothelial cancer originates [8]. Several groups have constructed superficial Raman probes using ball lenses. [7,11,12,21,22] The sampling range of these probes is minimized to 40-300 μm and focuses on the urothelial cancer origin. Unfortunately, ball lenses are generally composed of sapphire which generates high fluorescence background signals that might interfere with the urothelial tissue Raman signal. Consequently, we aimed to design a probe using silica, which has a lower fluorescence background compared with sapphire [13,23].

In conclusion, to our knowledge the superficial Raman probe presented here is the first clinically applicable urological endoscopic probe with a shallow sampling range and with minimal signal interference from the materials used. Although, it has a sampling range of 0-200 μm , this absolute determination of sampling range only allows comparison of the two probes described here. No comparison can be made with the probes described in table 2 as these research groups might have used different definitions of sampling range and measuring methods.

The sampling range and SNR results of this new superficial Raman probe are improved compared with the non-superficial probe in the phantom tissue model. Nevertheless, the clinical diagnostic sensitivity, specificity and accuracy of this new probe needs to be examined in a clinical situation, because the materials used in the phantom model are a simplification of real tissue. Our group is currently investigating this in an ongoing clinical trial on in vivo Raman spectroscopy for bladder cancer diagnosis. To date, monitoring of the probe performance (80 patients) has shown acceptable variations in the constancy test and mechanical integrity during each new procedure after sterilization. For commercial acceptability, additional sterilization contamination tests are required.

Table 2. Information on the Raman probe developed since the 1990s

Authors	Year	Probe diameter (mm)	Sampling range	Acquisition time (sec)	Biocompatible	Sterilizable	Design
Mahadevan-Jansen et al. [10]	1998	12	900 μm \varnothing	90	NA	NA	
Shim et al. [13]	1999	1.5	0-600 μm (10 ^o)	1	NA	NA	Beam steering beveled probes fibers in 0 ^o , 5 ^o and 10 ^o
Motz et al. [12]	2004	3	500 μm	10	NA	NA	Sapphire
Hattori et al. [8]	2007	2.5	10 mm focal depth	50	NA	NA	
Day et al. [7]	2009	2.8	147 μm	2 and 10	Yes	Yes	Microscopic system with grin lens
Mo et al. [11]	2009	8	700 μm max depth	1	Yes	NA	Sapphire ball lens
Mo et al. [21]	2010	3	40-300 μm	NA	Yes	NA	Different refractive indexes Ball lens Sapphire
Draga et al. [3]	2010	2.1	0-300 μm	0.5x10	Yes	Yes	
Wang et al. [22]	2013	1.8	NA		Yes?	NA	Ball lens Refractive index 1.76
Agenant et al.	2013	2.1	0-200 μm	0.5x10	Yes	Yes	

NA=not applicable



CONCLUSION

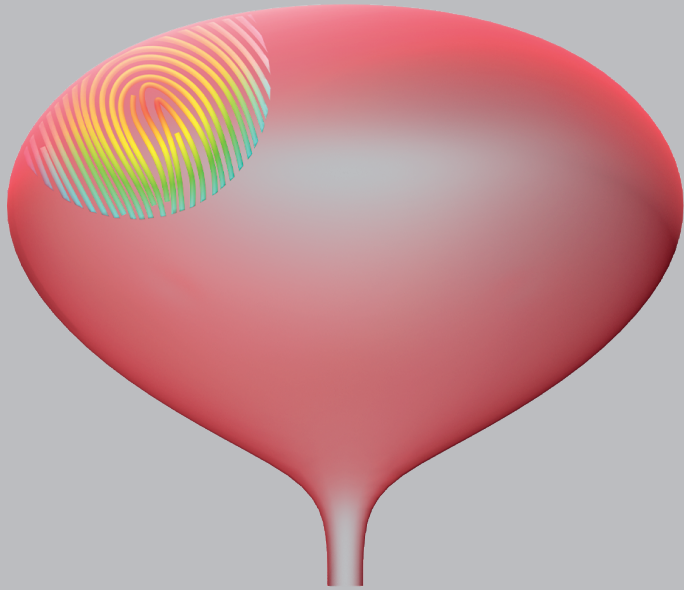
Since the 1990s, substantial research led to the design and development of several Raman probes for real-time clinical cancer diagnosis. However, a probe meeting MDD and functional requirements for clinical urothelial carcinoma diagnosis has not yet been developed. A superficial clinical Raman probe design, approved for investigative use, is presented. It has a superficial sampling range of 0-200 μm which should improve the diagnosis of (superficial) urothelial carcinoma, and has an improved SNR compared with the non-superficial probe used in the our earlier clinical feasibility study. The ultimate goal is to detect urothelial (pre) carcinoma with high accuracy in real-time using an optical non-invasive Raman measurement in the outpatient clinic, rather than an invasive biopsy in the operating room.

REFERENCES

- 1 Bergholt MS, Zheng W, Lin K, Ho KY, Teh M, Yeoh KG, et al. In vivo diagnosis of gastric cancer using Raman endoscopy and ant colony optimization techniques. *Int J Cancer*. 2011 Jun;128(11):2673–80.
- 2 Crow P, Uff JS, Farmer JA, Wright MP, Stone N. The use of Raman spectroscopy to identify and characterize transitional cell carcinoma in vitro. *BJU Int*. 2004 Jun;93(9):1232–6.
- 3 Draga ROP, Grimbergen MCM, Vijverberg PLM, van Swol CFP, Jonges TGN, Kummer JA, et al. In vivo bladder cancer diagnosis by high-volume Raman spectroscopy. *Anal Chem*. 2010 Jul;82(14):5993–9.
- 4 Kanter EM, Vargis E, Majumder S, Keller MD, Woeste E, Rao GG, et al. Application of Raman spectroscopy for cervical dysplasia diagnosis. *J Biophotonics*. 2009 Feb;2(1–2):81–90.
- 5 Molckovsky A, Song L-MWK, Shim MG, Marcon NE, Wilson BC. Diagnostic potential of near-infrared Raman spectroscopy in the colon: differentiating adenomatous from hyperplastic polyps. *Gastrointest Endosc*. 2003 Mar;57(3):396–402.
- 6 Shetty G, Kendall C, Shepherd N, Stone N, Barr H. Raman spectroscopy: elucidation of biochemical changes in carcinogenesis of oesophagus. *Br J Cancer*. 2006 May;94(10):1460–4.
- 7 Day JCC, Bennett R, Smith B, Kendall C, Hutchings J, Meaden GM, et al. A miniature confocal Raman probe for endoscopic use. *Phys Med Biol*. 2009 Dec;54(23):7077–87.
- 8 Hattori Y, Komachi Y, Asakura T, Shimosegawa T, Kanai G-I, Tashiro H, et al. In vivo Raman study of the living rat esophagus and stomach using a micro-Raman probe under an endoscope. *Appl Spectrosc*. 2007 Jun;61(6):579–84.
- 9 Huang Z, Teh SK, Zheng W, Mo J, Lin K, Shao X, et al. Integrated Raman spectroscopy and trimodal wide-field imaging techniques for real-time in vivo tissue Raman measurements at endoscopy. *Opt Lett*. 2009 Mar;34(6):758–60.
- 10 Mahadevan-Jansen A, Mitchell MF, Ramanujam N, Utzinger U, Richards-Kortum R. Development of a fiber optic probe to measure NIR Raman spectra of cervical tissue in vivo. *Photochem Photobiol*. 1998 Sep;68(3):427–31.
- 11 Mo J, Zheng W, Low JJH, Ng J, Ilancheran A, Huang Z. High wavenumber Raman spectroscopy for in vivo detection of cervical dysplasia. *Anal Chem*. 2009 Nov;81(21):8908–15.
- 12 Motz JT, Hunter M, Galindo LH, Gardecki JA, Kramer JR, Dasari RR, et al. Optical fiber probe for biomedical Raman spectroscopy. *Appl Opt*. 2004 Jan;43(3):542–54.
- 13 Shim MG, Wilson BC, Marple E, Wach M. Study of Fiber-Optic Probes for in vivo Medical Raman spectroscopy. *Appl Spectrosc*. 1999 Jun;53(6):619–27.
- 14 Marple ET. Filtered fiber optic probe. 2012 May [cited 2023 Apr 19]. Available from: <https://patents.google.com/patent/US8175423B2/en>
- 15 Di Ninni P, Martelli F, Zaccanti G. Effect of dependent scattering on the optical properties of Intralipid tissue phantoms. *Biomed Opt Express*. 2011 Aug;2(8):2265–78.
- 16 Ninni PD, Martelli F, Zaccanti G. Intralipid: towards a diffusive reference standard for optical tissue phantoms. *Phys Med Biol*. 2011 Jan;56(2):N21–28.
- 17 Thompson CA, Reynolds JS, Webb KJ, Laplant FP, Ben-Amotz D. Raman spectroscopic studies of diamond in Intralipid. *Opt Lett*. 1995 May;20(10):1195–7.

- 18 van Staveren HJ, Moes CJ, van Marie J, Prah SA, van Gemert MJ. Light scattering in Intralipid-10% in the wavelength range of 400-1100 nm. *Appl Opt.* 1991 Nov;30(31):4507-14.
- 19 Lieber CA, Mahadevan-Jansen A. Automated method for subtraction of fluorescence from biological Raman spectra. *Appl Spectrosc.* 2003 Nov;57(11):1363-7.
- 20 John Wiley & Sons, Ltd. Signal-to-Noise in Raman spectroscopy. *Raman spectroscopy for Chemical Analysis.* 2000; pp 49-71.
- 21 Mo J, Zheng W, Huang Z. Fiber-optic Raman probe couples ball lens for depth-selected Raman measurements of epithelial tissue. *Biomed Opt Express.* 2010 Jun;1(1):17-30.
- 22 Wang J, Bergholt MS, Zheng W, Huang Z. Development of a beveled fiber-optic confocal Raman probe for enhancing in vivo epithelial tissue Raman measurements at endoscopy. *Opt Lett.* 2013 Jul;38(13):2321-3.
- 23 Shim MG, Wilson BC. Development of an In Vivo Raman Spectroscopic System for Diagnostic Applications. *Journal of Raman spectroscopy.* 1997 Feb;28(2-3):131-42.





CHAPTER 3

IN VIVO RAMAN SPECTROSCOPY FOR BLADDER CANCER DETECTION USING A SUPERFICIAL RAMAN PROBE COMPARED TO A NONSUPERFICIAL RAMAN PROBE

Stomp-Agenant M
van Dijk T
Onur A
Grimbergen M
van Melick H
Jonges T
Bosch R
van Swol C

J Biophotonics. 2022 Jun;15(6)

ABSTRACT

Raman spectroscopy is promising as a non-invasive tool for cancer diagnosis. A superficial Raman probe might improve classification of bladder cancer, because information is gained solely from the diseased tissue and irrelevant information from deeper layers is omitted. We compared Raman measurements of a superficial to a non-superficial probe, in bladder cancer diagnosis. Two hundred sixteen Raman measurements and biopsies were taken in vivo from at least one suspicious and one unsuspecting bladder location in 104 patients. A Raman classification model was constructed based on histopathology, using a Principal-Component fed Linear-Discriminant-Analysis and Leave-one-person-out cross-validation. The diagnostic ability measured in Area Under the Receiver Operating Characteristics Curve, was 0.95 and 0.80, the sensitivity was 90% and 85% and the specificity was 87% and 88% for the superficial and the non-superficial probe, respectively. We found inflammation to be a confounder and also an indication of a gradual transition from benign to low-grade to high-grade urothelial carcinoma. Raman spectroscopy provides additional information to histopathology, and the use of a superficial probe the diagnostic value.

INTRODUCTION

Bladder cancer is the tenth most common malignancy worldwide [1,2], and urothelial carcinoma is the most prominent subtype. Generally, detection of bladder cancer is performed using white light cystoscopy, which has a limited sensitivity (62-82%) and specificity (43-98%) [3–5]. Subsequently, transurethral resection of a bladder tumor (TURBT) using white light cystoscopy is performed for pathologic assessment, but it is also therapeutic. Because recurrence and progression rates are high, up to 55% after non-muscle-invasive bladder cancer (NMIBC) resection, patients are being exposed to an extensive follow-up program [6]. Recurrence and progression could result from tumor residual after incomplete resection, or from malignant tissue that was not recognized as such, as occurs with flat lesions like carcinoma in situ (CIS).

To improve urothelial carcinoma detection and to avoid residual tumor after resection, novel diagnostic techniques are being investigated and some have been recently implemented. Photodynamic diagnosis (fluorescence cystoscopy) has been introduced supplementing white light cystoscopy during TURBT. This optical technique enhances the contrast between benign and malignant tissue using violet-blue light after pre-operative instillation of the bladder with a photosensitive dye. Photodynamic diagnosis has a sensitivity of 92%, compared to 71% of white light cystoscopy alone [7]. This technique offers improved tumor detection, resulting in reduced residual tumor rates after TURBT and superior detection of CIS compared to white light cystoscopy. However, photodynamic diagnosis has a limited specificity that leads to up to 26% false positive biopsies [7]. This results in unnecessary tissue resection, stress to the patient with a burden of unnecessary care and corresponding complications. Therefore, a more specific diagnostic optical technique could improve the overall diagnostic value.

Raman spectroscopy is a well-established, highly specific optical technique that allows biochemical cancer diagnosis in various organs, without removing any tissue [8–15]. This technique is based on an inelastic interaction of monochromatic light photons with molecular bonds of biological tissue. As a consequence, the scattered photons are frequency-shifted. The frequency shift depends on the particular molecular bond that the photons interact with. By obtaining a spectrum of these frequency-shifted photons, a distinct biochemical fingerprint is acquired. It makes label free biochemical identification possible.

There are several publications describing Raman spectroscopy in bladder cancer diagnosis [16–18]. Chen et al. showed that it is possible to identify and characterize bladder cancer by a fiber-optic Raman probe ex vivo in 32 bladder tissue samples [19].

Our group previously reported results of using a Raman system in vivo during clinical practice for bladder cancer diagnosis [20,21]. We used a non-superficial Raman probe, that collected spectra from multiple tissue layers, i.e., high volume, and reached a sensitivity of 85% and specificity of 79% [10]. It was hypothesized that the sensitivity and specificity for bladder cancer detection and grading ability would increase if a superficial Raman probe would be used, because information is gained solely from interaction of photons in the superficial diseased tissue and irrelevant information from deeper layers is omitted. Ideally, the sampled volume should match the volume of the investigated tissue layer. Therefore, a measuring depth of 0-200 μm would be adequate for NMIBC diagnosis, as the thickness of benign urothelial tissue is 3-7 cell layers thick (100-200 μm) covering an underlying stromal tissue layer that yields minimal information. In a phantom study, we demonstrated the feasibility of a clinical superficial Raman probe with a measuring depth of 0-200 μm [22]. Other groups also have published results on confocal Raman probes [23,24].

In this study we calculated the Area Under the Receiver Operating Characteristic Curve (AUROCC), sensitivity and specificity of urothelial carcinoma detection and grading in vivo, using the superficial probe measurements compared to the non-superficial probe measurements with the Raman setup used in the previous study [10]. We also present the in vivo signal-to-noise ratio differences of these probes. Furthermore, we investigate the confounding influence on the classification of inflammation of the tissue. Finally, we present the gradual progression from benign to low-grade and high-grade in the principal component space.

MATERIALS AND METHODS

Data collection was conducted at the St. Antonius Hospital, the Netherlands. Ethical approval was obtained to perform in vivo Raman measurements from suspicious bladder lesions and locations not suspect for malignancy before biopsy/resection (MREC UMC Utrecht). Informed consent was obtained from all patients. The data processing algorithms were developed in GNU octave version 6.1.0. [25].

Patient inclusion

Patients of at least 18 years old with a scheduled TURBT were included after informed consent, from March 2013 until December 2014. Patients with excessive hematuria, that hindered direct visualization of lesions during the procedure, were excluded.

Sixty-six new patients (156 unique biopsy sites) were included in this study alongside 38 patients (60 unique biopsy sites) from the dataset of Draga et al. [10].

Raman system

The used Raman system has been described by Draga et al.[10]. The system consists of a 785 nm diode laser (DFB-0785-1000, Sacher Lasertechnik, Marburg, Germany), a spectrograph (HoloSpec Imaging Spectrograph fl1.8i (HSG-785-LF), Kaiser Optical Systems, Ecully, France), a charge-coupled device camera (PIXIS 256 BRDD, Princeton Instruments, Trenton, New Jersey, USA), a personal computer and a superficial and non-superficial probe (EmVision LLC, Loxahatchee, Florida, USA) that have been described by Agenant et al. [22]. The non-superficial Raman probe is a standard fiber bundle style probe with collection fibers surrounding an excitation fiber. The superficial probe uses the same external dimensions, however to enable sampling of a superficial layer, an overlap of focus of the excitation beam and collection region is created by a convergent lens as is shown in figure 1.

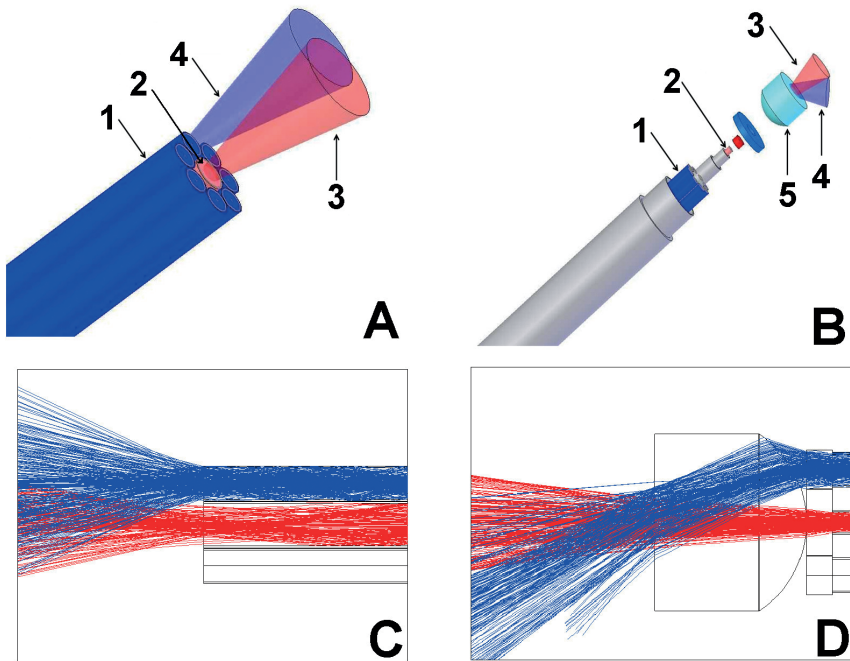


Figure 1. Top left (A) and right (B) are exploded views of the distal probe tip of the non-superficial and superficial Raman probe with a sampling depth of $300\mu\text{m}$ and $200\mu\text{m}$, respectively. The Raman laser excitation region and the direction of the Raman collection cone(s) create an overlap with the laser cone at the surface of the lens and is illustrated for the non-superficial Raman probe (A) and the superficial Raman probe (B). (1 = collection fibers, 2 = excitation fiber, 3 = Raman laser cone, 4 = Raman collection cone, 5 = convergent lens). Bottom left (C) and right (D) are Zemax traces by EMVISION of the non-superficial and superficial Raman probe using the refractive index of water, respectively [22].

Raman spectroscopy procedures

In the operating room, a white light cystoscopy was performed and the location and number of lesions was determined. Subsequently, a Raman measurement and a tissue biopsy of one to four locations suspect for malignancy were performed as well as from one normal appearing location from the posterior bladder wall.

During the procedure, the Raman probe and the biopsy forceps were advanced parallel to each other through an angled cystoscope, into the bladder. After minimizing the ambient light and, disconnecting the light cable, the Raman probe was placed in gentle contact to the lesion for a Raman measurement (10 consecutive spectra with an acquisition time of 500 ms each). After this, the light cable was reconnected and a corresponding biopsy was taken. Each biopsy was separately fixated in formalin and sent for pathology analysis as in standard care. After the patient left the operating room, the calibration measurements were performed in the same lighting conditions as the *in vivo* measurements. All biopsies were evaluated using the WHO 2004 classification system for malignancy grading of bladder cancer, by a pathologist specialized in uro-oncology (G.N. Jonges).

Spectra exclusion and pre-processing

Spectra of biopsy samples that could not be classified by the pathologist due to limited or damaged tissue were excluded. Some spectra were excluded due to saturation of the CCD camera. After excluding these spectra, 5-10 spectra were included per biopsy location. Depending on the number of remaining spectra there was a difference in acquisition time. To correct for this inequality in total acquisition time, the spectra per biopsy specimen were summed and divided by their total acquisition time. The Raman signal was collected in the 400-1800 cm^{-1} spectral region with spectral resolution of 4 cm^{-1} . Using Raman measurements of specific calibration substances, the spectra were calibrated: spectral dispersion of the detection system was corrected using a neon-argon light, standardization of the Raman shift axis was performed using acetaminophen.

The following preprocessing steps were executed in order:

1. Calibrate wavelengths
2. Reject overexposed spectra
3. Sum spectra at each tissue sample/biopsy
4. Separate noise with Savitsky-Golay filter (order 3, frame length 13)
5. Normalize measurement by exposure time
6. Subtract autofluorescence [26]
7. Divide by total autofluorescence
8. Perform extended multiplicative scatter correction (EMSC) [27]

Signal-to-noise ratio

To determine signal-to-noise-ratio we separated the measured spectrum in a Raman signal component and a noise component (step 4 of preprocessing). First, we obtained the Raman signal by applying a digital filter to smooth the measurement data (Savitzky-Golay filter, order 3, width 13 points, or 18.2 wavenumbers). Then, we took the noise to be the absolute value of the difference between this Raman component and the measured spectrum. For a given spectrum we defined the signal-to-noise ratio as the sum over wavenumbers of the Raman signal, divided by the sum over wavenumbers of the noise. We have verified that the noise obtained in this manner is proportional to the square root of the fluorescence signal, which is characteristic of photon shot noise. To compare SNR between measurements with differing acquisition times we made a correction by dividing by the square root of the acquisition time.

Classification

For the classification we excluded all biopsies that contained inflammation to enable comparison to the dataset of Draga et al., as we only had access to the biopsies of Draga et al. that do not contain inflammation. The preprocessed data were used to train a diagnostic classification model. The diagnostic classification model was based on the Principal-Component fed Linear-Discriminant-Analysis (PCA/LDA) as described by Crow et al. [9]. To reduce the class imbalance, synthetic minority oversampling (SMOTE) was applied [28]. A classification is an average over 10 runs with SMOTE. A leave-one-person-out cross-validation model was used. As a performance metric the AUROCC is reported. The number of principal components was obtained by optimizing the AUROCC. Using the optimized number of principal components we repeated the classification 100 times. This resulted in a mean and standard deviation of the sensitivity and specificity and AUROCC as performance metrics, generated from 100 confusion matrices.

RESULTS & DISCUSSION

Patient characteristics

Spectra were taken from 156 unique biopsy locations, in 66 patients. The patient and pathologic characteristics are described in table 1 and are equally distributed in each pathology groups. Due to saturation, 15 out of 1560 spectra were excluded, which resulted in 1445 spectra of 156 biopsy locations. We excluded biopsies that contained inflammation according to the histopathologic analysis resulting in 57 non-inflamed biopsies and performed the same 5 preprocessing steps and analysis on their data [10].



Table 1. Patient and pathology characteristics. In the non-superficial data set, information about tumor grade and whether the tissue was suspected for malignancy was not documented and is therefore absent.

Patient parameters	Superficial probe data set	Superficial probe data set excluding inflammation	Non-superficial data set
Number of included patients	66	37	38
Number of Biopsies/Raman Measurements	156	57	60
Mean age (years)	64.6	64.8	70
Pathology groups			
Benign	109	38	28
Benign not suspect for malignancy	58	29	-
Benign suspect for malignancy	51	9	-
Malignancy	47	19	32
Low grade malignancy	25	11	-
High grade malignancy + CIS	17 + 5	8	-

Signal-to-noise ratio

The median signal-to-noise ratio of all Raman spectra (benign and malignant together, including inflammation) for the superficial probe was 12.5, compared to 6.5 for the non-superficial probe, an increase with a factor 1.92 (figure 2).

Classification

The average spectra of the three pathological groups are presented in figure 3. Specific band intensities that differed between pathology groups are more clearly shown in figure 4. This figure presents the difference spectra of two out of the three determined pathology groups. Figure 3 and 4 show bands that might be able to distinguish benign from malignant tissue, such as at 492, 1082, 1264, 1304 and 1444 cm^{-1} . Also, high-grade urothelial carcinoma could be distinguished from benign or low-grade urothelial carcinoma e.g. at the 1656 cm^{-1} band, which might be valuable in the classifier to distinguish the three pathology groups from each other. Nevertheless, the difference between low-grade and high-grade urothelial carcinoma is limited as is shown in figure 4.

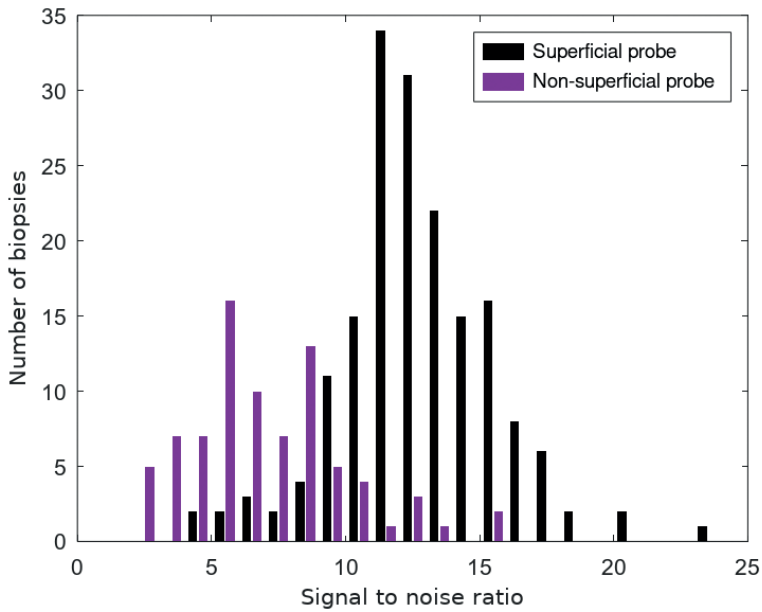


Figure 2. Histogram of signal-to-noise ratio of the superficial and non-superficial probe. The determined signal-to-noise ratios are set against the number of Raman spectra (after preprocessing).

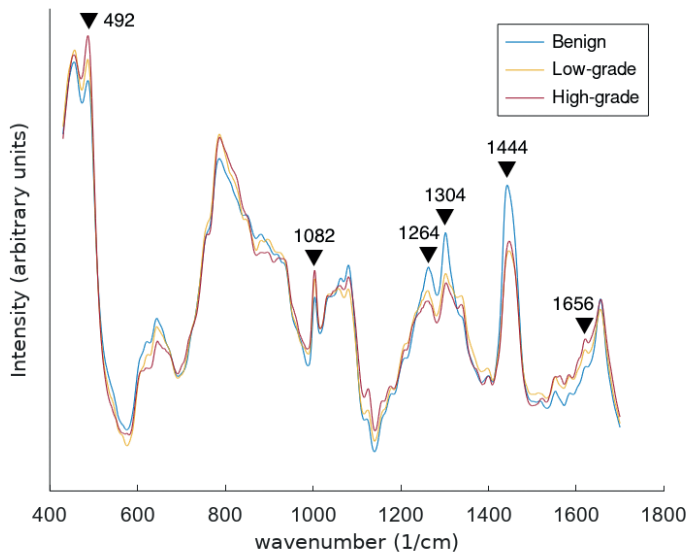


Figure 3. Mean Raman spectra of each pathology group of the superficial probe (inflammation excluded).



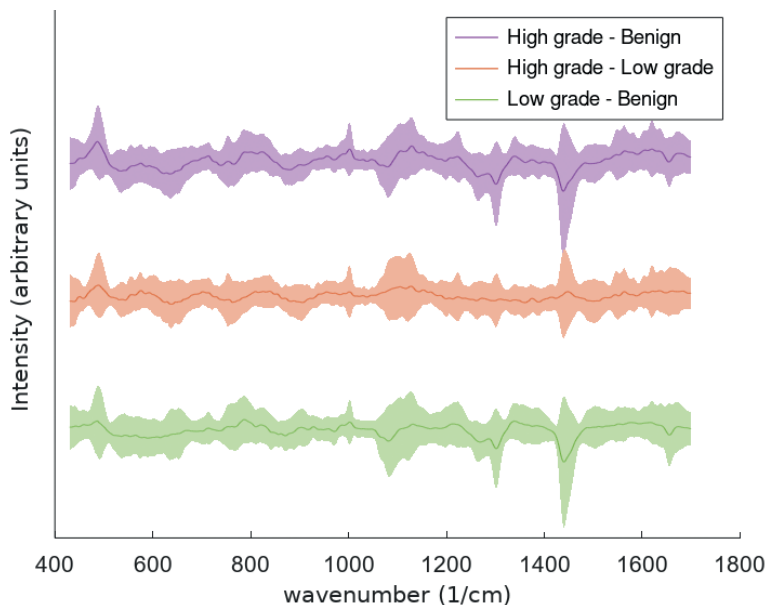


Figure 4. Difference of mean spectra and the standard deviation between every 2 pathology groups (inflammation excluded): (green) low-grade minus benign, (orange) high-grade minus low-grade and (purple) high-grade minus benign.

Analysis

After the preprocessing, PCA was implemented for dimensional reduction of the datasets of the superficial and non-superficial Raman probes, separately. Our dataset consisted of superficial Raman spectra of 156 biopsy locations. The dataset from the previous study (Draga et al.) consisted of non-superficial Raman spectra of 60 biopsy locations that were dimensionally reduced using principal components. The number of principal components was chosen to optimize the AUROCC of the classification model per measurement set, to enable probe comparing.

The confusion matrices after the linear discriminant analysis and the leave-one-person-out cross validation of both probes are presented in table 2. The sensitivity, specificity and AUROCC for the superficial probe was 90% ($\pm 4\%$), 87% ($\pm 4\%$) and 0,95 (± 0.01), and for the non-superficial probe 80% ($\pm 2\%$), 85% ($\pm 3\%$) and 0.88 (± 0.01), respectively. The number of principal components necessary to optimize the AUROCC was 18 for the non-superficial probe and 10 for the superficial probe. For correct comparison of our clinical study to the clinical study of Draga et al. the same exclusion criteria and preprocessing was used on both data sets. As a consequence, slightly different values are reported compared to the ones published by Draga et al. [10].

Table 2. Mean and standard deviation over 100 confusion matrices using the optimized number of PC's for leave-one-person out cross-validation of logistic regression-based Raman decision algorithm compared to the histopathologic assessment which is the "gold standard" describing benign and malignant tissue for the superficial probe and the non-superficial probe, excluding inflamed biopsies.

			Histopathology ("gold standard")	
			Malignant	Benign
Raman spectroscopy	Superficial probe	Malignant	17.2 ± 0.7	5.1 ± 1.4
		Benign	1.8 ± 0.7	32.9 ± 1.4
		AUOCC: 0.95 ± 0.01	Sensitivity: 90% ± 4%	Specificity: 87% ± 4%
	Non-superficial probe	Malignant	25.5 ± 0.6	4.1 ± 0.9
		Benign	6.5 ± 0.6	23.9 ± 0.9
		AUOCC: 0.88 ± 0.01	Sensitivity: 80% ± 2%	Specificity: 85% ± 3%

Figure 5 presents the ROC curve of the superficial and non-superficial Raman probe (compared to Random 1). The area under the curve of the superficial and non-superficial probe is 0.95 and 0.88, respectively. This indicates that the performance of the superficial probe is better than the non-superficial probe. In addition, the ROC curve of the superficial probe with inflammation in the biopsy is shown. In this situation the performance of the probe is reduced which could be explained by different Raman signals that will be obtained from an inflamed biopsy location, as a range of different cells that will be present in an ongoing inflammation. Nevertheless, as inflammatory cells will be present as a reaction of the immune system to a tumor, this might be unavoidable and it would be better to include the inflamed biopsy locations. Maybe, the amount of inflammation could be prognostic for the progression of the tumor or the response to immune therapy, which is under development by others. More research will be needed to evaluate this.

Finally, we performed the PCA-LDA analysis with leave-one-out cross validation for the three pathology groups; benign, low-grade and high-grade urothelial carcinoma. In this analysis only 2 PC's were used. The confusion matrix is listed in table 3 and the total accuracy was 63%. The biopsies that contained CIS were limited in number and therefore we combined them with the high-grade urothelial carcinoma because CIS shows high-grade histopathological characteristics.

Unfortunately, it was not possible to compare the probe performance for grading between both probes precisely, as the data of Draga et al. was pathologically assessed using the WHO 1997 grading classification in grade 1, 2 and 3, as opposed to the assessment in the current study, using the 2004 WHO grading classification in low-grade and high-grade urothelial carcinoma.



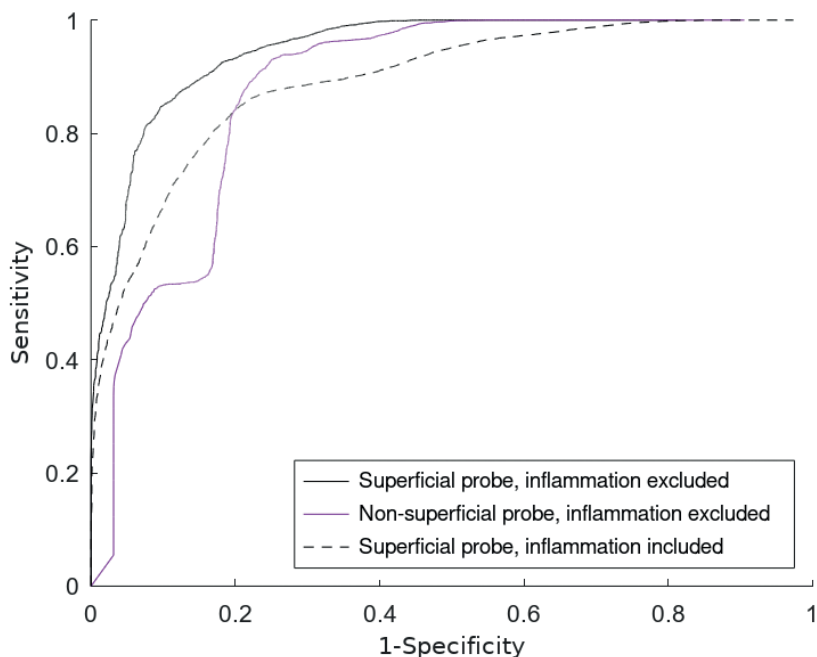


Figure 5. ROC curve of the diagnostic accuracy for the superficial and non-superficial Raman probe.

Table 3. Confusion matrix for leave-one out cross-validation of logistic regression-based Raman decision algorithm compared to the histopathologic assessment which is the “gold standard” describing benign urothelium, low-grade urothelial carcinoma and high-grade urothelial carcinoma, resulting in an accuracy of 59%. The numbers are calculated from the database without inflammation, and in parentheses are the numbers including biopsies that contained inflammation.

		Histopathology (“gold standard”)		
		Benign	Low-grade	High-grade
Raman spectroscopy	Benign	22.3 (59.0)	1.2 (3.7)	0.7(3.9)
	Low-grade	10.3 (24.7)	5.4 (9.1)	1.3 (4.6)
	High-grade	5.4 (25.3)	4.4 (12.2)	6.0 (13.5)

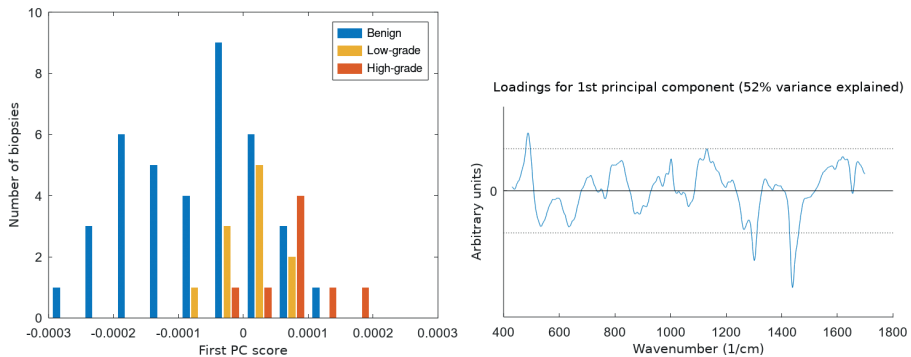


Figure 6. The left part shows a histogram, representing the separation of the 3 classes (excluding inflammation) along the first principal component (for the ternary classification excluding infections). It indicates that progressive evolution from benign to low-grade to high-grade urothelial carcinoma is contained in the Raman spectra. The right part of the figure shows the loadings for the 1st principal component.

The limited accuracy is due to the small differences between the low-grade and high-grade urothelial carcinoma spectra that could be explained by the relevant differences, which may cover just a small percentage of the total signal and may therefore not always come to light. Alternatively, there might be a sampling error in the measurement because only a small volume of the tumor is sampled by the Raman probe. This small volume might not be of the highest grade in the total lesion that has been biopsied because a tumor can be heterogeneous. Another hypothesis is that the small difference might be explained by a distribution of molecular biochemical characteristics within one pathology group. In our opinion, there is no clear biochemical cut-off value between low-grade and high-grade urothelial carcinoma, but it is probably a continuum of malignant biochemical characteristics that gradually increase when becoming more malignant in the development of urothelial carcinoma. Figure 6 indicates this progressive evolution from benign to low-grade to high-grade urothelial carcinoma. This progressive trend in Raman signal from benign to low-grade to high grade urothelial carcinoma was also proposed by Chen et al. [19]. If there is a gradual change, this might explain the high inter- and intra-observer variability of the histopathologic assessment [29]. Raman spectroscopy measures quantitative biochemical changes as opposed to histopathologic analysis, which assesses morphologic and histopathologic differences. Maybe the poor reproducibility of the histopathologic analysis could be solved using Raman spectroscopy. To empower this hypothesis, future research should be performed using Raman spectroscopy in a higher resolution and larger data set, to develop an improved diagnostic algorithm.

CONCLUSION

This study investigated the in vivo clinical potential of our superficial probe in diagnosis of NMIBC. The signal-to-noise ratio was improved with a factor 1.92, compared to the non-superficial probe, used by Draga et al. [10]. This is a confirmation our group's earlier phantom model results with this new probe [22]. The sensitivity, specificity and AUROCC for the superficial probe were 90%, 87% and 0.95, and for the non-superficial probe 80%, 85% and 0.88, respectively in discriminating benign from malignant tissue. Therefore, the performance of the superficial probe is superior to the non-superficial probe. This might be due to the improved signal-to-noise ratio. However, we think that the decreased measuring depth of the probe is also responsible, as the tissue information is expected to be solely from the diseased depth and deeper unaffected tissue do not cloud the result. We have not been able to quantify this yet. As a next step, it would be interesting to link our Raman shift findings at specific wavenumbers and to its biochemical bonds where the Raman signals originates from. We also found an indication that there exists a progressive evolution from benign to low-grade to high-grade UC. Tissue inflammation leads to a worse classification performance, but cannot be excluded as the immune system responds with inflammation to tumor development.

Further research needs to be performed to differentiate low-grade from high-grade urothelial carcinoma. In our opinion, the transition between benign, low-grade and high-grade urothelial carcinoma in different patients should be evaluated with a higher spatial resolution, e.g., ex vivo in cystectomy specimens over a grid of locations, generating a larger data set. This will provide us with more information about the biochemical nature of the malignancy leading to an improved diagnostic algorithm for Raman spectroscopy.

ACKNOWLEDGEMENTS

Eric Marple for probe production and Olivier Wegelin for measuring Raman spectra.

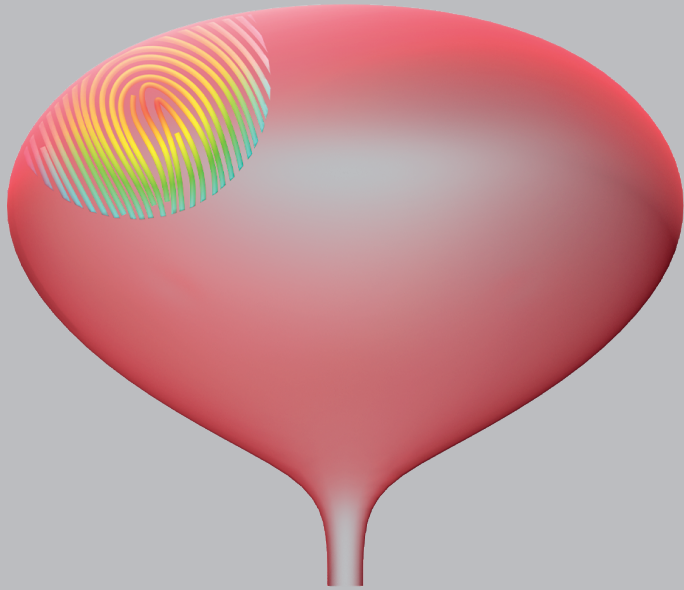
REFERENCES

- 1 Antoni S, Ferlay J, Soerjomataram I, Znaor A, Jemal A, Bray F. Bladder Cancer Incidence and Mortality: A Global Overview and Recent Trends. *Eur Urol.* 2017;71(1):96–108.
- 2 Cumberbatch MGK, Jubber I, Black PC, Esperto F, Figueroa JD, Kamat AM, et al. Epidemiology of Bladder Cancer: A Systematic Review and Contemporary Update of Risk Factors in 2018. *Eur Urol.* 2018 Dec;74(6):784–95.
- 3 Brunckhorst O, Ong QJ, Elson D, Mayer E. Novel real-time optical imaging modalities for the detection of neoplastic lesions in urology: a systematic review. *Surg Endosc.* 2018 Nov DOI: 10.1007/s00464-018-6578-1
- 4 Cauberg Evelyne CC, de la Rosette JJMCH, de Reijke TM. Emerging optical techniques in advanced cystoscopy for bladder cancer diagnosis: A review of the current literature. *Indian J Urol.* 2011 Apr;27(2):245–51.
- 5 Jocham D, Stepp H, Waidelich R. Photodynamic Diagnosis in Urology: State-of-the-Art. *European Urology.* 2008 Jun;53(6):1138–50.
- 6 Babjuk M, Burger M, Comperat E, Gontero P, Liedberg F. EAU guidelines on Non-muscle-invasive Bladder Cancer (TaT1 and CIS). 2021 Apr Available from: <https://uroweb.org/wp-content/uploads/EAU-Guidelines-on-Non-muscle-invasive-Bladder-Cancer-TaT1-2021V2.pdf>
- 7 Rink M, Babjuk M, Catto JWF, Jichlinski P, Shariat SF, Stenzl A, et al. Hexyl aminolevulinic acid-guided fluorescence cystoscopy in the diagnosis and follow-up of patients with non-muscle-invasive bladder cancer: a critical review of the current literature. *Eur Urol.* 2013 Oct;64(4):624–38.
- 8 Bergholt MS, Zheng W, Lin K, Ho KY, Teh M, Yeoh KG, et al. In vivo diagnosis of gastric cancer using Raman endoscopy and ant colony optimization techniques. *Int J Cancer.* 2011 Jun;128(11):2673–80.
- 9 Crow P, Uff JS, Farmer JA, Wright MP, Stone N. The use of Raman spectroscopy to identify and characterize transitional cell carcinoma in vitro. *BJU Int.* 2004 Jun;93(9):1232–6.
- 10 Draga ROP, Grimbergen MCM, Vijverberg PLM, van Swol CFP, Jonges TGN, Kummer JA, et al. In vivo bladder cancer diagnosis by high-volume Raman spectroscopy. *Anal Chem.* 2010 Jul;82(14):5993–9.
- 11 Kanter EM, Vargis E, Majumder S, Keller MD, Woeste E, Rao GG, et al. Application of Raman spectroscopy for cervical dysplasia diagnosis. *J Biophotonics.* 2009 Feb;2(1–2):81–90.
- 12 Molckovsky A, Song L-MWK, Shim MG, Marcon NE, Wilson BC. Diagnostic potential of near-infrared Raman spectroscopy in the colon: differentiating adenomatous from hyperplastic polyps. *Gastrointest Endosc.* 2003 Mar;57(3):396–402.
- 13 Shim MG, Wilson BC, Marple E, Wach M. Study of Fiber-Optic Probes for in vivo Medical Raman spectroscopy. *Appl Spectrosc.* 1999 Jun;53(6):619–27.
- 14 Song JH, Francis IR, Platt JF, Cohan RH, Mohsin J, Kielb SJ, et al. Bladder tumor detection at virtual cystoscopy. *Radiology.* 2001 Jan;218(1):95–100.
- 15 Stone N, Kendall C, Smith J, Crow P, Barr H. Raman spectroscopy for identification of epithelial cancers. *Faraday Discuss.* 2004;126:141–57; discussion 169-183.



- 16 de Jong BWD, Bakker Schut TC, Wolffenbuttel KP, Nijman JM, Kok DJ, Puppels GJ. Identification of Bladder Wall Layers by Raman spectroscopy. *J Urol*. 2002 Oct;168(4 Pt 2):1771–8.
- 17 Stone N, Hart Prieto MC, Crow P, Uff J, Ritchie AW. The use of Raman spectroscopy to provide an estimation of the gross biochemistry associated with urological pathologies. *Anal Bioanal Chem*. 2007 Mar;387(5):1657–68.
- 18 Cordero E, Ruger J, Marti D, Mondol AS, Hasselager T, Mogensen K, et al. Bladder tissue characterization using probe-based Raman spectroscopy: Evaluation of tissue heterogeneity and influence on the model prediction. *J Biophotonics*. 2020 Feb;13(2):e201960025.
- 19 Chen H, Li X, Broderick N, Liu Y, Zhou Y, Han J, et al. Identification and characterization of bladder cancer by low-resolution fiber-optic Raman spectroscopy. *J Biophotonics*. 2018 Sep;11(9):e201800016.
- 20 Draga ROP, Grimbergen MCM, Kok ET, Jonges TN, van Swol CFP, Bosch R, et al. The quality of 5-aminolevulinic acid-induced photodynamic diagnosis and transurethral resection of bladder tumors: does the urologist play a role? *Urol Int*. 2012;89(3):326–31.
- 21 Grimbergen MCM, van Swol CFP, van Moorselaar RJA, Uff J, Mahadevan-Jansen A, Stone N. Raman spectroscopy of bladder tissue in the presence of 5-aminolevulinic acid. *J Photochem Photobiol B, Biol*. 2009 Jun;95(3):170–6.
- 22 Agenant M, Grimbergen M, Draga R, Marple E, Bosch R, van Swol C. Clinical superficial Raman probe aimed for epithelial tumor detection: Phantom model results. *Biomed Opt Express*. 2014 Apr;5(4):1203–16.
- 23 Day JCC, Bennett R, Smith B, Kendall C, Hutchings J, Meaden GM, et al. A miniature confocal Raman probe for endoscopic use. *Phys Med Biol*. 2009 Dec;54(23):7077–87.
- 24 Latka I, Dochow S, Krafft C, Dietzek B, Popp J. Fiber optic probes for linear and nonlinear Raman applications - Current trends and future development: Fiber optic Raman probes. *Laser & Photonics Reviews*. 2013 Sep;7(5):698–731.
- 25 Eaton JW, Bateman D, Hauberg S, Wehbring R. GNU Octave version 6.1.0 manual: a high-level interactive language for numerical computations. 2020 Available from: <https://www.gnu.org/software/octave/doc/v6.1.0/>
- 26 Lieber CA, Mahadevan-Jansen A. Automated method for subtraction of fluorescence from biological Raman spectra. *Appl Spectrosc*. 2003 Nov;57(11):1363–7.
- 27 Martens H, Stark E. Extended multiplicative signal correction and spectral interference subtraction: New preprocessing methods for near infrared spectroscopy. *Journal of Pharmaceutical and Biomedical Analysis*. 1991 Jan;9(8):625–35.
- 28 Chawla NV, Bowyer KW, Hall LO, Kegelmeyer WP. SMOTE: Synthetic Minority Over-sampling Technique. *Journal of Artificial Intelligence Research*. 2002 Jun;16:321–57.
- 29 Tosoni I, Wagner U, Sauter G, Egloff M, Knonagel H, Alund G, et al. Clinical significance of interobserver differences in the staging and grading of superficial bladder cancer. *BJU Int*. 2000 Jan;85(1):48–53.





CHAPTER 4

RAMAN SPECTROSCOPY IN THE EVALUATION OF TISSUE SURROUNDING MALIGNANCY IN RADICAL CYSTECTOMY SPECIMENS

Stomp-Agenant M*
ten Dam A*
Onur A
Jonges G
Bosch J
van Dijk T

*Both authors contributed equally

Submitted: Biomedical Optics Express

ABSTRACT

Purpose

To investigate spatial urothelial carcinoma (UC) distribution in cystectomy specimens by Raman spectroscopy. We focus on regions surrounding malignant tissue, to enable accurate resection during transurethral resection of a bladder tumor.

Materials & method

Raman measurements and pathologic evaluation were performed throughout the urothelial surface of 3 cystectomy specimens. The sensitivity, specificity and area under the curve (AUC) were projected onto 2D Raman-maps. Finally, we present the malignancy distribution with different probability thresholds for classification as being malignant.

Results

The sensitivity, specificity and AUC were 93%, 86% and 92%, respectively. A gradual spatial transition from *benign* to *malignant* was observed, which could be explained by tissue heterogeneity and/or a biochemical transition into malignancy.

Conclusion

Spatially applied Raman spectroscopy gives insight in the spatial UC distribution. Detection of transition into malignancy might lead to more accurate resections, less residuals and/or lower recurrence rates of bladder malignancy after TURBT.

INTRODUCTION

Bladder cancer is worldwide the ninth most frequently diagnosed malignancy [1]. When a malignancy is suspected during white light cystoscopy of the bladder, a transurethral resection of a bladder tumor (TURBT) is performed to enable pathological evaluation of the suspected tissue. Urothelial carcinoma (UC) of the bladder is known to have high recurrence and progression rates, up to 15-70% and 7-40%, respectively [2,3]. To minimize those rates, early detection, adequate treatment including complete resection and intensive monitoring is essential. New techniques have been implemented clinically to reduce the amount of recurrence. Examples are a single post-operative intravesical instillation of chemotherapy in low-grade UC that reduces the risk of recurrence by 35% [4]. Another example is photodynamic diagnosis (PDD), which has been proven to increase the sensitivity of white light cystoscopy from 62-82% to 79-100% [5-8]. Despite these measures, recurrences are frequent. Previous studies have shown heterogeneity of malignant tissue [9,10]. We hypothesize that pathologically determined benign tissue surrounding a malignancy, might be heterogeneous as well and/or partially (pre-)malignant, while these changes are yet unrecognized as such by the pathologist. Thus, tumor margins might be wider than optically visible; and not recognizing these might lead to inadequate resections during TURBT and recurrences. Accordingly, new techniques are required to evaluate the tumor margins adequately to improve the quality of bladder tumor resection, such as clinically applied Raman spectroscopy.

Raman spectroscopy is an optical technique that uses molecular-specific, inelastic scattering of light photons to interrogate biological tissues [11]. When tissue is illuminated by laser light, photons interact with the intramolecular bonds. The photon then donates energy to, or receives energy from the bond. This leads to a change in the bond's vibrational state. When it subsequently exits the tissue, the photon has an altered energy level, hence a different wavelength compared to the original laser light. This wavelength change is called a Raman shift. Raman peaks in many cases can be associated with the specific vibration of a particular chemical bond in a molecule. Thus, Raman spectroscopy is a molecular specific technique that can be used as a biochemical tool for study of various materials [12]. It has shown a high sensitivity and specificity in tumor detection in various tissues [13-17]. Raman spectroscopy could be used to generate an "optical non-invasive biopsy" that represents the chemical composition of biological tissue. Raman spectroscopy has been investigated in bladder UC both ex vivo and in vivo [18-25]. In some studies, microscopic Raman was applied spatially to generate 2-dimensional (2D) map of healthy and malignant bladder tissue [9,20]. Using Raman, De Jong, et al. presented the chemical composition of different bladder layers from a frozen section compared to its pathological assessment [21]. In 2D-maps from

microscopic Raman measurements, Cordero, et al. showed that some malignant tumors are molecularly heterogeneous [9].

In this study, we investigate tissue heterogeneity surrounding malignant bladder tissue using Raman spectroscopy and pathologic evaluation (gold standard) in three cystectomy specimens. We provide a detailed description of the used data processing and classification model. Sensitivity, specificity and Area-Under-the-Curve (AUC) were calculated as performances metrics. We present 2D-maps of all cystectomy specimens according to different analysis: pathologic assessment and Raman classifier output (prediction) and Raman probability. Finally, we present the Raman prediction per location for decreasing the malignancy thresholds to evaluate whether changing the threshold could eventually lead to a more accurate resection.

MATERIALS & METHOD

The data used in this study was collected at the University Medical Center Utrecht, The Netherlands. Ethical approval was obtained via Biobank protocol by standard hospital agreements. The data processing was done using algorithms developed in MATLAB 2017b (The Mathworks Inc., Natick Massachusetts).

Data inclusion

Three Freshly resected cystectomy specimens (49, 89 and 53 measurement locations, respectively) were included. These specimens were derived from patients suffering from bladder cancer who had undergone therapeutic radical cystectomy, conform the guidelines of the European Association of Urology. Specimens with less than three pathological entities were excluded.

Measurement protocol

Over a grid of locations, three independent Raman measurements were taken from each urothelial location of freshly resected cystectomy specimens (stretched on paraffin block after ventral incision as in standard pathology assessment, before formalin fixation). Each measurement consisted of ten consecutive Raman spectra (500 ms acquisition time, each). A colored pin was placed as a location marker to ensure corresponding pathology assessment. This is shown in figure 1. The probe was positioned with the intention to avoid movement or pressure change during the measurements.

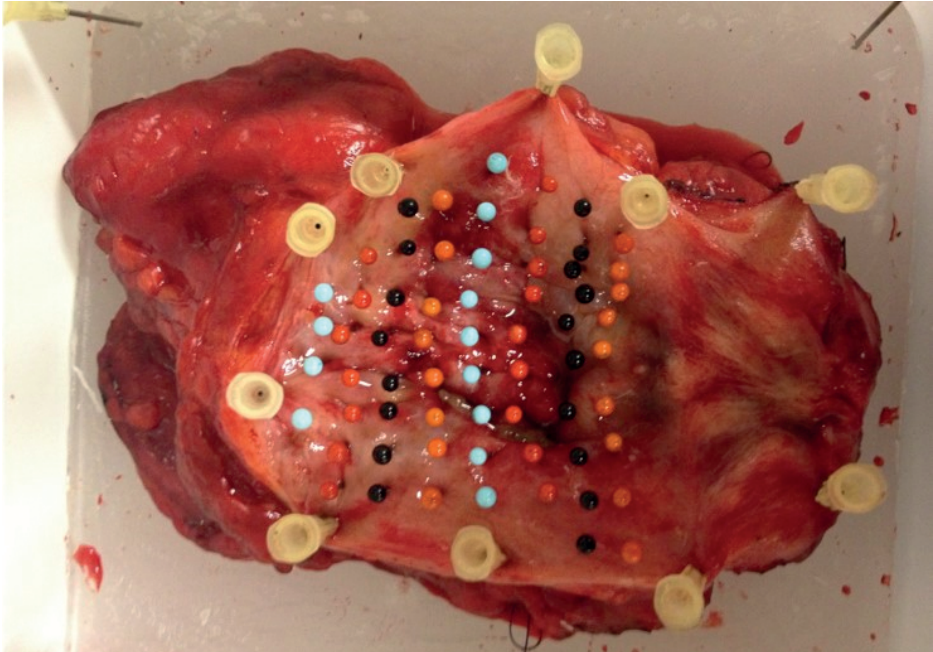


Figure 1. All measurement locations are precisely localized by pins (a different color for each row). After the Raman measurements were taken, the pin was inserted and the tissue was prepared for pathological assessment per pin location.

The used Raman system setup was described by Draga et al. [19]. It includes a 785 nm diode laser (DFB-0785-1000, Sacher Lasertechnik, Marburg, Germany) and the superficial probe with a sampling depth of 200 μm (EmVision LLC, Loxahatchee, Florida, USA) described by Agenant et al. [26]. After the Raman measurements, the specimen was formalin-fixed and each location was pathologically analyzed by a uro-pathologist (GJ), according to the WHO 1974 classification system.

Pre-Processing

The Raman shift axis was standardized by calibration using acetaminophen. Saturated spectra were excluded from the measurements. Subsequently, the measurements were normalized based on the total exposure time. For noise reduction, a 3rd-order Savitzky-Golay filter was used (window width 18.2 cm^{-1}). The autofluorescence background was removed using a 4th-order iterative polynomial fit [27]. After removal of the autofluorescence, the Raman signal was divided by the autofluorescence to normalize the spectra.

Classification model

Classification of the Raman measurements according to the pathological assessment per specimen was performed using Linear Discriminant Analysis with a leave-one-out

cross-validation. Partial Least Squares was used for reduction of the dimensions. Per specimen was the number of PLS components optimized for AUC (between 4 and 7). Classification in two and in three pathology-sets was performed (table 1). Synthetic Minority Over-sampling Technique (SMOTE) was used to correct the imbalance in the data set [28]. To correct for the small difference between the synthetic spectra per cycle, the whole classification loop was performed with ten iterations. The results presented are the averages of these iterations.

Performance evaluation

For the performance evaluation, a *benign* and a *malignant* set were constructed based on the pathology results. The *benign* set includes normal tissue, reactive atypia and dysplasia and the *malignant* set includes UC and carcinoma in situ (CIS) (table 1). Although CIS is a pre-malignancy, we chose to assign CIS to the *malignant* set because it requires active treatment. Grade 1 UC was not present in any specimen. Sensitivity, specificity and AUC are used as metrics for performance evaluation of the classification.

Table 1. The pathological classification for the performance (two-set classification) and for the spatial distribution (three-set classification) evaluation.

	WHO grading 1974	Performance: Two-set-classification	Spatial evaluation: Three-set-classification
Benign ↓ Malignant	Normal	benign	benign – normal
	Reactive atypia	benign	benign – abnormal
	Dysplasia	benign	benign – abnormal
	CIS	malignant	malignant
	Grade 2 UCC	malignant	malignant
	Grade 3 UCC	malignant	malignant

Spatial tissue evaluation

For spatial tissue evaluation we have created 2D-Raman maps using a three-set-classification. The *benign* set was divided into normal and abnormal. Reactive atypia and dysplasia were assigned to the *benign abnormal* set, whereas normal tissue was assigned to the *benign normal* set (table 1). An example of the Raman spectra we generated and its classification into three pathology-sets is shown in figure 2.

2D-maps are constructed per specimen based on the pathological classification and the Raman classification. The definition of the different 2D-maps is described below. Although, classification is performed on all three independent measurements in each

location, only the mean results of these independent measurements are presented in the 2D-maps.

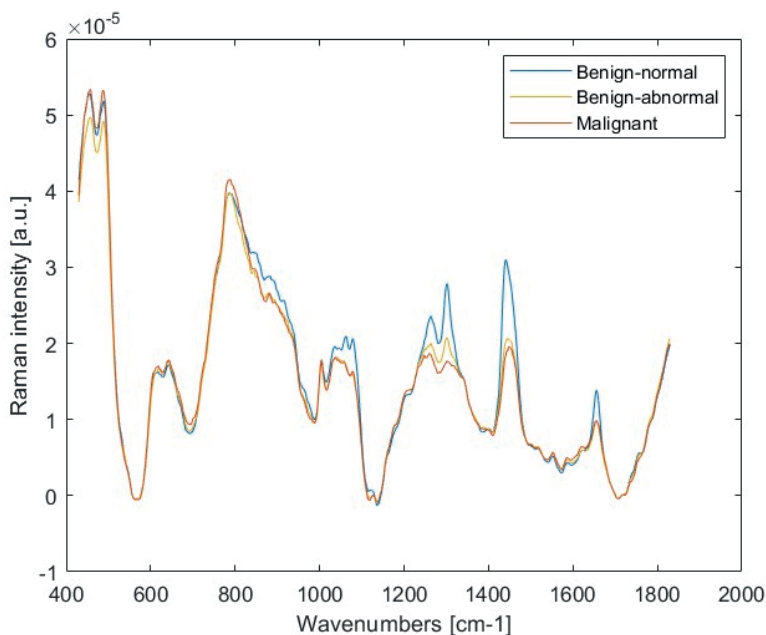


Figure 2. The mean Raman spectra of the three pathology-sets of specimen 2.

Histopathology

Pathological 2D-maps are created per specimen. These maps show the location and the pathology-set according to pathologic evaluation. Each pathology-set is depicted in a primary color. Hence, the pathological distribution of *benign normal* (blue), *benign abnormal* (yellow) and *malignant* (red) is mapped (table 1).

Prediction

In the 2D-maps underneath, each location is assigned to a primary color (consequent to the used colors for each pathology-set in the pathological 2D-map), based on the prediction of the Raman classification. The predicted class is determined according to the class with the highest probability (figure 3). The differences and agreement of the Raman prediction and the pathological classification can be observed in the first two 2D-maps.

Probability

To show the certainty of the Raman prediction, the underlying probabilities are presented in the 2D-maps below. Figure 3 demonstrates how each color on the probability 2D-maps

is derived from the Raman classification. A transitional or blended color is determined per location, based on the mean classification probability of the three independent Raman measurements. The contribution of each primary color is proportional to the corresponding probabilities per pathology-set. The summed probabilities of each pathology-set always add up to 1. Measurements that have a more distinctive probability for one pathology-set will be presented in the 2D-map by a color close to that corresponding primary color. Less distinctive probabilities are presented more blended colors.

Malignant classification using different thresholds

To evaluate whether tissue bordering malignant areas has Raman characteristics of a malignancy, 2D-maps were created using lowered threshold for Raman classification. If the probability for belonging to the *malignant* set exceeds the threshold, the predicted class is depicted as *malignant* (red). Otherwise, the set with the highest probability for either *benign - normal* (blue) or *benign - abnormal* (yellow) is depicted. 2D-maps are created using thresholds of 0.3, 0.1, and 0.05. That is, 30%, 10% and 5% probability of being malignant.

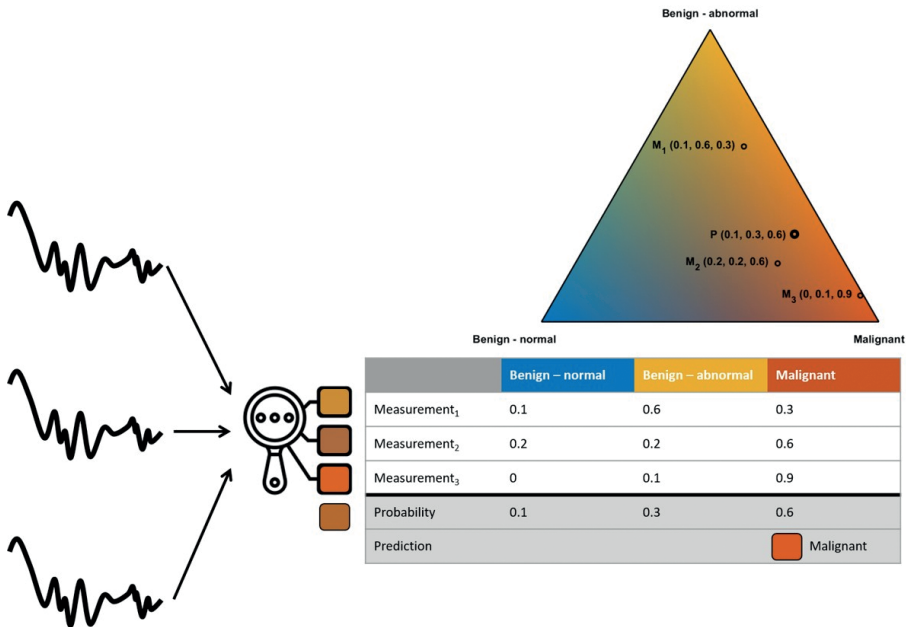


Figure 3. The Raman classification model classifies the three independent measurements at one location independently. This results in a probability of each pathology-set per measurement. Only the average of these three independent measurements is presented in a 2D-map. For the (mean) probability, the color in the 2D-map is determined based on the probability for each set of the pathology classification as is visualized in the triangular in this plot.

RESULTS

Table 2 shows the number of included measurements in this study and their pathological classification. In total 569 measurements were taken at 191 location in three bladders. At five locations, only two measurements were taken instead of three as was required per protocol. At one location, an additional measurement has been taken. These missing and added measurements are not corrected for, because only the average of the measurements is presented per location.

Table 2. Number of Raman measurements and their pathological classification. The number of measurement locations is shown between brackets.

	Specimen 1	Specimen 2	Specimen 3	Accumulated
Normal	111 (37)	150 (50)	61 (21)	322 (108)
Reactive atypia	29 (10)	57 (19)	89 (30)	175 (59)
Dysplasia	-	3 (1)	-	3 (1)
CIS	-	27 (9)	-	27 (9)
UC Grade 2	6 (2)	-	-	6 (2)
UC Grade 3	-	30 (10)	6 (2)	36 (12)

Performance evaluation

The classification model was validated by the sensitivity, specificity and AUC, for all three specimens using the two-set classification. The results are shown in table 3.

Table 3. The classifier performance of all three specimens using the two-set-classification.

	Specimen 1	Specimen 2	Specimen 3	Mean
AUC	0.98	0.84	0.95	0.92
Sensitivity	1	0.79	1	0.93
Specificity	0.91	0.77	0.90	0.86

Spatial tissue evaluation

Figure 4 represents the spatial tissue evaluation in 2D-maps of the pathological and Raman classifications.



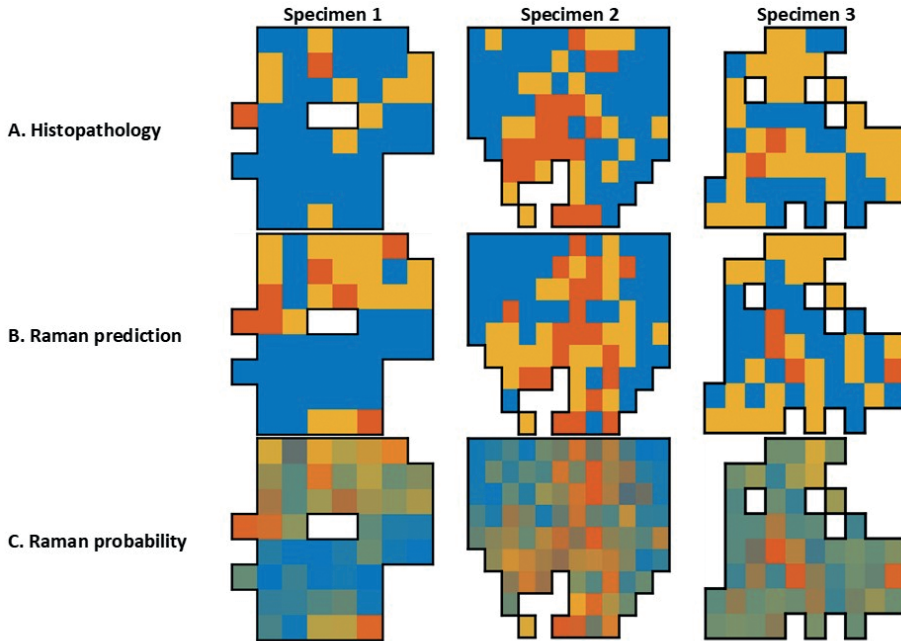


Figure 4. 2D-maps for spatial tissue evaluation per specimen; In row A and B, primary colors are allocated to each specific pathology-set: *benign normal* (blue), *benign abnormal* (yellow) and *malignant* (red). Row A shows the pathological classification and row B the Raman prediction. Row C depicts the underlying probability for the prediction, which is displayed in blended colors.

Histopathology

Row A shows the pathological classification per location in each specimen. The three-set-classification is used and the different sets are represented by a primary color; *benign normal* (blue), *benign abnormal* (yellow) and *malignant* (red).

Prediction

The Raman classifier output (prediction) is presented in row B in the corresponding primary colors according to the sets of the 2D-maps in row A. In line with the two-set-classification performance presented in table 3, large similarities are observed between the pathological evaluation (figure 5A) and the Raman prediction (figure 5B).

Probability

The prediction in row B is derived from the underlying classification probability, which is presented in row C. The 2D-Raman-maps in this row show a gradual transition from one pathology-set to another. We found that surrounding *malignant* areas the probability is less distinctive, hence a less distinctive presence of primary colors (more blended colors) and a higher prediction uncertainty.

Malignant classification using different thresholds

In figure 5, the 2D-maps of Raman predictions are presented using different thresholds for classification into *malignancy*. The *malignant* areas expand at *malignant* margins, as the threshold is lowered. Vice versa, *benign-(ab)normal* locations are not randomly depicted as *malignant*, even for a low threshold of 5% probability on being *malignant* (figure 5C).

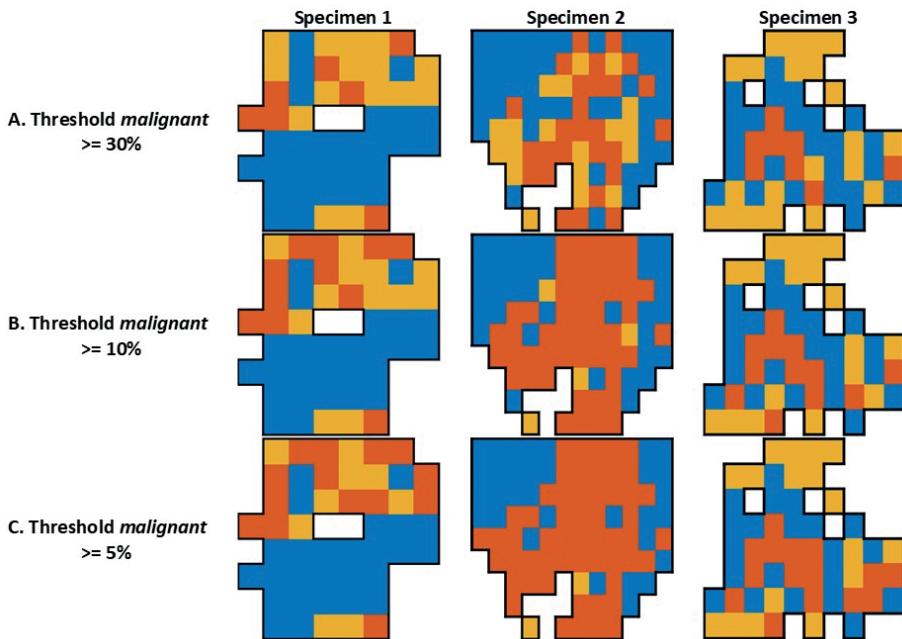


Figure 5. 2D-maps of the Raman prediction per specimen with a lowering threshold for the malignant set; The thresholds are 30%, 10%, and 5% for row A, B and C, respectively. The primary colors are allocated to each specific pathology-set: *benign normal* (blue), *benign abnormal* (yellow) and *malignant* (red).

DISCUSSION

To our knowledge, this is the first presentation of 2D-maps of the pathological and biochemical constitution of therapeutic radical cystectomy specimens containing bladder cancer. Three cystectomy specimens were included in this experiment; all of which contained UC, and one specimen also contained CIS. In all specimens, normal tissue was present.

Performance evaluation

To evaluate the general performance of the Raman classification system, a two-set classification was performed. The results are equivalent to the performance of other systems [14–17]. This Raman system is therefore adequate in discriminating tissue of being benign or malignant. In specimen 2, the specificity was limited compared to the other specimens; this could be explained by the higher number of pathological entities in the pathology-sets (5) compared to only three pathological entities in the other two specimens. Combining different pathological entities, that may have different biochemical compositions, in one pathology-set makes classification more complex.

Spatial evaluation

From the 2D-Raman-maps in figure 4, less distinctive probabilities and higher prediction uncertainty were found mostly surrounding pathologically assessed *malignant* areas. There are two theories that could explain this observation: Firstly, the higher prediction uncertainty could be explained by the presence of tissue heterogeneity [29,30]. Multiple cells in one tissue location are evaluated in a Raman spectrum. Therefore, the generated spectra include information of multiple biochemical compositions, which might belong to different pathology-sets. Furthermore, we consider that the measured tissue could slightly differ between the three independent Raman measurements in one location. Also, tumor heterogeneity with diverse characteristics within one tumor, could be of importance. This has been investigated before [9]. In future, when using Raman clinically, multiple independent measurements might be required for the definitive classification of the tissue. The second theory is based on the presence of a smooth transition of normal tissue into malignant tissue [31]. Raman spectroscopy enables detection of biochemical transitions, which might not yet be detectable by the pathologists (using cut-off values for classification). Therefore, Raman spectroscopy could be used as an early indicator for progression or recurrences.

The 2D-maps in figure 5 endorse these theories. By setting a threshold for *malignant* allocation, risk-based resection margins are visualized and might be of added value in clinical practice. When using spatial Raman spectroscopy clinically and changing

the threshold of malignancy detection, more accurate tumor resections could result that would lead to less residuals and/or recurrence. To define the correct threshold more clinical (prospective) research should be performed. Especially the margins of *malignant* areas should be of focus in further research for clinical application of Raman spectroscopy.

In future, it would also be valuable to evaluate the Raman characteristics of the disagreeing Raman and pathologically classified locations. This could give insight in the biochemical substrate that might be responsible for a transition into malignancy. Furthermore, it could be interesting to further explore the spatial application of Raman spectroscopy. E.g. micro-Raman in cystectomy specimens using a measurement grid that contains more measurement location in the same surface.

CONCLUSION

In this study we have investigated the spatial application of Raman spectroscopy *ex vivo*, resulting in 2D-Raman-maps of cystectomy specimens. We observed a discrepancy in Raman classification compared to the pathologic classification, especially at *malignant* margins. We hypothesize that this is due to tissue heterogeneity and/or a biochemical transition into malignancy. This was supported by the increased *malignant* classification surrounding pathological *malignant* margins when lowering the classification threshold. Either of the hypotheses could pose an explanation for inaccurate resections during TURBT and subsequent UC and/or CIS recurrences. Further development of clinically applied spatial Raman spectroscopy could create a valuable supportive technique in bladder cancer diagnosis to enable accurate resection and less residuals and/or recurrences of UC.



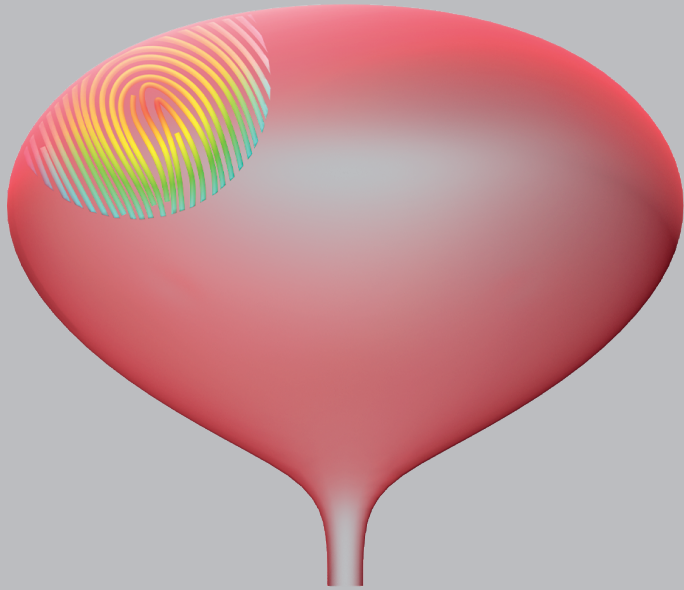
REFERENCES

- 1 Antoni S, Ferlay J, Soerjomataram I, Znaor A, Jemal A, Bray F. Bladder Cancer Incidence and Mortality: A Global Overview and Recent Trends. *Eur Urol*. 2017;71(1):96–108.
- 2 Brausi M, Collette L, Kurth K, van der Meijden AP, Oosterlinck W, Witjes JA, et al. Variability in the recurrence rate at first follow-up cystoscopy after TUR in stage Ta T1 transitional cell carcinoma of the bladder: a combined analysis of seven EORTC studies. *Eur Urol*. 2002 May;41(5):523–31.
- 3 Sylvester RJ, van der Meijden APM, Oosterlinck W, Witjes JA, Bouffouix C, Denis L, et al. Predicting recurrence and progression in individual patients with stage Ta T1 bladder cancer using EORTC risk tables: a combined analysis of 2596 patients from seven EORTC trials. *Eur Urol*. 2006 Mar;49(3):466–465; discussion 475–477.
- 4 Sylvester RJ, Oosterlinck W, Holmang S, Sydes MR, Birtle A, Gudjonsson S, et al. Systematic Review and Individual Patient Data Meta-analysis of Randomized Trials Comparing a Single Immediate Instillation of Chemotherapy After Transurethral Resection with Transurethral Resection Alone in Patients with Stage pTa–pT1 Urothelial Carcinoma of the Bladder: Which Patients Benefit from the Instillation? *European Urology*. 2016 Feb;69(2):231–44.
- 5 Brunckhorst O, Ong QJ, Elson D, Mayer E. Novel real-time optical imaging modalities for the detection of neoplastic lesions in urology: a systematic review. *Surg Endosc*. 2018 Nov DOI: 10.1007/s00464-018-6578-1
- 6 Cauberg Evelyne CC, de la Rosette JJMCH, de Reijke TM. Emerging optical techniques in advanced cystoscopy for bladder cancer diagnosis: A review of the current literature. *Indian J Urol*. 2011 Apr;27(2):245–51.
- 7 Rink M, Babjuk M, Catto JWF, Jichlinski P, Shariat SF, Stenzl A, et al. Hexyl aminolevulinate-guided fluorescence cystoscopy in the diagnosis and follow-up of patients with non-muscle-invasive bladder cancer: a critical review of the current literature. *Eur Urol*. 2013 Oct;64(4):624–38.
- 8 Jin H, Lin T, Han P, Yao Y, Zheng D, Hao J, et al. Efficacy of Raman spectroscopy in the diagnosis of bladder cancer: A systematic review and meta-analysis. *Medicine (Baltimore)*. 2019 Nov;98(47):e18066.
- 9 Cordero E, Ruger J, Marti D, Mondol AS, Hasselager T, Mogensen K, et al. Bladder tissue characterization using probe-based Raman spectroscopy: Evaluation of tissue heterogeneity and influence on the model prediction. *J Biophotonics*. 2020 Feb;13(2):e201960025.
- 10 da Costa JB, Gibb EA, Nykopp TK, Mannas M, Wyatt AW, Black PC. Molecular tumor heterogeneity in muscle invasive bladder cancer: Biomarkers, subtypes, and implications for therapy. *Urol Oncol*. 2022 Jul;40(7):287–94.
- 11 Crow P, Stone N, Kendall CA, Persad RA, Wright MPJ. Optical diagnostics in urology: current applications and future prospects. *BJU Int*. 2003 Sep;92(4):400–7.
- 12 Rao AR, Hanchanale V, Javle P, Karim O, Motiwala H. Spectroscopic view of life and work of the Nobel Laureate Sir C.V. Raman. *J Endourol*. 2007 Jan;21(1):8–11.
- 13 Stone N, Kendall C, Shepherd N, Crow P, Barr H. Near-infrared Raman spectroscopy for the classification of epithelial pre-cancers and cancers. *Journal of Raman spectroscopy*. 2002;33(7):564–73.

- 14 Bergholt MS, Zheng W, Lin K, Ho KY, Teh M, Yeoh KG, et al. In Vivo Diagnosis of Esophageal Cancer Using Image-Guided Raman Endoscopy and Biomolecular Modeling. *Technol Cancer Res Treat*. 2011 Apr;10(2):103–12.
- 15 Kanter EM, Vargis E, Majumder S, Keller MD, Woeste E, Rao GG, et al. Application of Raman spectroscopy for cervical dysplasia diagnosis. *J Biophotonics*. 2009 Feb;2(1–2):81–90.
- 16 Molckovsky A, Song L-MWK, Shim MG, Marcon NE, Wilson BC. Diagnostic potential of near-infrared Raman spectroscopy in the colon: differentiating adenomatous from hyperplastic polyps. *Gastrointest Endosc*. 2003 Mar;57(3):396–402.
- 17 Bergholt MS, Zheng W, Lin K, Ho KY, Teh M, Yeoh KG, et al. In vivo diagnosis of gastric cancer using Raman endoscopy and ant colony optimization techniques. *Int J Cancer*. 2011 Jun;128(11):2673–80.
- 18 Grimbergen MCM, van Swol CFP, Draga ROP, van Diest P, Verdaasdonk RM, Stone N, et al. Bladder cancer diagnosis during cystoscopy using Raman spectroscopy. In: Kollias N, Choi B, Zeng H, Malek RS, Wong BJ, Ilgner JFR, et al., editors. San Jose, CA; 2009; p 716114.
- 19 Draga ROP, Grimbergen MCM, Vijverberg PLM, van Swol CFP, Jonges TGN, Kummer JA, et al. In vivo bladder cancer diagnosis by high-volume Raman spectroscopy. *Anal Chem*. 2010 Jul;82(14):5993–9.
- 20 Crow P, Uff JS, Farmer JA, Wright MP, Stone N. The use of Raman spectroscopy to identify and characterize transitional cell carcinoma in vitro. *BJU Int*. 2004 Jun;93(9):1232–6.
- 21 de Jong BWD, Schut TCB, Maquelin K, van der Kwast T, Bangma CH, Kok D-J, et al. Discrimination between nontumor bladder tissue and tumor by Raman spectroscopy. *Anal Chem*. 2006 Nov;78(22):7761–9.
- 22 Kerr LT, Domijan K, Cullen I, Hennelly B. Applications of Raman spectroscopy to the urinary bladder for cancer diagnostics. 2014 DOI: 10.1515/plm-2014-0004
- 23 Krafft C, Guo S, Bocklitz T, Popp J, Bronsert P, Miernik A. Raman spectroscopy to Characterize Bladder Tissue for Multidimensional Diagnostics of Cancer in Urology. *Current Directions in Biomedical Engineering*. 2020 Sep;6(3):250–3.
- 24 Kim DK, Kim YH, Lee HY, Lee S, Doo SW, Yang WJ, et al. Diagnostic accuracy of Raman spectroscopy for the diagnosis of bladder cancer: A systematic review and meta-analysis. *J Cancer Res Ther*. 2021 Jun;17(2):426–33.
- 25 Stomp-Agenant M, van Dijk T, R Onur A, Grimbergen M, van Melick H, Jonges T, et al. In vivo Raman spectroscopy for bladder cancer detection using a superficial Raman probe compared to a nonsuperficial Raman probe. *J Biophotonics*. 2022 Mar;e202100354.
- 26 Agenant M, Grimbergen M, Draga R, Marple E, Bosch R, van Swol C. Clinical superficial Raman probe aimed for epithelial tumor detection: Phantom model results. *Biomed Opt Express*. 2014 Apr;5(4):1203–16.
- 27 Lieber CA, Mahadevan-Jansen A. Automated method for subtraction of fluorescence from biological Raman spectra. *Appl Spectrosc*. 2003 Nov;57(11):1363–7.
- 28 Chawla NV, Bowyer KW, Hall LO, Kegelmeyer WP. SMOTE: Synthetic Minority Over-sampling Technique. *Journal of Artificial Intelligence Research*. 2002 Jun;16:321–57.

- 29 Cheng L, Neumann RM, Nehra A, Spotts BE, Weaver AL, Bostwick DG. Cancer heterogeneity and its biologic implications in the grading of urothelial carcinoma. *Cancer*. 2000 Apr;88(7):1663–70.
- 30 Minoli M, Kiener M, Thalmann GN, Kruithof-de Julio M, Seiler R. Evolution of Urothelial Bladder Cancer in the Context of Molecular Classifications. *Int J Mol Sci*. 2020 Aug;21(16):E5670.
- 31 Rao JY, Hemstreet GP, Hurst RE, Bonner RB, Jones PL, Min KW, et al. Alterations in phenotypic biochemical markers in bladder epithelium during tumorigenesis. *Proc Natl Acad Sci U S A*. 1993 Sep;90(17):8287–91.





CHAPTER 5

REAL-TIME BLADDER LESION REGISTRATION AND NAVIGATION: A PHANTOM STUDY

Agenant M
Noordmans HJ
Koomen W
Bosch JL

PLoS One. 2013;8(1)

ABSTRACT

Background

Bladder cancer is the fourth most common malignancy in men, with a recurrence rate of 33-64%. Tumor documentation during cystoscopy of the bladder is suboptimal and might play a role in these high recurrence rates.

Objective

In this project, a bladder registration and navigation system was developed to improve bladder tumor documentation and consequently increase reproducibility of the cystoscopy.

Materials/Methods

The bladder registration and navigation system consists of a stereo-tracker that tracks the location of a newly developed target, which is attached to the endoscope during cystoscopy. With this information the urology registration and navigation software is able to register the 3D position of a lesion of interest. Simultaneously, the endoscopic image is captured in order to combine it with this 3D position. To enable navigation, navigational cues are displayed on the monitor, which subsequently direct the cystoscopist to the previously registered lesion. To test the system, a rigid and a flexible bladder phantom were developed. The system's robustness was tested by measuring the accuracy of registering and navigating the lesions. Different calibration procedures were compared. It was also tested whether system accuracy is limited by using a previously saved calibration, to avoid surgical delay due to calibration. Urological application was tested by comparing a rotational camera (fixed to the rotating endoscope) to a non-rotational camera (dangling by gravity), used in standard urologic practice. Finally, the influence of volume differences on registering and navigating was tested.

Results/Conclusion

The bladder registration and navigation system has an acceptable accuracy for bladder lesion registration and navigation. Limitations for patient determinants included changes in bladder volume and bladder deformation. In vivo studies are required to measure the effect of these limitations, and functionality in urological practice as a tool to increase reproducibility of the cystoscopy.

INTRODUCTION

In western countries, bladder cancer is the fourth most common malignancy in men [1,2]. Most bladder tumors are confined to the mucosa (stage Ta or CIS) or submucosa (T1). These are defined as non-muscle-invasive bladder cancer (NMIBC) and are diagnosed by inspection of the entire bladder wall during a cystoscopy, mostly using a 30° endoscope [3]. Treatment consists of transurethral resection of the bladder tumor (TURBT) in which most of the tumors are completely resected. Nevertheless, recurrence and residual tumors are common issues that can lead to disease progression, even with additional intravesical (chemo- or immuno-) therapy [4–7]. For T1 or high-grade NMIBC, recurrence rates of 33–64%, residual tumor rates of 28–37% and progression rates of 11–27% have been reported [2,8–10]. If there is a high risk for recurrence or residual tumor after initial resection, a re-TURBT is performed after 6 weeks to evaluate the completeness of resection or to define the total tumor invasion [3,11]. There are two problems associated with the current diagnostic approach. First, there is no certainty that the whole bladder has been inspected during a cystoscopy as the urologist might overlook a small part of the bladder that contains a suspect lesion. Second, conventional tumor documentation is suboptimal, which is a major limitation for patient follow-up and treatment.

The tumor location is currently registered in the patient’s medical record by making a provisional hand-made drawing of lesions on a bladder schedule. Subsequent follow-up cystoscopy, or cystoscopy during TURBT, is then performed with specific attention paid to these marked areas on the schedule. However, this approach lacks documentation accuracy because of the inter- and intra-urologist variability related to the drawing and interpretation. In addition, information on the size and shape of the tumor is inadequate. Although, endoscopic images containing that information can be saved, they still lack information on the location of the lesion.

To overcome these problems, we developed a bladder registration and navigation system. This system registers which parts of the bladder have been inspected during a cystoscopy. Furthermore, it allows to capture the 3D position of endoscopic images to generate a panoramic bladder wall overview. This enables a cystoscopic comparison of new and previously performed inspections. This serves to improve patient follow-up and increases the reproducibility of the cystoscopy.

The aim of this study is to demonstrate the first concept of the bladder registration and navigation system. It is a stage 0 preclinical study, according to the IDEAL recommendations [12–14]. Tests are performed to analyze the technical determinants of the system, i.e. the stability of registering a location, navigating back to that location, how

and when to calibrate the system and the influence of the dangling endoscopic camera. Secondly, as navigation in the bladder places extra demands on the system, (e.g., the deformable nature of the bladder), additional tests are performed to study these effects.

MATERIALS & METHODS

Bladder navigation system

The bladder navigation system consists of a conventional cystoscopic system equipped with 3 extra components, to register and navigate positions in the 3D space inside the bladder (figure 1). The first component is a tracking target connected to the endoscope which moves together with the scope. The second component is a stereotracker which can be placed above the standard endoscopic monitor and subsequently measures the 3D position of the tracking target. The third component is a computer that converts analog imaging data of the endoscopic camera to digital data and combines it with the 3D position information of the endoscope tip, which is generated from the stereotracker and tracking target.

Tracking target

First, we experimented with conventional tracking targets, where near-infrared reflecting spheres are mounted on a frame (figure 1). Although conventional tracking targets are easily clamped to an endoscope, two problems arose which severely hampered their use for a urological application. First, while rotational movement is essential during cystoscopy and TURBT, the tracking camera lost sight of the conventional tracking target when the endoscope was turned upside down. Secondly, the target was easily lost by the system because the sight path from the camera to the tracking target was often disturbed by aspects required in the urological application i.e., the light cable, the head of the surgeon, and the legs of the patient that are placed in stirrups.

To overcome these two problems, we devised two new tracking targets i.e., the butterfly target and the foil target (figure 1). Both of these are equipped with retro-reflective patches instead of the reflecting spheres. In addition to being constantly visible by the tracking camera, we stipulated that the target could be clamped to the endoscope in one unique way. In this way, a previously obtained calibration can be loaded into the software, avoiding surgical delay due to calibration.

In a dedicated test (results not shown), the foil target outperformed the conventional and butterfly design in overall visibility and user friendliness; therefore, this foil target was used for all subsequent tests.

The stereotracker

For this project we used a *PS-Tech* stereo-tracking camera, which is a motion-based tracker that determines the position and orientation (POSE) of arbitrary objects in a coordinate system relative to a known origin. In this stereotracker two major components can be distinguished:

- The infrared lighting panel illuminates the workspace with near-infrared light.
- Two infrared cameras observe the tracking space with a frequency of 55 Hz, each from a slightly different viewpoint. This infrared illumination is synchronized with the cameras enabling capture of the reflected near-infrared light from the retro-reflective patches of the target.

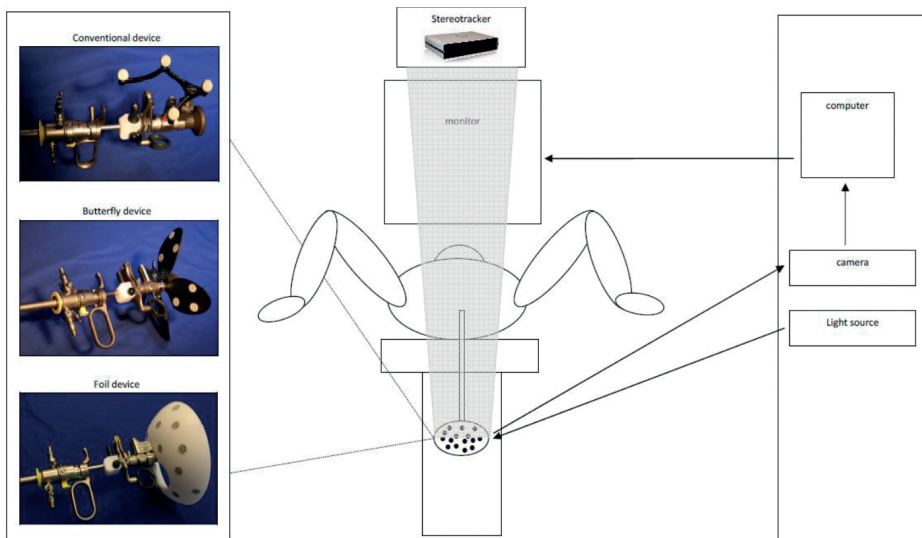


Figure 1. Schematic bladder navigation system; the typical position of a patient during cystoscopy or TURBT, with the legs in stirrups. The cystoscope set is connected to the light source, endoscopic camera and a tracking target (conventional, butterfly or foil) The camera sends image data to a computer that converts the analogous imaging data to digital imaging information. This is combined by a computer with positional information of the tracking target, which is read by the stereo-tracking camera. Standard endoscopic images edited with navigational directions are displayed on the monitor.

Computer software

For registration, 3D positions are captured by a medically-approved computer during cystoscopy in a shared coordinate system, which indicates the relative 3D distance to each other in space. To enable navigation, the cystoscopist is guided to the registered 3D positions by multiple directional cues, i.e. arrows and point markers. The arrows indicate the 3D direction in which the cystoscopist should direct the scope, and the

point markers are virtual representations of the registered points that increase in size when the tip of the scope approaches the registered 3D location. To achieve this, the endoscopic video stream is captured by the computer and the navigation cues are superimposed over the digitized endoscopic video stream. Subsequently, the combined video stream is transferred to a second endoscope monitor that shows the augmented reality view. This monitor is placed next to the original endoscopic monitor, so that both monitors are shown during cystoscopy. To enable this, the entire endoscopic imaging and tracking chain is modeled. First, the 3D position of the endoscope and attached target is determined with the use of triangulation methods and by measuring the 3D Euclidean transformation of the target [15]. Second, to achieve the augmented reality view, it is necessary to model the projective properties of the endoscope using two parts.

- The *intrinsic* part is based on the pinhole camera model and contains the parameters that are invariant under motion [16,17]. It is represented by the 3 by 4 matrix, which is called \mathbf{K} :

$$s \begin{bmatrix} x \\ y \\ 1 \end{bmatrix} = \mathbf{K} \begin{bmatrix} X \\ Y \\ Z \\ 1 \end{bmatrix}, \quad \mathbf{K} = \begin{bmatrix} f_x & 0 & c_x & 0 \\ 0 & f_y & c_y & 0 \\ 0 & 0 & 1 & 0 \end{bmatrix}$$

X , Y and Z are elements of a 3D point defined in camera space, x and y are the coordinates of the projected 3D point and s is an arbitrary scale factor. The elements f_x and f_y in matrix \mathbf{K} , describe the focal length in pixels along the x - and y -axes and c_x and c_y indicate the location of the principal point.

- The *extrinsic* part describes the transformation from world space coordinates to camera space coordinates. In our model it is defined by two matrices: \mathbf{A} and \mathbf{T} . Matrix \mathbf{A} is a 4 by 4 Euclidean transformation matrix that is completely defined by the POSE of the tracking target which is attached to the endoscope in real-time. This results in a change of parameters, when the endoscope is moved through the workspace. Because the coordinate frame of the tracking target and the coordinate frame of the endoscope camera do not align, we have to incorporate an offset transformation into our model: a 4 by 4 Euclidean transformation matrix \mathbf{T} . This matrix transforms the 3D coordinates from the coordinate space of the tracking target to the endoscope's camera coordinate space.

The full cystoscopic projection model is defined as:

$$s \begin{bmatrix} x \\ y \\ 1 \end{bmatrix} = \mathbf{K}(\mathbf{T}\mathbf{A}^{-1}) \begin{bmatrix} X \\ Y \\ Z \\ 1 \end{bmatrix}$$

Matrix \mathbf{T} and \mathbf{K} are fixed and matrix \mathbf{A} is updated every frame, using parameters that are retrieved from the stereo-tracking camera.

Calibration method

All parameters of the cystoscopic projection model are determined using one integrated calibration method. Several snapshots (at least two) are taken by pointing the endoscope to a planar checkerboard-patterned calibration board, which itself is tracked using retro-reflective patches. The POSE of the calibration board and the tracking target are saved, together with a set of 2D points extracted from the endoscopic camera image. From the entire set of 2D points the intrinsic parameters are calculated; simultaneously, the extrinsic camera parameters are determined for every snapshot, both by using Zhang's calibration method [17].

In addition to the linear pinhole model, the optics of the endoscope show significant amounts of non-linear distortion. For this reason we modeled the non-linear distortion using a 5-parameter version of the Brown distortion model (3 for radial distortion and 2 for the tangential distortion) [18]. Offset matrix \mathbf{T} can easily be calculated as the relation between the pose of the calibration board, tracking target and the endoscopic camera, and is known from Zhang's calibration procedure.

Registering locations

To register locations of interest, the user moves the endoscope until the tip is touching the location of interest. By pushing a pedal or a key on the computer, the 3D position of the tip of the endoscope that allocates a lesion of interest is stored in the system. At the same time the endoscopic image is captured and stored as digital image (PNG) to enable generation of panoramic overviews and comparison with previously obtained cystoscopy information.

Navigating locations

The cystoscopist effectuates navigation by moving the tip of the endoscope to a previously registered 3D position, by navigation cues that denote the direction and

distance to that position. To enable that, the 3D position of the location is transferred to the current image space.

Phantoms

Because no commercial functional phantom was available to measure the accuracy of registering and navigating lesions without fluid leakage during introduction of the scope, we designed two phantoms. The first is a dry 'box phantom' with graph paper on the inside (figure 2A) and the second a 'balloon phantom' which can be filled with different volumes of water (figure 2B and 2C). The endoscope is introduced through openings in the phantom that simulate the bladder neck, which connects the 'bladder' (box or balloon, respectively). The 'balloon phantom' contains a luer lock trocar holder connection in the opening, which provides a fluid-filled balloon without leakage. Similar to the original anatomy where bony structures and the rectum surround the bladder, the balloon expands specifically to the ventral side because sponge material surrounds the other parts of the balloon. Adjusting the volume of water in the balloon simulates bladder content increase/decrease, and deformation. In both 'bladders', four 'lesions' were drawn (on the floor, right wall, left wall and back wall), to facilitate 3D position registering and navigation. A lesion in the dome of the balloon was omitted, because the thin balloon wall deformed very easily at the ventral side when the scope touched the wall, due to the surrounding air instead of sponge material. Therefore, these measurements are incomparable to the stiffer real bladder. An example of registering the lesions and which hints are shown for navigation is shown in figure 3AB.

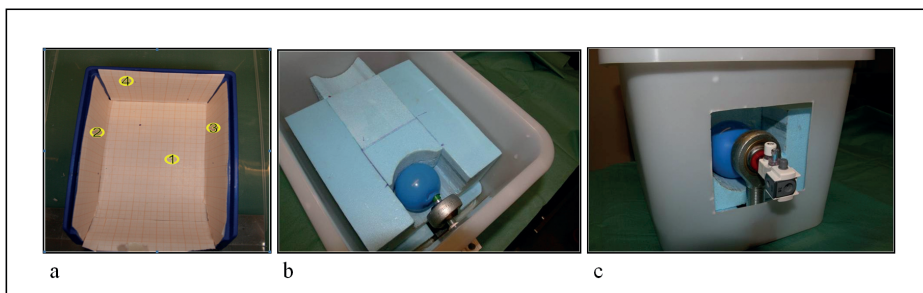


Figure 2. Both phantoms; A is the box phantom with four lesions drawn on the inside; B and C are the balloon phantom with four lesions drawn inside the balloon, coupled to the trocard holder.

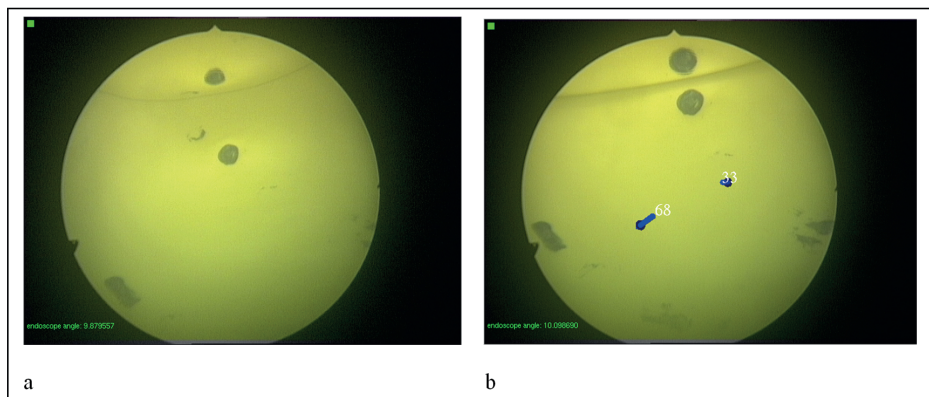


Figure 3. Endoscopic balloon phantom; Views through the endoscope before and after registering lesion number 68 and 33. Note that one lesion is mirrored in the air bubble.

Tests

Technical determinants

All technical determinant tests were performed in the box phantom to test the robustness of the system itself.

The *registering-accuracy* of the system was evaluated after conventional calibration with 24 snapshots. By registering each lesion 16 times, 64 3D positions in the bladder were recorded. The mean position per lesion was calculated. Then, Euclidean distance between each registered 3D point and the mean 3D point was calculated, per lesion.

Navigation feasibility was tested in the box phantom after conventional calibration with 24 snapshots. Each registered 3D position (one per lesion) was navigated 16 times by the cystoscopist, based on navigation cues on the monitor in the absence of endoscopic images. At the same time, the researcher observed another monitor that displayed both the navigation cues and the endoscopic imaging. When the cystoscopist finished navigation, the researcher subsequently documented whether the navigation was successful by designating whether the lesion was 'on' or 'off' screen.

To determine the minimum number of snapshots required for a functional calibration procedure, the registration-accuracy test was repeated 4 times; the first after standard calibration with 24 snapshots, which was then compared to calibrations using 18, 12 and 6 snapshots in the box phantom, respectively. We call this the *snapshot-calibration* test. The mean 3D position of each lesion of the standard calibration (24 snapshots) was

calculated and the Euclidean distance between each registered 3D point and the mean standard 3D position was measured, per lesion.

To test whether a previously obtained calibration can be loaded into the software to avoid surgical delay due to calibration, the robustness of the target clamp is tested in the *calibration-requirement* test in the box model. After calibration using 24 snapshots, the back lesion was registered 16 times, then the cystoscope set and target were disassembled and reassembled 19 times and, each time, the registration was repeated 16 times. The mean 3D position of the set just after calibration, without taking the cystoscope set and target apart, was calculated and the Euclidean distance between each registered 3D point to that mean 3D point was calculated.

To assess whether an endoscope camera dangling to gravity was properly modeled by the software, the *rotation-correction* test was performed by repeating the navigation-feasibility test twice. First with the camera fixed to the endoscope (i.e. the conventional navigation system) and secondly with a dangling camera as in standard urological practice and, subsequently, a software correction, the rotation correction was investigated.

Patient determinants

Both of the patient determinant tests were performed in the balloon phantom, to enable analyses of the influence of volume differences in the bladder. The influence of changing volume on the registering accuracy was verified (*registering-volume-influence* test). The registering-accuracy test was repeated 7 times using different volumes of water as follows: first the volume was stepwise decreased in increments of 60 cc (i.e. 480-420-360-300 cc) and then stepwise increased (i.e., 360-420-480 cc). A mean 3D position for the balloon filled with 300 cc water was calculated and the Euclidean distance between each registered 3D point and that mean 3D point was calculated, per lesion.

Finally, the influence of changing the volume was also tested on navigation, by repeating the navigation-feasibility test (*navigation-volume-influence* test). Lesions were registered in a balloon filled with 420 cc water and the registered 3D positions were navigated, as described in the navigation-feasibility test. Navigation was first performed within the same volume and then again after reducing the volume to 300 cc.

General conditions

All tests were performed in an operating room on a surgical table with clinical cystoscopic instruments (Storz). The test phantoms were strapped to the table, to prevent movement

of the phantom itself. All registration and navigation characteristics were recorded and the mean and spread of measure sets were calculated.

RESULTS

Technical determinants

The mean Euclidean distances and standard deviations of all registration tests are depicted in table 1 for each location and for all the locations together. Table 1 also includes the percentages of the correctly navigated lesions for the *navigation-feasibility* test, the *rotational-correction* test and the *navigation-volume-influence* test.

The *registering-accuracy* test shows that the overall mean Euclidean distance to the mean position was 3.0 mm. The minimal and maximal mean distances were 2.4 mm for the left wall lesion to 3.8 mm for the floor lesion (table 1 and figure 4).

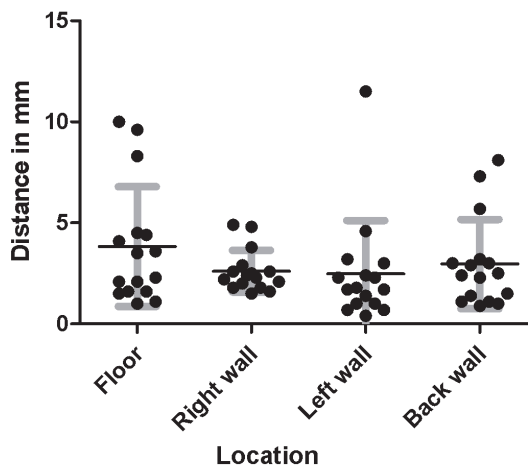


Figure 4. Registering-accuracy test; Mean and spread of the Euclidian distance of registered 3D points to the mean 3D point, per lesion.

The results of the *navigation-feasibility* test indicate that navigation within the box phantom is feasible (table 1), with successful navigation in 93.8%. There was no clear difference between the lesions for navigation success.

The results of the *snapshot-calibration* test, show that on average the registration error decreases when 18 or more calibration snapshots are used. The mean Euclidian distance for all lesions using 18 snapshots was 1.0 mm and standard deviation was 0.8 mm (table 1 and figure 5).

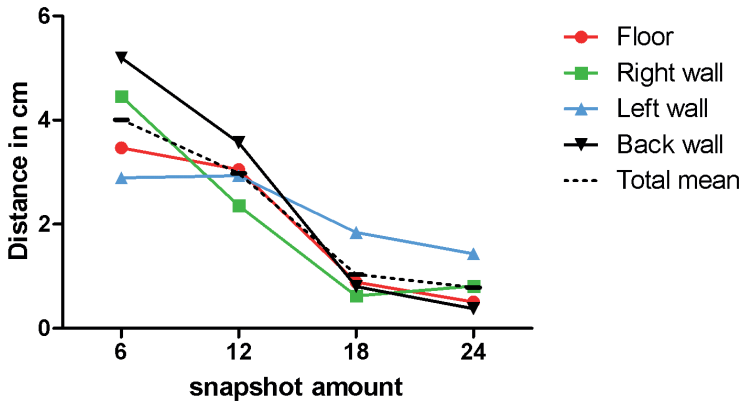


Figure 5. Snapshot-calibration test; to determine how many snapshots are minimally required to calibrate the urology navigation system. Errors clearly decrease using 18 or more snapshots.

The *calibration-requirement* test shows that there is no trend of differences in accuracy after disassembling and reassembling the instrument parts and target up to 19 times (table 1 and figure 6). Compared to the registrations of not taking apart the set with an Euclidian distance to the mean of the same set of 0,6 mm, the maximal Euclidian distance (8.9 mm) was measured after the set was taken apart the fourth time and the minimal Euclidian distance (2.3 mm) was measured after the set was taken apart the eleventh time.

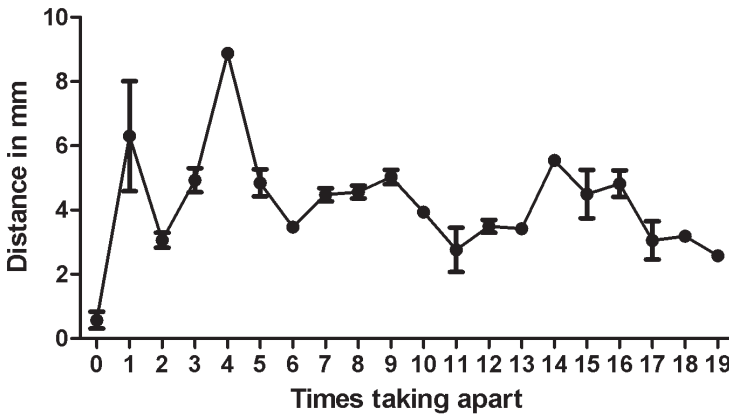


Figure 6. Calibration-requirement test; to assess whether a previously obtained calibration can be loaded into the software, to avoid delay in surgery due to calibration. The accuracy did not decrease after disassembling and reassembling the cystoscopy set and target several times.

The *rotational-correction* test reveals no clear difference in navigation accuracy when using the rotational software correction in the standard urologic system (dangling camera), compared to no rotational software correction in the conventional navigation system (fixed camera). Using the non-rotational setting, one lesion out of 64 navigations was off screen, whereas all lesions of the 64 navigations were on screen using the rotational setting.

Patient determinants

The *registering-volume-influence* test shows a decrease in Euclidian distance when the balloon volume decreases (table 1 and figure 7). In contrast, the Euclidian distances were not increased after increasing the volume again.

The *navigation-volume-influence* test showed no significant difference between navigation success in the 300 cc compared to the 420 cc filled balloon (table 1).

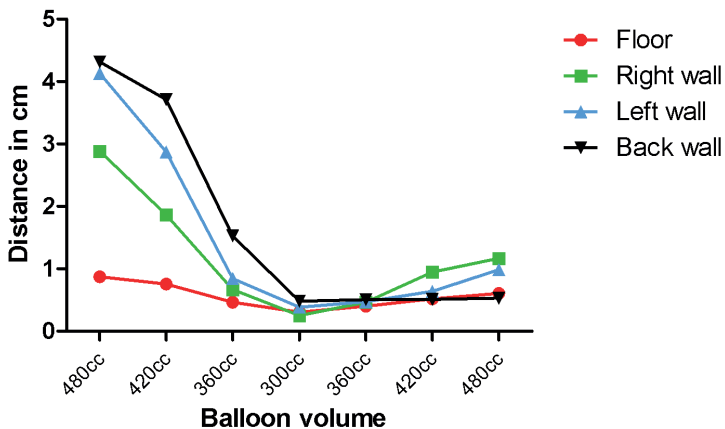


Figure 7. Registering-volume-influence test; to determine the influence of volume differences on the registering accuracy in the balloon phantom. For each measurement set per volume, the Euclidian distance between the registered 3D points and the mean registered 3D point of the 300 cc filled balloon were calculated per lesion.

Table 1. Results overview; all tests results are shown numerically summarized. The mean and standard deviation of the Euclidean distance to the reference positions are depicted (of every 16 registrations per lesion and per variable). The navigation tests (including the rotational-correction test) do not show a mean distance, but a percentage of the correctly navigated lesions, that were 'on screen' after navigation (also of every 16 navigations per lesion and variable).

Variables	Floor		Right wall		Left wall		Back wall		Total		
	Mean	Std	Mean	Std	Mean	Std	Mean	Std	Mean	Std	
Registering-accuracy test (box/mm)	3.8	3.0	2.6	1.0	2.5	2.6	3.0	2.2	3.0	2.3	
Navigation-feasibility test (box/%)	100%		100%		100%		75%		93.8%		
Snapshot-calibration test (box/mm)	6 snapshots	3.5	1.3	4.5	1.5	2.9	0.5	5.2	0.8	4.0	1.4
	12 snapshots	3.1	0.3	2.4	0.3	2.9	1.0	3.6	0.8	3.0	0.8
	18 snapshots	0.9	0.2	0.6	0.4	1.8	1.0	0.8	0.6	1.0	0.8
	24 snapshots	0.5	0.4	0.8	0.4	1.4	1.0	0.4	0.2	0.8	0.7
Calibration-requirement test (box/mm)	0 x taken apart						0.6	0.3			
	1 x taken apart						6.3	1.7			
	2 x taken apart						3.1	0.2			
	3 x taken apart						4.9	0.4			
	4 x taken apart						8.9	0.2			
	5 x taken apart						4.9	0.4			
	6 x taken apart						3.5	0.1			
	7 x taken apart						4.5	0.2			
	8 x taken apart						4.6	0.2			
	9 x taken apart						5.0	0.2			
	10 x taken apart						3.9	0.2			
	11 x taken apart						2.8	0.7			
	12 x taken apart						3.5	0.2			
	13 x taken apart						3.4	0.2			
	14 x taken apart						5.5	0.2			
	15 x taken apart						4.5	0.8			
	16 x taken apart						4.8	0.4			
	17 x taken apart						3.1	0.6			
	18 x taken apart						3.2	0.2			
19 x taken apart						2.6	0.1				

Table 1. (Continued)

Variables		Floor		Right wall		Left wall		Back wall		Total	
		Mean	Std	Mean	Std	Mean	Std	Mean	Std	Mean	Std
Rotational-correction test (box/%)	Fixed	100%		100%		94%		100%		99%	
	Rotation	100%		100%		100%		100%		100%	
Registering-volume-influence test (balloon/cm)	480 cc	0.9	0.4	2.9	0.5	4.1	0.7	4.3	0.2	3.1	1.5
	420 cc	0.8	0.4	1.9	0.3	2.9	0.5	3.7	0.2	2.3	1.2
	360 cc	0.5	0.2	0.7	0.2	0.8	0.3	1.5	0.4	0.9	0.5
	300 cc	0.3	0.3	0.3	0.2	0.4	0.2	0.5	0.2	0.4	0.3
	360 cc	0.4	0.3	0.5	0.1	0.5	0.2	0.5	0.2	0.5	0.2
	420 cc	0.5	0.1	0.9	0.3	0.6	0.3	0.5	0.1	0.7	0.3
	480 cc	0.6	0.2	1.2	0.2	1.0	0.4	0.5	0.4	0.8	0.4
Navigation-volume-influence test (balloon/%)	420 cc	81%		56%		50%		100%		72%	
	300 cc	94%		100%		81%		100%		94%	
Registering-accuracy test (box/mm)		3.8	3.0	2.6	1.0	2.5	2.6	3.0	2.2	3.0	2.3
Navigation-feasibility test (box/%)		100%		100%		100%		75%		93.8%	
Snapshot-calibration test (box/mm)	6 snapshots	3.5	1.3	4.5	1.5	2.9	0.5	5.2	0.8	4.0	1.4
	12 snapshots	3.1	0.3	2.4	0.3	2.9	1.0	3.6	0.8	3.0	0.8
	18 snapshots	0.9	0.2	0.6	0.4	1.8	1.0	0.8	0.6	1.0	0.8
	24 snapshots	0.5	0.4	0.8	0.4	1.4	1.0	0.4	0.2	0.8	0.7
Calibration-requirement test (box/mm)	0 x taken apart							0.6	0.3		
	1 x taken apart							6.3	1.7		
	2 x taken apart							3.1	0.2		
	3 x taken apart							4.9	0.4		
	4 x taken apart							8.9	0.2		
	5 x taken apart							4.9	0.4		
	6 x taken apart							3.5	0.1		
	7 x taken apart							4.5	0.2		
	8 x taken apart							4.6	0.2		
	9 x taken apart							5.0	0.2		

Table 1. (Continued)

	Variables	Floor		Right wall		Left wall		Back wall		Total	
		Mean	Std								
	10 x taken apart							3.9	0.2		
	11 x taken apart							2.8	0.7		
	12 x taken apart							3.5	0.2		
	13 x taken apart							3.4	0.2		
	14 x taken apart							5.5	0.2		
	15 x taken apart							4.5	0.8		
	16 x taken apart							4.8	0.4		
	17 x taken apart							3.1	0.6		
	18 x taken apart							3.2	0.2		
	19 x taken apart							2.6	0.1		
Rotational-correction test (box/%)	Fixed	100%		100%		94%		100%		99%	
	Rotation	100%									
Registering-volume-influence test (balloon/cm)	480 cc	0.9	0.4	2.9	0.5	4.1	0.7	4.3	0.2	3.1	1.5
	420 cc	0.8	0.4	1.9	0.3	2.9	0.5	3.7	0.2	2.3	1.2
	360 cc	0.5	0.2	0.7	0.2	0.8	0.3	1.5	0.4	0.9	0.5
	300 cc	0.3	0.3	0.3	0.2	0.4	0.2	0.5	0.2	0.4	0.3
	360 cc	0.4	0.3	0.5	0.1	0.5	0.2	0.5	0.2	0.5	0.2
	420 cc	0.5	0.1	0.9	0.3	0.6	0.3	0.5	0.1	0.7	0.3
	480 cc	0.6	0.2	1.2	0.2	1.0	0.4	0.5	0.4	0.8	0.4
Navigation-volume-influence test (balloon/%)	420 cc	81%		56%		50%		100%		72%	
	300 cc	94%		100%		81%		100%		94%	

DISCUSSION

This study shows that our developed system is robust enough to register and navigate lesions. A 10 mm cut-off value for registering accuracy was determined based on the minimal field of view visible on screen during cystoscopy. The *registration-accuracy* test is representative of the system accuracy, which should be below or comparable to other errors in the system. The overall accuracy of 3 mm is therefore adequate. The outliers of this test (distances of 10 mm and 9.6 mm on the floor and 11.5 mm on the left wall) might be caused by interference of the light cable that might have changed its position with respect to the cystoscope set and target, as we have observed during the tests. The light cable consequently might block the retro-reflection of some patches to the stereotracker and if other patches reflect onto the stereo-tracking camera, the 3D position might deviate more than the characteristic spread of the system.

The *navigation-feasibility* test showed that navigation was successful, even in the worst-case scenario: navigation on navigational cues only, in the absence of endoscopic imaging. This is comparable to limited visibility in the bladder of patients with severe hematuria. Navigation of the back wall lesion was probably worse due to the smaller field of view (± 1 cm) when the 30° endoscope is held against that lesion, compared to the side lesions that show a field of view of > 2.5 cm.

To operate correctly, the system requires calibration that enables tracking by correctly assigning the visual tools on the augmented overlay. We showed that the overall tracking and image modeling can be calibrated in one step using several captures of a checker board. In practice, special care is required to capture snapshots from as many different angles as possible, to avoid extrapolation errors when a specific position has not been covered during calibration. Based on this assumption, 24 snapshots are sufficient for adequate calibration, which may be reduced to 18 snapshots to save time.

We also investigated whether a previously obtained calibration could be loaded into the software to avoid the need for calibration during surgery. As the tracking target can be remounted with considerable precision, no additional errors were introduced after disassembling and reassembling. As a result, calibration may be performed outside the surgical flow. However, figure 6 suggests that firmly connecting the cystoscope set and target is influenced by a learning curve of re-mounting and registering by the cystoscopist using the system. Furthermore, it should be mentioned that different scopes have different optical characteristics and consequently, that calibration should be performed for each endoscope separately. Finally, to make the registration reproducible, special care is required because the cystoscope set has some flexibility in assembly.

Furthermore, rotational corrections do not negatively affect navigation of registered lesions.

In contrast, the first patient determinants test shows that decreasing the balloon volume does affect the registering accuracy; this was expected because the 3D position of a lesion changes when the balloon volume decreases. Nevertheless, increasing the balloon volume showed no change in the registered 3D position of the lesion. This might be explained by the surrounding sponge material and the non uniform stretching of the balloon: i.e. when reducing the balloon volume the walls shrink and slide along the sponge material; conversely when increasing the volume again the balloon might stick to the sponge material and only extends to the ventral side where no sponge material is present. A limitation of this test is that the extension of the ventral side could not be proven because no lesion was drawn on that side. Furthermore, volume reduction did not affect navigation accuracy. This was expected because during navigation, arrows indicate the direction to the registered 3D position, which is unchanged when using a smaller volume. Therefore, either way, the tip of the scope will reach the lesion. Influence of volume increase on navigation was not tested.

We present a newly developed system to register and navigate bladder lesions. Furthermore, we show that bladder tumors can be registered and subsequently navigated with acceptable accuracy in phantom models based on urologic conditions. This system has additional diagnostic value and can be used together with other advanced optical techniques to improve tumor detection, e.g. photodynamic diagnosis (PDD), narrow band imaging (NBI) and optical coherence tomography (OCT) [19]. Because small lesions can be diagnosed by cystoscopy, this system allows to register the location and to navigate lesions of all sizes. This is in contrast to the virtual cystoscopy techniques (currently being developed) that detect and register only those tumors measuring ≥ 5 mm using CT [20–27], MRI [20,28] and sonography [29,30]. An advantage of these latter techniques is that invasion can be distinguished and therefore (in the future) a combination of both advantageous properties for bladder registration and navigation may be preferable. In addition, unlike CT or MRI-based navigation techniques, no pre-operative imaging or anatomical or artificial landmarks (fiducials) are required [31]. Furthermore, the system allows direct feedback to the cystoscopist. The augmentation of endoscopic imaging results has only a few milliseconds time delay, which is very short compared to the mosaicking algorithms that are being developed to construct panoramic images of the bladder wall [32–37].

Other applications for navigation are cases with severe hematuria, where lesions can be easily found and quickly treated. During PDD, the endoscope is held closer to the

bladder wall due to the blue light, which has low illumination power. Consequently, diagnosing multifocal tumors is improved because the system avoids the limitation of the small field of view. The translation from the balloon phantom to the real bladder remains uncertain. Other studies have analyzed the influence of volume differences on the bladder structure and found bladder deformation [38,39]. In our model, expansion of the bladder wall due to an increase in volume was not proportionate for all sides, probably due to pressure of the surrounding 'tissues'. Therefore, predicting the 3D position changes of lesions due to volume changes in the bladder remains difficult. Furthermore, the ease of use and duration of the surgical time, needs to be evaluated using this system.

We will perform an in vivo pilot study to test the feasibility of the bladder navigation and registration system, focusing on the 3D position change of different lesions (including the dome) after volume increase/decrease and bladder deformation. To analyze this using the current system, the bladder registration and navigation accuracy will be tested and compared using different fixed bladder volumes. This is a challenge during TURBT because the bladder is rinsed to prevent blood in the urine that limits vision. In the future, some analytical software adjustments might be developed when creating the bladder map for different volumes.

Registering the inspected parts of the bladder during cystoscopy will reduce the concern related to possibly overlooking a small part of the bladder that might contain a suspect lesion. Therefore, this system can be used as a quality control during urologic procedures; once feasibility has been demonstrated this should be tested. A prospective multi-center study is needed to measure the clinical feasibility of the bladder registration and navigation in urological practice and its inter-user variances. This proposed study will investigate whether the bladder registration and navigation system improves the reproducibility of the cystoscopy. Consequently, a reduction of residual and recurrent tumors due to better registration, follow up and more complete surgery of bladder lesions might be expected as a result. An improvement of disease-free survival will be the ultimate goal of implementing this clinical tool.

CONCLUSION

The bladder registration and navigation system was developed to improve the reproducibility of the cystoscopy by improved bladder tumor documentation according to tumor size, number, shape and especially location, in real-time during a cystoscopy. It is hoped that this will lead to a reduction in residual and recurrent tumors and,

consequently, to an improved disease-free survival. Because the system successfully functioned in its form for urological purposes in phantom models, it can now be used in clinical trials. In vivo tests will be performed at our department to examine feasibility for the urological clinic, focusing on the effects of volume differences and bladder deformation. Future studies are required to evaluate the ultimate goal: reduction in the number of residual and recurrent tumors and consequently improved disease-free survival.

ACKNOWLEDGEMENTS

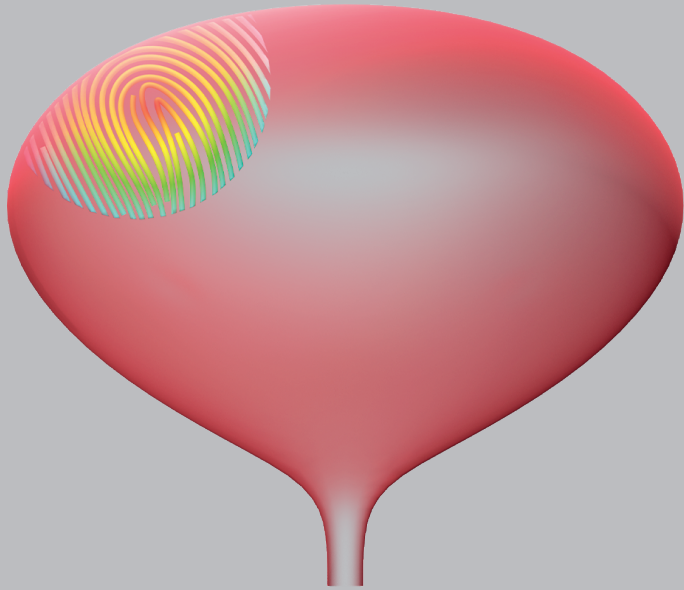
We would like to thank PS-tech for using their stereotracker and software and for their encouragement and guidance during this project. Furthermore, we would like to express our gratitude towards Froukje Euwe, Technical Developer at the UMCU, who helped developing the tracking targets.

REFERENCES

- 1 Siegel R, Ward E, Brawley O, Jemal A. Cancer statistics, 2011: the impact of eliminating socioeconomic and racial disparities on premature cancer deaths. *CA Cancer J Clin.* 2011 Aug;61(4):212–36.
- 2 Kirkali Z, Chan T, Manoharan M, Algaba F, Busch C, Cheng L, et al. Bladder cancer: epidemiology, staging and grading, and diagnosis. *Urology.* 2005 Dec;66(6 Suppl 1):4–34.
- 3 Babjuk M, Burger M, Comperat E, Gontero P, Liedberg F. EAU guidelines on Non-muscle-invasive Bladder Cancer (TaT1 and CIS). 2021 Apr Available from: <https://uroweb.org/wp-content/uploads/EAU-Guidelines-on-Non-muscle-invasive-Bladder-Cancer-TaT1-2021V2.pdf>
- 4 Hall RR, Parmar MK, Richards AB, Smith PH. Proposal for changes in cystoscopic follow up of patients with bladder cancer and adjuvant intravesical chemotherapy. *BMJ.* 1994 Jan;308(6923):257–60.
- 5 Palou J, Rodríguez-Rubio F, Millán F, Algaba F, Rodríguez-Faba O, Huguet J, et al. Recurrence at three months and high-grade recurrence as prognostic factor of progression in multivariate analysis of T1G2 bladder tumors. *Urology.* 2009 Jun;73(6):1313–7.
- 6 Sylvester RJ, Oosterlinck W, Witjes JA. The schedule and duration of intravesical chemotherapy in patients with non-muscle-invasive bladder cancer: a systematic review of the published results of randomized clinical trials. *Eur Urol.* 2008 Apr;53(4):709–19.
- 7 Weizer AZ, Tallman C, Montgomery JS. Long-term outcomes of intravesical therapy for non-muscle invasive bladder cancer. *World J Urol.* 2011 Feb;29(1):59–71.
- 8 Peyromaure M, Zerbib M. T1G3 transitional cell carcinoma of the bladder: recurrence, progression and survival. *BJU Int.* 2004 Jan;93(1):60–3.
- 9 Liu J-J, Droller MJ, Liao JC. New optical imaging technologies for bladder cancer: considerations and perspectives. *J Urol.* 2012 Aug;188(2):361–8.
- 10 Ramírez-Backhaus M, Domínguez-Escrig J, Collado A, Rubio-Briones J, Solsona E. Re-staging transurethral resection of bladder tumor for high-risk stage Ta and T1 bladder cancer. *Curr Urol Rep.* 2012 Apr;13(2):109–14.
- 11 Schwaibold HE, Sivalingam S, May F, Hartung R. The value of a second transurethral resection for T1 bladder cancer. *BJU Int.* 2006 Jun;97(6):1199–201.
- 12 Barkun JS, Aronson JK, Feldman LS, Maddern GJ, Strasberg SM, Balliol Collaboration, et al. Evaluation and stages of surgical innovations. *Lancet.* 2009 Sep;374(9695):1089–96.
- 13 Ergina PL, Cook JA, Blazeby JM, Boutron I, Clavien P-A, Reeves BC, et al. Challenges in evaluating surgical innovation. *Lancet.* 2009 Sep;374(9695):1097–104.
- 14 McCulloch P, Altman DG, Campbell WB, Flum DR, Glasziou P, Marshall JC, et al. No surgical innovation without evaluation: the IDEAL recommendations. *Lancet.* 2009 Sep;374(9695):1105–12.
- 15 A.J. Rhijn V. Configurable input devices for 3D interaction using optical tracking. 2007 DOI: 10.6100/IR616370
- 16 Hartley R, Zisserman A. *Multiple View Geometry in Computer Vision.* 2 edition. Cambridge, UK ; New York: Cambridge University Press; 2004.
- 17 Zhang Z. A flexible new technique for camera calibration. *IEEE Transactions on Pattern Analysis and Machine Intelligence.* 2000 Nov;22(11):1330–4.
- 18 Brown DC. Close-Range Camera Calibration. 12.

- 19 Cauberg Evelyne CC, de la Rosette JJMCH, de Reijke TM. Emerging optical techniques in advanced cystoscopy for bladder cancer diagnosis: A review of the current literature. *Indian J Urol*. 2011 Apr;27(2):245–51.
- 20 Dighe MK, Bhargava P, Wright J. Urinary bladder masses: techniques, imaging spectrum, and staging. *J Comput Assist Tomogr*. 2011 Aug;35(4):411–24.
- 21 Kagadis GC, Siablis D, Liatsikos EN, Petsas T, Nikiforidis GC. Virtual endoscopy of the urinary tract. *Asian J Androl*. 2006 Jan;8(1):31–8.
- 22 Karabacak OR, Cakmakci E, Ozturk U, Demirel F, Dilli A, Hekimoglu B, et al. Virtual cystoscopy: the evaluation of bladder lesions with computed tomographic virtual cystoscopy. *Can Urol Assoc J*. 2011 Feb;5(1):34–7.
- 23 Kim JK, Ahn JH, Park T, Ahn HJ, Kim CS, Cho K-S. Virtual cystoscopy of the contrast material-filled bladder in patients with gross hematuria. *AJR Am J Roentgenol*. 2002 Sep;179(3):763–8.
- 24 Kishore TA, George GK, Bhat S. Virtual cystoscopy by intravesical instillation of dilute contrast medium: preliminary experience. *J Urol*. 2006 Mar;175(3 Pt 1):870–4.
- 25 Kivrak AS, Kiresi D, Emlik D, Odev K, Kilinc M. Comparison of CT virtual cystoscopy of the contrast material-filled bladder with conventional cystoscopy in the diagnosis of bladder tumours. *Clinical Radiology*. 2009 Jan;64(1):30–7.
- 26 Song JH, Francis IR, Platt JF, Cohan RH, Mohsin J, Kielb SJ, et al. Bladder tumor detection at virtual cystoscopy. *Radiology*. 2001 Jan;218(1):95–100.
- 27 Yazgan C, Fitoz S, Atasoy C, Turkolmez K, Yagci C, Akyar S. Virtual cystoscopy in the evaluation of bladder tumors. *Clin Imaging*. 2004 Apr;28(2):138–42.
- 28 Avcu S, Koseoglu MN, Ceylan K, Bulut MD, Dbulutand M, Unal O. The value of diffusion-weighted MRI in the diagnosis of malignant and benign urinary bladder lesions. *Br J Radiol*. 2011 Oct;84(1006):875–82.
- 29 Gulsen F, Dikici S, Mihmanli I, Ozbayrak M, Onal B, Obek C, et al. Detection of bladder cancer recurrence with real-time three-dimensional ultrasonography-based virtual cystoscopy. *J Int Med Res*. 2011;39(6):2264–72.
- 30 Li Q, Tang J, He E, Li Y, Zhou Y, Zhang X, et al. Clinical utility of three-dimensional contrast-enhanced ultrasound in the differentiation between noninvasive and invasive neoplasms of urinary bladder. *Eur J Radiol*. 2012 Nov;81(11):2936–42.
- 31 Hung AJ, Ma Y, Zehnder P, Nakamoto M, Gill IS, Ukimura O. Percutaneous radiofrequency ablation of virtual tumours in canine kidney using Global Positioning System-like technology. *BJU Int*. 2012 May;109(9):1398–403.
- 32 Behrens A, Bommers M, Stehle T, Gross S, Leonhardt S, Aach T. Real-time image composition of bladder mosaics in fluorescence endoscopy. *Comput Sci Res Dev*. 2011 Feb;26(1):51–64.
- 33 Behrens A, Stehle T, Gross S, Aach T. Local and global panoramic imaging for fluorescence bladder endoscopy. *Conf Proc IEEE Eng Med Biol Soc*. 2009;2009:6990–3.
- 34 Behrens A, Grimm J, Gross S, Aach T. Inertial navigation system for bladder endoscopy. *Conf Proc IEEE Eng Med Biol Soc*. 2011;2011:5376–9.
- 35 Hernández-Mier Y, Blondel WCPM, Daul C, Wolf D, Guillemin F. Fast construction of panoramic images for cystoscopic exploration. *Comput Med Imaging Graph*. 2010 Oct;34(7):579–92.
- 36 Seshamani S, Lau W, Hager G. Real-time endoscopic mosaicking. *Med Image Comput Comput Assist Interv*. 2006;9(Pt 1):355–63.

- 37 Weibel T, Daul C, Wolf D, Rösch R, Ben-Hamadou A. Endoscopic bladder image registration using sparse graph cuts. 2010 IEEE International Conference on Image Processing. 2010; pp 157–60.
- 38 Lotz HT, Remeijer P, van Herk M, Lebesque JV, de Bois JA, Zijp LJ, et al. A model to predict bladder shapes from changes in bladder and rectal filling. *Med Phys*. 2004 Jun;31(6):1415–23.
- 39 Lotz HT, van Herk M, Betgen A, Pos F, Lebesque JV, Remeijer P. Reproducibility of the bladder shape and bladder shape changes during filling. *Med Phys*. 2005 Aug;32(8):2590–7.



CHAPTER 6

SUMMARY AND GENERAL CONCLUSION

RAMAN SPECTROSCOPY IN BLADDER CANCER DIAGNOSIS

SUMMARY AND GENERAL CONCLUSION

The main aim of this thesis is to understand the value of Raman spectroscopy for bladder cancer diagnosis and to find ways to improve its application. We evaluated a newly developed Raman probe in a phantom model and in vivo. We also used this probe to evaluate tissue heterogeneity in cystectomy specimens. As a spin-off to enable repeat Raman measurements of specific locations, a bladder registration and navigation tool was developed and we evaluated this in a phantom model.

In the introduction (**Chapter 1**) the standard diagnostic and treatment practice of bladder cancer (mostly urothelial carcinoma (UC)) is described. The background of Raman spectroscopy is explained and publications on the use of Raman spectroscopy in bladder cancer diagnosis are reviewed. In **Chapter 2** two different fiber optic probes are compared to each other in a phantom model. A superficial and non-superficial Raman probe are evaluated regarding depth response function and signal-to-noise ratio. As the urothelial layer is only 3-7 cell layers thick, which is about 200 micron, a probe should be aimed at this superficial layer in order to reduce the irrelevant response of deeper layers. The sampling range of the superficial probe was 0-200 micron and of the non-superficial probe 0-300 micron. In addition, the superficial probe had a two-times increased signal-to-noise ratio at a measurement depth of 200 micron. Therefore, this newly developed superficial Raman probe is expected to improve the urothelial cancer detection in vivo.

In **Chapter 3**, the superficial probe was compared to the non-superficial probe for in vivo measurements. In vivo Raman measurements were acquired during transurethral resection of a bladder tumor (TURBT) before resection and pathological evaluation. Newly acquired superficial probe measurements were compared to previous in vivo measurements obtained with the non-superficial probe [1]. The performance of the superficial probe for urothelial carcinoma detection was improved compared to the non-superficial probe; the area under the curve of the receiver operating characteristic curve increases from 0.88 to 0.95, the sensitivity from 80% to 90% and the specificity from 85% to 87%. This may partly be due to the improved signal-to-noise ratio of the superficial probe with a factor of 1.92 compared to the non-superficial probe, also described in chapter 2. Another explanation for this superior performance could be the limited measuring depth of the superficial probe in which the spectrum is not 'contaminated'

by Raman signals from deeper tissue layers. Although we observed clearly a qualitative improvement, we were not able to quantify this; further research is required to confirm this hypothesis. In chapter 3, the superficial probe was also evaluated in its capacity to distinguish different grades of UC. The ability to distinguish high-grade from low-grade UC was limited. We think that this might be due to tissue heterogeneity (sampling error), or due to a continuum of biochemical tumor characteristics that gradually increase when becoming more malignant in the development of UC.

Chapter 4 describes a spatial evaluation of bladder cancer using Raman spectroscopy in cystectomy specimens. A representation consisting of a 2D-map was created of the entire surface of three cystectomy specimens according to both the histopathologic analysis and its Raman spectrum for each measurement location. For tumor detection an AUC of 93%, sensitivity of 86% and specificity of 92% were obtained. The regions surrounding tumorous tissue showed to have a higher prediction uncertainty than the tumor itself and also the tissue further away from the tumor. Therefore, the Raman spectroscopy data suggested a gradual spatial transition from benign to malignant tissue. This may be explained by two theories; first tissue heterogeneity (sampling error), in which multiple cells in one tissue location are evaluated in one Raman spectrum and different biochemical compositions can be measured that belong to different pathologic entities. The second theory is based on the presence of a smooth transition of normal tissue into malignant tissue, meaning no hard cut-off between tumor and healthy tissue. Some (pre-)malignant changes were detected by Raman spectroscopy while not being obvious in the pathologic evaluation (using cut-off values for classification). Therefore, Raman spectroscopy may be used as an early indicator for progression or recurrence, and also as a more accurate way to describe the tumor boundary. If Raman spectroscopy could detect these (pre-) malignant changes, more accurate tumor resections could be performed, that could result in less residuals and recurrences.

A spin-off of this Raman spectroscopic research is presented in **Chapter 5**. Current diagnostic tools such as photodynamic diagnosis (PDD) can be used for screening an entire bladder for bladder malignancies. Techniques like this have a high sensitivity but lack specificity [2]. This means that many lesions are detected, and false positives are frequent, resulting in unnecessary resections of benign tissue in current standard practice. Raman spectroscopy can be used in combination with such a diagnostic screening tool to acquire optical biopsies at specific suspect locations, with a high specificity. To follow up specific lesions by Raman spectroscopy, we developed a real-time registration and navigation system. A repeat measurement at the exact location could possibly indicate a transition into malignancy in time and its need for resection at the right time. In this chapter, we present a phantom study of a real-time



bladder registration and navigation process. The newly developed system showed an acceptable accuracy for bladder lesion registration and navigation. The advantage of the developed system is that detection is not limited to lesions of >5 mm as in CT, MRI and/or sonography [3–13]. Also, no pre-operative imaging or artificial landmarks (fiducials) are required. This system can also be used in patients with severe hematuria that limits vision during cystoscopy or when the light is reduced as in PDD. We found some limitations such as limited accuracy due to volume changes of the model. In vivo studies are required to measure the feasibility of navigation with different bladder volumes and with different rectal filling statuses.

DISCUSSION, FUTURE PERSPECTIVES AND CONCLUSION

Instant optical biopsies in bladder cancer diagnosis

Diagnosing bladder cancer takes time. When a patient suffers from hematuria, a cystoscopy is performed in the outpatient clinic. A suspect lesion is detected, and then the patient is planned for a transurethral resection of a bladder tumor (TURBT). After approval of the anesthesiologist, the operation is performed, mostly within a few weeks. The resected tissue or biopsies are evaluated by the pathologist, which takes about 10 days. Eventually the patient has a doctor's appointment and starts the appropriate follow up and/or treatment scheme after about a month or more. When an instant biopsy is performed at the outpatient clinic, a lot of time and costs are saved and possibly unnecessary treatments are avoided. Obtaining a direct diagnosis at the outpatient clinic enables decisions such as following up lesions instead of direct resections, planning postoperative chemotherapeutic instillations or direct upstaging to cystectomy without TURBT. Such an instant biopsy should be highly specific and easily tolerated by the patient in that specific office setting.

Endoscopic Raman spectroscopy is such a technique, that is both non-invasive and highly specific by revealing the biochemical substrate of lesions. The biggest obstacle in the utilization of Raman spectroscopy in clinical practice is that the signal from Raman scattering is very weak, one in 10^6 - 10^8 scattering photons. This inefficient scattering requires a high laser power and long acquisition times [14]. Translation and implementation into the clinic is consequently hampered. Compromises to reduce acquisition times can decrease the diagnostic accuracy. Nevertheless, new strategies are being developed to address this limitation. Hardware developments to improve collection of the Raman signal but also software developments such as different analytical methods are being evaluated to improve the diagnostic ability of Raman spectroscopy. Imaging modalities based on non-linear Raman scattering, multimodal

integration of Raman spectroscopy and selective-sampling Raman Microscopy (RM), are tools to empower Raman spectroscopy. In addition, the use of nanomaterials and photonic structures to enhance the Raman signals are being evaluated. New analysis methods that are being explored include Artificial Intelligence techniques such as Deep Convolutional Neural Networks and Spatial bagging [15,16]. All these accomplishments are important steps toward maximizing the diagnostic accuracy and speed of Raman spectroscopy. Further improvement will lead to more cost-effective solutions that are likely to be adopted into clinical practice [17].

In this thesis, a hardware design to improve signal collection is evaluated. A new superficial Raman probe was developed that is biocompatible, complies with the Medical Device Directive requirements and is suitable for endoscopic evaluation. This superficial probe is aimed at the required measurement depth and with an increased signal-to-noise ratio, compared to a non-superficial probe. Also, signals generated from the probe, silica in this case, do not interfere with the Raman signal of urothelium, as opposed to the substance of other beveled or ball lens probes that have a limited field (and depth) of view. The measurement depth and increase in signal-to-noise ratio were confirmed in both the phantom model and the in vivo evaluation (chapter 2 and chapter 3). The use of Raman spectroscopy to discriminate benign from malignant tissue was shown to be adequate in chapter 3; however, discrimination between different grades of UC was limited in the in vivo study. This could be explained by tissue heterogeneity or a transition into malignancy. To adopt this technique into the outpatient clinic, adjustments should be made to enable use of the Raman probe through a flexible cystoscope.

To improve the diagnostic ability of Raman spectroscopy, more than just hardware and software improvements are required. Sufficient data is necessary to improve the Raman spectroscopic knowledge on bladder cancer. In future, a spatial micro-Raman analysis using a more dense measurement grid with automated placement of the probe on a cystectomy specimen, could evaluate the impact of tissue heterogeneity in UC. Generation of a larger multi-center database of Raman measurements and biopsies of different UC entities (more power) could increase the diagnostic accuracy of Raman spectroscopy, because the diagnostic algorithm is based on prior Raman measurements. Knowledge about specific Raman contributions of certain biochemical tumor compositions, linked to their corresponding biochemical alterations, provides information about tumor biology.

Raman characteristics of disagreeing Raman and pathological classification in one tissue location gives insight into the biochemical substrate responsible for a transition into

malignancy. These findings could consecutively lead to more therapeutic targets in bladder cancer treatment or be the basis of research on bladder cancer (recurrence or progression) prevention. Because Raman spectroscopy determines a biological fingerprint of tissue without necessity of human interpretation, this technique could possibly overcome some inter- and intra-observer variability of the pathologist. Raman spectroscopy measures biochemical characteristics as opposed to the histopathologic analysis, which assesses morphologic and histopathologic characteristics. Maybe the poor reproducibility of the histopathological analysis could be resolved by adding Raman spectroscopy to this analysis.

Finally, if Raman spectroscopy generates an instant optical biopsy with high accuracy and is applicable in the outpatient clinic, immediate treatment decisions could be made as described above. When a lesion requires follow up, the exact same location should be evaluated again at follow-up. Bladder registration and navigation would enable such repeat measurements. In combination with deep learning augmented bladder tumor detection, the accuracy of the navigation systems and reproducibility of cystoscopy can be improved. Also, quality verification of cystoscopies could be accomplished by improving the documentation of findings during cystoscopy by such a system. Nevertheless, this registration and navigation system is still in its infancy. Combinations of techniques should be explored in future clinical studies.

Other Raman spectroscopic applications in bladder cancer

As described in chapter 1, more implementations of Raman spectroscopy in bladder cancer diagnosis are under development, such as evaluation of urine or serum constituents. Raman spectroscopy on urine samples is being evaluated to detect early recurrences. Alternatives to urine cytology and repeat cystoscopy in the follow up of UC, are being searched for. High sensitivities, specificities and accuracies of Raman spectroscopy on urine have been presented [15,16,18–23]. However, none of these has been implemented in standard care. All these cystoscopies are invasive and not cost-effective and the patient waiting lists are increasing. A paradigm shift is required in favor of the diagnostic costs, time and complications of cystoscopy and cytology that may cause a few more false negative findings which could be registered to avoid unnecessary biopsies.

Alternative applications of Raman spectroscopy are being investigated in basic research. Several studies were designed to evaluate bladder tumor specific biomarkers by (Surface Enhanced) Raman spectroscopy (SERS). For example, anti EGFR antibody, circulating cancer-derived small extracellular vesicles, Alfa-1-Antitrypsin antigen and Hyaluronic acid-ase and telomerase activity were investigated to enable tumor detection in urine.

In the future, detection of these biomarkers by Raman spectroscopy could be used as an alternative to urine cytology [24–29]. In search for alternatives to urine cytology, other biomarkers are also being investigated. For example Circulating Tumor Cells, urinary long non-coding RNA's (prognostic marker for Non Muscle Invasive Bladder Carcinoma (NMIBC)), neutrophil-to-lymphocyte ratio (prognostic prediction marker in primary T1HG UC), and systematic inflammatory biomarkers that are related to the oncological outcomes in patients with high-risk NMIBC, are being explored [30–34]. In the future, Raman spectroscopy could be used as a tool to enable detection of such markers.

Raman spectroscopy was also used to evaluate bladder cancer detection in serum, another form of liquid biopsy [35,36]. Interesting is that these groups evaluated whether serum samples could detect NMIBC and Muscle-Invasive Bladder Cancer (MIBC), while logically when the disease is limited to the bladder, no cancerous characteristics would be detectable in serum. In contrast, when (micro) metastasis are present these would be detectable in serum as they can be spread by serum. This indicates another application for Raman spectroscopy; a detection tool of (micro-)metastasis that are not detectable by regular imaging, which is vital for the appropriate treatment. The 5-year overall survival rate after cystectomy is about 50% and has not improved in the last decades [37,38]. Many patients die because of preoperatively undetected micro-metastasis. Therefore, more research should be performed on detection of micro-metastasis in serum pre-cystectomy, and Raman spectroscopy is an adequate tool.

To improve outcomes of this patient group, a response prediction to (neo-)adjuvant therapy (chemo- or immunotherapy) is important. When patients are unresponsive to neo-adjuvant therapy, cystectomy is delayed while the tumor has more time to advance and metastasize. Raman spectroscopy might enable detection of specific tumor characteristics that predict an adequate response to (neo-)adjuvant therapy to choose the correct (neo-)adjuvant therapy or omit this therapy. One point of interest is the amount and kind of inflammation present in the tumor and serum. This might be related to the response of the immune system to tumorigenesis. Maybe the kind and amount of inflammation, detectable by Raman spectroscopy could be prognostic for the progression of the tumor, or the response to immunotherapy.

Raman spectroscopy is also being investigated for detection of biochemical processes in bladder tumor development. Raman spectroscopy enables detection of Green Fluorescent Protein in bladder cancer cell lines. The corresponding gene is used as tool in gene engineering for determining changes in function or expression to evaluate cellular biology, especially of gene silencing [39]. In another study, SERS was used



to evaluate leak-resistance DNA hybridization chain reaction in urine samples. This detection is an important tool in DNA nanotechnology studies to gain information about DNA breakage in tumor development [40]. Also, SERS was used to detect an enhanced surface permeability and retention effect in human bladder cancer tissue [41]. Finally, preliminary results have been published on using Raman spectroscopy for detection of intracellular nano-transporters that could contain therapeutic and/or imaging agents, to enable targeted drug delivery in the field of oncology [42].

CONCLUSION

In this thesis improvements for the clinical application of Raman spectroscopy are being evaluated. The way is being smoothed for the use of Raman spectroscopy in bladder cancer diagnosis *in vivo*.

Non-invasive bladder cancer diagnosis is an ongoing challenge, because the gold standard cystoscopy and TURBT are invasive procedures and are timely and costly. Raman spectroscopy is a powerful analytical method that enables measurements of chemical compounds in complex biological samples, such as cells, tissues and biological fluids. The equipment for *in vivo* measurements has been developed, but the system is not yet applicable in the outpatient clinic with flexible cystoscopes. When discriminating malignant from benign tissue or cells, high accuracy rates are achieved. For liquid biopsies, Raman spectroscopy outperforms the current standard pathologic urine cytology. Furthermore, Raman spectroscopy has an added value in basic research. Thus, Raman spectroscopy has many opportunities and more research is required to increase the ease of clinical use and applicability in order to improve the quality of bladder cancer diagnosis.

SAMENVATTING EN ALGEMENE CONCLUSIE (DUTCH)

Het belangrijkste doel van dit proefschrift is de waarde van Ramanspectroscopie in blaaskanker diagnostiek te begrijpen en manieren te vinden om de toepassing te verbeteren. Wij evalueerden een nieuw ontwikkelde Ramanprobe in een fantoommodel en in vivo. We gebruikten deze probe ook om weefselheterogeniteit te onderzoeken in cystectomiepreparaten. Als spin-off, om herhaalde Ramanmetingen te kunnen doen op specifieke locaties, ontwikkelden we een blaasregistratie en navigatiesysteem en evalueerden we dit systeem in een fantoommodel.

In de introductie (**Hoofdstuk 1**) wordt de standaard diagnostiek en behandeling van blaaskanker (urotheelcarcinoom (UC)) beschreven. De achtergrond van Ramanspectroscopie wordt besproken en we beoordeelden de publicaties over het gebruik van Ramanspectroscopie in blaaskankerdiagnostiek. In **Hoofdstuk 2** worden twee verschillende fiber-optische probes geëvalueerd en vergeleken met elkaar in een fantoommodel. Een oppervlakkige en een niet-oppervlakkige Ramanprobe worden geëvalueerd met betrekking tot de signaaldiepte en signaal-ruis verhouding. Omdat de urotheellaag maar 3-7 cellagen dik is, ongeveer 200 micron, zou een probe gericht moeten zijn op de oppervlakkige laag, om het irrelevante signaal van diepere lagen te beperken. De signaaldiepte van de oppervlakkige probe was 0-200 micron, terwijl de signaaldiepte van de niet-oppervlakkige probe 0-300 micron was. Hiernaast had de oppervlakkige probe ook een tweemaal zo hoge signaal-ruis verhouding bij meting op 200 micron diepte. Om deze reden verwachten we dat de nieuw ontwikkelde oppervlakkige Ramanprobe een betere in vivo urotheelcarcinoom detectie zal hebben.

In **Hoofdstuk 3** wordt de oppervlakkige probe met de niet-oppervlakkige probe vergeleken bij in vivo metingen. In vivo Ramanmetingen werden verricht tijdens een transurethrale resectie van een blaastumor (TURBT) voorafgaand aan de resectie en pathologische evaluatie. Nieuw verkregen oppervlakkige probe metingen werden vergeleken met eerder verkregen in vivo metingen van de niet-oppervlakkige probe [1]. De kwaliteit (performance) van de oppervlakkige probe voor UC detectie was beter in vergelijking met de niet-oppervlakkige probe op verschillende kwaliteitsparameters; de oppervlakte onder de curve van de receiver operating characteristic curve (wat is een maat berekend uit het aantal echte-positieven en vals-positieven) verbeterde van 0.88 naar 0.95, de sensitiviteit van 80% naar 90% en de specificiteit van 85% naar 87%. Dit kan deels verklaard worden door de verbeterde signaal-ruis verhouding van de oppervlakkige probe met een factor van 1.92 vergeleken met de niet-oppervlakkige probe, vergelijkbaar met de resultaten van hoofdstuk 2. Een andere verklaring voor deze superieure prestatie kan de beperkte signaaldiepte van de oppervlakkige probe

zijn, waarbij het spectrum niet "vervuild" wordt door Ramansignalen van diepere weefsellagen. Ondanks dat we een duidelijke kwalitatieve verbetering zagen, konden we dit niet kwantificeren; verder onderzoek is nodig om deze hypothese te bevestigen. In hoofdstuk 3 wordt de oppervlakkige probe ook geëvalueerd in zijn capaciteit om verschillende graden UC te kunnen onderscheiden. Hooggradig UC was niet duidelijk van laaggradig UC te onderscheiden op basis van de Ramanmetingen. Wij denken dat dit te verklaren is door weefselheterogeniteit (sampling error), of doordat de biochemische karakteristieken van weefsel geleidelijk van benigne naar maligne veranderen in de ontwikkeling van UC.

Hoofdstuk 4 beschrijft een ruimtelijke evaluatie van blaaskanker met het gebruik van Ramanspectroscopie op cystectomiepreparaten. Een representatie van het gehele oppervlakte van drie cystectomiepreparaten wordt gepresenteerd in een 2D-kaart overeenkomstig met de histopathologische diagnose en de Ramanuitkomst voor elke meetlocatie. Voor tumordetectie werden een AUC van 93%, sensitiviteit van 86% en specificiteit van 92% behaald. De regio's rondom tumorweefsel lieten een hogere Ramandiagnose-onzekerheid zien dan de tumor zelf en weefsel verder weg van de tumor. Daarom suggereert deze Ramanspectroscopiedata een geleidelijke ruimtelijke verandering van benigne naar maligne weefsel. Dit kan verklaard worden door twee theorieën; De eerste is weefsel heterogeniteit (sampling error), waarbij meerdere cellen in een weefsel locatie worden geëvalueerd in een Ramanspectrum. Hierbij worden verschillende biochemische composities gemeten die toebehoren aan verschillende pathologische entiteiten. De tweede theorie is gebaseerd op de aanwezigheid van een geleidelijke overgang van normaal weefsel naar maligne weefsel, wat betekent dat er geen harde afkapwaarden zijn tussen tumor en normaal weefsel. Sommige (pre-) maligne veranderingen worden dan gedetecteerd door Ramanspectroscopie, terwijl ze nog niet duidelijk zijn in de pathologische evaluatie (die harde afkapwaarden gebruikt voor de classificatie). Daarom zou Ramanspectroscopie gebruikt kunnen worden als een vroege indicator voor progressie of recidief, en ook als een meer accurate manier om de tumorgrens te markeren. Als Ramanspectroscopie deze (pre-) maligne veranderingen detecteert, kunnen meer accurate resecties worden verricht welke kunnen leiden tot minder residuen en recidieven.

Een spin-off van dit Ramanspectroscopie onderzoek wordt gepresenteerd in **Hoofdstuk 5**. Huidige diagnostische hulpmiddelen zoals phothodynamische diagnostiek (PDD) worden gebruikt om een gehele blaas te beoordelen om blaaskanker te detecteren. Technieken zoals deze hebben een hoge sensitiviteit maar hebben een beperkte specificiteit [2]. Dit betekent dat veel afwijkingen worden gedetecteerd, maar dat vals positieven vaak voorkomen wat resulteert in onnodige resecties van benigne

weefsel in de huidige urologische praktijk. Ramanspectroscopie kan worden gebruikt in combinatie met zulke technieken als diagnostisch screeningstool om een optisch biopt te verkrijgen op specifieke verdachte locaties, met een hoge specificiteit. Om specifieke locaties te vervolgen met Ramanspectroscopie is een real-time registratie en navigatie systeem ontwikkeld. Herhaalde metingen op specifieke locaties zouden een verandering naar maligniteit in tijd kunnen aantonen zodat deze gereceerd kan worden op het juiste moment. In dit hoofdstuk presenteren we een fantoom studie met dit real-time blaasregistratie en navigatieproces. Het nieuw ontwikkelde systeem liet een acceptabele nauwkeurigheid zien voor blaasafwijkingregistratie en navigatie. Het voordeel van het ontwikkelde systeem is dat de detectie niet wordt gelimiteerd tot afwijkingen van >5 mm, zoals bij CT, MRI en/of echografie [3–13]. Tevens zijn er geen pre-operatieve beeldvormingstechnieken of kunstmatige oriëntatiepunten nodig. Dit systeem zou eventueel ook kunnen worden gebruikt in patiënten met ernstige hematurie, die het zicht belemmert tijdens cystoscopie of als het licht wordt gereduceerd zoals tijdens PDD. We constateerden beperkingen zoals verminderde nauwkeurigheid bij volumeveranderingen van het model. In vivo studies zijn nodig om de haalbaarheid van navigatie te beoordelen met verschillende blaasvolumina en verschillende rectale vullingstadia.

DISCUSSIE, TOEKOMSTPERSPECTIEVEN EN CONCLUSIE

Directe optische biopten in blaaskanker diagnostiek

Blaaskankerdiagnostiek kost tijd. Als een patiënt bloed plast (hematurie heeft) wordt een cystoscopie verricht op de polikliniek. Wanneer een verdachte afwijking wordt gedetecteerd tijdens cystoscopie, wordt de patiënt ingepland voor een transurethrale resectie van de blaastumor (TURBT). Na akkoord van de anesthesioloog wordt de operatie uitgevoerd, meestal binnen een aantal weken. Het gereceerde weefsel of de biopten worden beoordeeld door de patholoog, wat ongeveer 10 dagen tijd kost. Uiteindelijk komt de patiënt bij de uroloog voor de uitslag en wordt het vervolg plan opgesteld, dat kan bestaan uit follow up of aanvullende behandelingen. Vanaf het eerste polikliniek bezoek tot de definitieve therapie zal het in totaal ongeveer een maand of meer duren. Als een direct biopt op de polikliniek afgenomen zou kunnen worden, worden veel tijd, kosten en mogelijk onnodige behandelingen bespaard. Een direct optisch biopt op de polikliniek kan leiden tot een langer afwachtend beleid, voorafgaand inplannen van de juiste blaasspoelingen postoperatief of directe upstaging naar cystectomy, waarbij een TURBT niet meer nodig is. Zo een biopt zal moeten voldoen aan bepaalde eisen zoals hoge specificiteit en goede tolerantie voor de patiënt op de polikliniek.



Endoscopische Ramanspectroscopie is een dergelijke techniek, die niet-invasief is met hoge specificiteit waarmee van de biochemische achtergrond van een afwijking bepaald kan worden. Het grootste obstakel voor het gebruik van Ramanspectroscopie in de klinische praktijk is dat het signaal van Raman scattering erg zwak is, een van de 10^6 - 10^8 verstrooide fotonen. Deze inefficiënte scattering zorgt ervoor dat een hoog laser vermogen en lange acquisitietijden nodig zijn [14]. Hierdoor wordt de translatie en implementatie naar de klinische praktijk gehinderd. Compromissen om de acquisitietijden te verkorten, resulteren in een verlaagde diagnostische nauwkeurigheid. Nieuwe strategieën om deze beperkingen tegen te gaan, zijn in ontwikkeling. Hardware ontwikkelingen voor verbeterde ontvangst van het Ramansignaal, maar ook softwareontwikkelingen zoals verschillende analytische methoden, worden door verschillende groepen geëvalueerd om de diagnostische mogelijkheden van Ramanspectroscopie te verbeteren. Beeldvorming modaliteiten gebaseerd op niet-lineaire Raman scattering, multimodale integratie van Ramanspectroscopie en selectieve sampling van Raman Microscopie (RM), zijn hulpmiddelen om Ramanspectroscopie te verbeteren. Hiernaast worden ook nanomaterialen en fotonische structuren geëvalueerd om het Ramansignaal te vergroten. Nieuw analysemethoden worden verkend waaronder artificiële intelligentie technieken zoals Deep Convolutional Neural Networks en Spatial Bagging [15,16]. Al deze ontwikkelingen zijn belangrijke stappen op weg naar verbetering van de diagnostische nauwkeurigheid en snelheid van Ramanspectroscopie. Verdere verbeteringen moeten ook leiden tot betere kosteneffectiviteit, waardoor Ramanspectroscopie gemakkelijker in klinische praktijk geïmplementeerd kan worden [17].

In dit proefschrift wordt een nieuw hardware ontwerp geëvalueerd, met als doel verbeterde signaalontvangst. Een nieuwe oppervlakkige Ramanprobe voor klinisch gebruik werd ontwikkeld die voldoet aan de Medical Device Directives vereisten en geschikt is voor endoscopisch gebruik. Deze oppervlakkige probe is gericht op de benodigde signaaldiepte en heeft een hogere signaal-ruis verhouding dan de niet-oppervlakkige probe. Hiernaast interfereren de componenten (waaronder silica) niet met het Ramansignaal van urotheel, in tegenstelling tot de componenten van andere probes met afgeschuinde of bal lenzen ten behoeve van een oppervlakkige meting. De signaaldiepte en verbeterde signaal-ruis verhouding werden bevestigd in de evaluatie met het fantoom model maar ook in vivo (hoofdstuk 2 en 3). Het was goed mogelijk om met behulp van Ramanspectroscopie benigne van maligne weefsel te onderscheiden in hoofdstuk 3; maar onderscheiden van verschillende graderingen van UC was beperkt in de in vivo studie. Dit kan worden verklaard door weefsel heterogeniteit of een transitie naar maligniteit. Om deze techniek toe te passen op de polikliniek zullen aanpassingen nodig zijn om de probe door een flexibele cystoscoop te kunnen laten passeren.

Om de diagnostische mogelijkheden van Ramanspectroscopie te verbeteren zijn meer dan alleen hardware- en softwareverbeteringen nodig. Voldoende data is nodig om de Ramanspectroscopische kennis van blaaskanker te ontwikkelen. De impact van weefsel heterogeniteit van UC kan in de toekomst geëvalueerd worden middels een ruimtelijke micro-Ramananalyse. Hierbij wordt gebruikt gemaakt van een meetrooster waarbij de verschillende metingen dichter op elkaar worden verricht met automatische plaatsing van de probe op een cystectomie preparaat. Ontwikkeling van een grote multicenter database van Ramanmetingen en biopten van verschillende UC entiteiten (meer power) kan de diagnostische nauwkeurigheid van Ramanspectroscopie verbeteren omdat het diagnostische algoritme is gebaseerd op eerdere Ramanmetingen. Kennis over specifieke Raman eigenschappen van bepaalde biochemische tumor samenstellingen, gelinkt aan de bijpassende biochemische veranderingen, geeft informatie over de tumorbiologie.

Raman karakteristieken van weefsel locaties waarbij de classificatie tussen Ramanspectroscopie en de pathologische evaluatie niet overeen komt, kunnen inzicht geven in het biochemische substraat dat verantwoordelijk is voor de verandering in maligniteit. Hieruit zouden therapeutische aangrijpingspunten voor blaaskankerbehandeling afgeleid kunnen worden. Tevens kan dit de basis zijn voor onderzoek naar preventie van blaaskanker recidieven of progressie. Omdat Ramanspectroscopie de biologische vingerafdruk van weefsel bepaalt, waarbij geen menselijke interpretaties nodig zijn, heeft deze techniek geen last van de inter- en intra-observer variabiliteit die inherent is aan de pathologische evaluatie. Ramanspectroscopie meet biochemische eigenschappen, in tegenstelling tot pathologische analyse die gebaseerd is op morfologische en histopathologische eigenschappen. De reproduceerbaarheid van de pathologische analyse zou mogelijk kunnen verbeteren als Ramanspectroscopie geïncorporeerd wordt in de pathologische analyse.

Tenslotte, als een direct optisch biopt mogelijk zou zijn op de polikliniek met een hoge nauwkeurigheid, zoals we verwachten van Ramanspectroscopie, kunnen directe behandelingsbeslissingen genomen worden zoals hierboven beschreven. Als een blaasafwijking vervolgd dient te worden, moet de exact zelfde locatie steeds beoordeeld worden. Een navigatie systeem voor blaasafwijkingen, zou in combinatie met deep learning augmented blaas tumor detectie, de nauwkeurigheid van navigatie systemen en de reproduceerbaarheid van cystoscopie kunnen verbeteren. Tevens kan de kwaliteit van cystoscopieën geverifieerd worden door middel van navigatie systemen en deze systemen zouden een rol kunnen spelen in de documentatie van cystoscopie bevindingen. Echter het beschreven registratie en navigatie systeem staat nog in de



kinderschoenen. Combinaties van verschillende navigatie technieken moeten worden verkend in verdere klinische studies.

Andere Raman spectroscopische toepassingen voor blaaskanker

Zoals beschreven in hoofdstuk 1, worden er in de huidige literatuur meer toepassingen van Ramanspectroscopie in blaaskanker diagnostiek onderzocht zoals de evaluatie van urine of serum bestanddelen. Ramanspectroscopie op urinemonsters wordt onderzocht om vroege recidieven op te sporen. We zoeken alternatieven voor urinecytologie en follow-up cystoscopieën. Hoge sensitiviteit, specificiteit en nauwkeurigheid van Ramanspectroscopie op urinemonsters worden gepresenteerd [15,16,18–23]. Echter is Ramanspectroscopie nog niet geïmplementeerd in de standaard blaaskankerdiagnostiek. De vele cystoscopieën zijn invasief en niet kosteneffectief en bovendien nemen de wachtlijsten toe. Een paradigma verandering is nodig om de diagnostische kosten, tijd en complicaties van cystoscopieën en cytologie te beperken, zodat ook niet klinisch relevante, vals positieve bevindingen geregistreerd kunnen worden en niet onnodig opnieuw gebiopteerd worden.

Alternatieve toepassingen worden geëxploreerd in basaal onderzoek. Verschillende studies zijn uitgevoerd om blaastumor specifieke biomarkers middels (Surface Enhanced) Raman spectroscopy (SERS) te detecteren. Voorbeelden van specifieke biomarkers om tumoren te detecteren in urine zijn: anti-EGFR antilichaam, circulating cancer-derived small extracellular vesicles, Alfa-1-Antitrypsin antigen en Hyaluron acid-ase en telomerase activiteit. In de toekomst zou cytologie vervangen kunnen worden door detectie van deze biomarkers [24–29]. In de zoektocht naar alternatieven voor urinecytologie, worden ook andere biomarkers onderzocht. Voorbeelden van deze biomarkers zijn; Circulating Tumor Cells, urinary long-coding RNA's (prognostische marker voor niet-spier-invasief blaascarcinoom (NMIBC)), neutrofiel-lymfocyt ratio (prognostische marker voor primair T1 hooggradig UC) en systemische inflammatie biomarkers die worden gerelateerd aan de oncologische uitkomsten van patiënten met hoog risico NMIBC [30–34]. In de toekomst zou Ramanspectroscopie ingezet kunnen worden om dit soort biomarkers te detecteren.

Ramanspectroscopie voor blaaskankerdetectie, wordt in bepaalde onderzoeken ook toegepast op serum, een andere vorm van een vloeibaar biopt [35,36]. Interessant is dat deze groepen NMIBC en spier invasief blaas carcinoom (MIBC) konden detecteren in het bloed, terwijl logischerwijs, als de ziekte beperkt is tot de blaas, geen kanker karakteristieken gevonden zouden moeten kunnen worden in het bloed. Omgekeerd, als (micro-)metastasen aanwezig zijn, zullen deze ook detecteerbaar kunnen zijn in serum omdat ze worden verspreid via het serum. Hierdoor ontstaat een nieuwe toepassing van

Ramanspectroscopie in blaaskankerdiagnostiek; als detectiehulpmiddel voor (micro-) metastasen, die niet te detecteren zijn middels reguliere beeldvormingstechnieken. Dit is belangrijk voor het kiezen van de juiste behandeling. De 5-jaars mortaliteit na cystectomie is ongeveer 50% en is onveranderd gedurende de laatste tientallen jaren [37,38]. Veel van deze patiënten overlijden door preoperatief niet-gedetecteerde (micro-) metastasen. Om deze reden is het nodig om meer onderzoek te doen naar detectie van (micro-) metastasen in serum vooraf aan cystectomie, wat middels Ramanspectroscopie mogelijk zou zijn.

Om de uitkomsten van deze patiëntengroep te verbeteren, is het ook belangrijk om te kunnen voorspellen wat de respons zal zijn op (neo-)adjuvante chemo- of immunotherapie. Als patiënten geen respons hebben op neo-adjuvante therapie, wordt de cystectomie ongewenst uitgesteld omdat de tumor dan meer tijd heeft om te verspreiden en metastaseren. Ramanspectroscopie zou bepaalde tumor karakteristieken kunnen detecteren die kunnen voorspellen wat de respons zal zijn op de (neo-)adjuvante therapie waardoor een keuze gemaakt kan worden voor het soort (neo-)adjuvante therapie of afgezien kan worden van de therapie. Een aangrijpingspunt kan het soort inflammatie in de tumor of serum zijn. Dit kan gerelateerd zijn aan de respons van het immuunsysteem op tumorgenese. Het soort en de kwantiteit van de inflammatie die gedetecteerd zou kunnen worden door Ramanspectroscopie kan een prognostische factor voor tumorprogressie zijn of voor de respons op immunotherapie.

Ramanspectroscopie wordt ook gebruikt om biochemische processen in blaastumor ontwikkeling te evalueren. Green Fluorescent Protein kan door Ramanspectroscopie worden gedetecteerd in blaaskanker cellijnen. Het corresponderende gen wordt gebruikt in gene engineering om bepaalde veranderingen in functie of expressie te kunnen detecteren binnen de celbiologie, speciaal voor gene silencing [39]. In een andere studie wordt SERS gebruikt om leak-resistance DNA hybridization chain reaction in urinemonsters te evalueren. Deze detectie is een belangrijk hulpmiddel in DNA nanotechnologie studies, om meer informatie te genereren over DNA breakage in tumorontwikkeling [40]. SERS wordt ook gebruikt om een enhanced surface permeability en retention effect in menselijk blaaskankerweefsel te detecteren [41]. Ten slotte, zijn er eerste resultaten gepubliceerd over het gebruik van Ramanspectroscopie voor de detectie van intracellulaire nano-transporters, die bestanddelen kunnen bevatten voor therapeutische targeted drug delivery of voor beeldvormende doeleinden binnen de oncologie [42].



CONCLUSIE

In dit proefschrift worden verbeteringen voor de klinische toepassing van Ramanspectroscopie geëvalueerd. Belangrijke stappen worden gemaakt voor het gebruik van Ramanspectroscopie bij blaaskankerdiagnostiek in vivo. Niet-invasieve blaaskankerdiagnostiek is een voortdurende uitdaging omdat de gouden standaarden, cystoscopie en TURBT, invasieve procedures zijn die veel tijd en geld kosten. Ramanspectroscopie is een veelbelovende analytische methode die de chemische bestanddelen in complexe biologische samenstellingen kan meten, zoals cellen, weefsel en biologische vloeistoffen. Wij hebben faciliteiten voor in vivo metingen ontwikkeld, maar het systeem is nog niet bruikbaar op de polikliniek met flexibele cystoscopen. Bij het onderscheiden tussen benigne en maligne cellen wordt een hoge nauwkeurigheid behaald. Voor vloeistofbiopten, zijn de resultaten beter dan de huidige standaard pathologische urine cytologie. Tevens heeft Ramanspectroscopie een rol in basaal onderzoek. Concluderend kan Ramanspectroscopie op vele manieren een rol hebben in onderzoek naar blaaskanker. Verdere studies zijn nodig om de klinische toepasbaarheid te verbeteren ten behoeve van de verbetering van blaaskankerdiagnostiek.

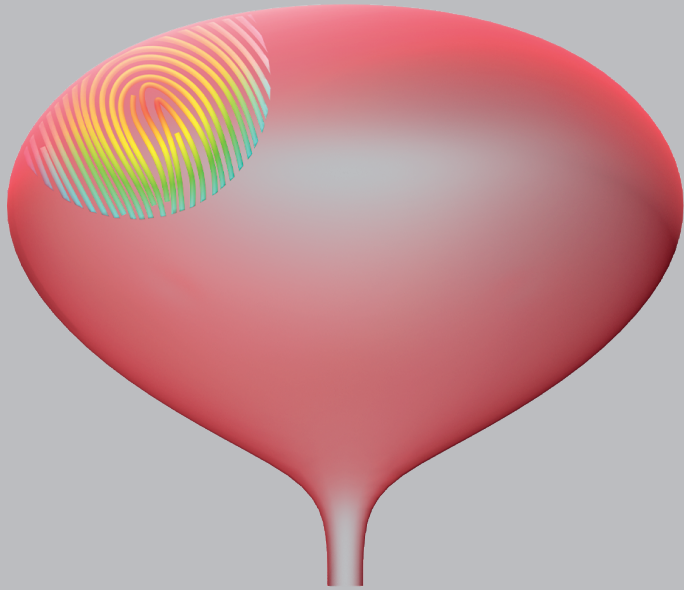
REFERENCES

- 1 Draga ROP, Grimbergen MCM, Vijverberg PLM, van Swol CFP, Jonges TGN, Kummer JA, et al. In vivo bladder cancer diagnosis by high-volume Raman spectroscopy. *Anal Chem*. 2010 Jul;82(14):5993–9.
- 2 Cauberg Evelyne CC, de la Rosette JJMCH, de Reijke TM. Emerging optical techniques in advanced cystoscopy for bladder cancer diagnosis: A review of the current literature. *Indian J Urol IJU J Urol Soc India*. 2011 Apr;27(2):245–51.
- 3 Dighe MK, Bhargava P, Wright J. Urinary bladder masses: techniques, imaging spectrum, and staging. *J Comput Assist Tomogr*. 2011 Aug;35(4):411–24.
- 4 Kagadis GC, Siablis D, Liatsikos EN, Petsas T, Nikiforidis GC. Virtual endoscopy of the urinary tract. *Asian J Androl*. 2006 Jan;8(1):31–8.
- 5 Karabacak OR, Cakmakci E, Ozturk U, Demirel F, Dilli A, Hekimoglu B, et al. Virtual cystoscopy: the evaluation of bladder lesions with computed tomographic virtual cystoscopy. *Can Urol Assoc J J Assoc Urol Can*. 2011 Feb;5(1):34–7.
- 6 Kim JK, Ahn JH, Park T, Ahn HJ, Kim CS, Cho K-S. Virtual cystoscopy of the contrast material-filled bladder in patients with gross hematuria. *AJR Am J Roentgenol*. 2002 Sep;179(3):763–8.
- 7 Kishore TA, George GK, Bhat S. Virtual cystoscopy by intravesical instillation of dilute contrast medium: preliminary experience. *J Urol*. 2006 Mar;175(3 Pt 1):870–4.
- 8 Kivrak AS, Kiresi D, Emlik D, Odev K, Kilinc M. Comparison of CT virtual cystoscopy of the contrast material-filled bladder with conventional cystoscopy in the diagnosis of bladder tumours. *Clin Radiol*. 2009 Jan;64(1):30–7.
- 9 Song JH, Francis IR, Platt JF, Cohan RH, Mohsin J, Kielb SJ, et al. Bladder tumor detection at virtual cystoscopy. *Radiology*. 2001 Jan;218(1):95–100.
- 10 Yazgan C, Fitoz S, Atasoy C, Turkolmez K, Yagci C, Akyar S. Virtual cystoscopy in the evaluation of bladder tumors. *Clin Imaging*. 2004 Apr;28(2):138–42.
- 11 Avcu S, Koseoglu MN, Ceylan K, Bulut MD, Dbulutand M, Unal O. The value of diffusion-weighted MRI in the diagnosis of malignant and benign urinary bladder lesions. *Br J Radiol*. 2011 Oct;84(1006):875–82.
- 12 Gulsen F, Dikici S, Mihmanli I, Ozbayrak M, Onal B, Obek C, et al. Detection of bladder cancer recurrence with real-time three-dimensional ultrasonography-based virtual cystoscopy. *J Int Med Res*. 2011;39(6):2264–72.
- 13 Li Q, Tang J, He E, Li Y, Zhou Y, Zhang X, et al. Clinical utility of three-dimensional contrast-enhanced ultrasound in the differentiation between noninvasive and invasive neoplasms of urinary bladder. *Eur J Radiol*. 2012 Nov;81(11):2936–42.
- 14 Kim DK, Kim YH, Lee HY, Lee S, Doo SW, Yang WJ, et al. Diagnostic accuracy of Raman spectroscopy for the diagnosis of bladder cancer: A systematic review and meta-analysis. *J Cancer Res Ther*. 2021 Jun;17(2):426–33.
- 15 Yosef HK, Krauß SD, Lechtonen T, Jütte H, Tannapfel A, Kafferlein HU, et al. Noninvasive Diagnosis of High-Grade Urothelial Carcinoma in Urine by Raman Spectral Imaging. *Anal Chem*. 2017 Jun;89(12):6893–9.



- 16 Krauß SD, Roy R, Yosef HK, Lechtonen T, El-Mashtoly SF, Gerwert K, et al. Hierarchical deep convolutional neural networks combine spectral and spatial information for highly accurate Raman-microscopy-based cytopathology. *J Biophotonics*. 2018 Oct;11(10):e201800022.
- 17 Kong K, Kendall C, Stone N, Notingher I. Raman spectroscopy for medical diagnostics--From in-vitro biofluid assays to in-vivo cancer detection. *Adv Drug Deliv Rev*. 2015 Jul;89:121–34.
- 18 Shapiro A, Gofrit ON, Pizov G, Cohen JK, Maier J. Raman molecular imaging: a novel spectroscopic technique for diagnosis of bladder cancer in urine specimens. *Eur Urol*. 2011 Jan;59(1):106–12.
- 19 Krauß SD, Yosef HK, Lechtonen T, Jütte H, Tannapfel A, Käßlerlein HU, et al. Integrating spatial, morphological, and textural information for improved cell type differentiation using Raman microscopy. *J Chemom*. 2018;32(1):e2973.
- 20 Pallaoro A, Mirsafavi RY, Culp WTN, Braun GB, Meinhardt CD, Moskovits M. Screening for canine transitional cell carcinoma (TCC) by SERS-based quantitative urine cytology. *Nanomedicine Nanotechnol Biol Med*. 2018 Jun;14(4):1279–87.
- 21 Huttanus HM, Vu T, Guruli G, Tracey A, Carswell W, Said N, et al. Raman chemometric urinalysis (Rametrix) as a screen for bladder cancer. *PloS One*. 2020;15(8):e0237070.
- 22 Cui X, Liu T, Xu X, Zhao Z, Tian Y, Zhao Y, et al. Label-free detection of multiple genitourinary cancers from urine by surface-enhanced Raman spectroscopy. *Spectrochim Acta A Mol Biomol Spectrosc*. 2020 Oct;240:118543.
- 23 Hu D, Xu X, Zhao Z, Li C, Tian Y, Liu Q, et al. Detecting urine metabolites of bladder cancer by surface-enhanced Raman spectroscopy. *Spectrochim Acta A Mol Biomol Spectrosc*. 2021 Feb;247:119108.
- 24 Yang Y-T, Hsu I-L, Cheng T-Y, Wu W-J, Lee C-W, Li T-J, et al. Off-Resonance SERS Nanoprobe-Targeted Screen of Biomarkers for Antigens Recognition of Bladder Normal and Aggressive Cancer Cells. *Anal Chem*. 2019 Jul;91(13):8213–20.
- 25 Zhang W, Jiang L, Diefenbach RJ, Campbell DH, Walsh BJ, Packer NH, et al. Enabling Sensitive Phenotypic Profiling of Cancer-Derived Small Extracellular Vesicles Using Surface-Enhanced Raman spectroscopy Nanotags. *ACS Sens*. 2020 Mar;5(3):764–71.
- 26 Kong KV, Leong WK, Lam Z, Gong T, Goh D, Lau WKO, et al. A rapid and label-free SERS detection method for biomarkers in clinical biofluids. *Small Weinh Bergstr Ger*. 2014 Dec;10(24):5030–4.
- 27 Si Y, Li L, He B, Li J. A novel surface-enhanced Raman scattering-based ratiometric approach for detection of hyaluronidase in urine. *Talanta*. 2020 Aug;215:120915.
- 28 Wang W, Li D, Zhang Y, Zhang W, Ma P, Wang X, et al. One-pot synthesis of hyaluronic acid-coated gold nanoparticles as SERS substrate for the determination of hyaluronidase activity. *Mikrochim Acta*. 2020 Oct;187(11):604.
- 29 Feng E, Zheng T, Tian Y. Dual-Mode Au Nanoprobe Based on Surface Enhancement Raman Scattering and Colorimetry for Sensitive Determination of Telomerase Activity Both in Cell Extracts and in the Urine of Patients. *ACS Sens*. 2019 Jan;4(1):211–7.
- 30 Jin H, Lin T, Han P, Yao Y, Zheng D, Hao J, et al. Efficacy of Raman spectroscopy in the diagnosis of bladder cancer: A systematic review and meta-analysis. *Medicine (Baltimore)*. 2019 Nov;98(47):e18066.

- 31 Busetto GM, Ferro M, Del Giudice F, Antonini G, Chung BI, Sperduti I, et al. The Prognostic Role of Circulating Tumor Cells (CTC) in High-risk Non-muscle-invasive Bladder Cancer. *Clin Genitourin Cancer*. 2017 Aug;15(4):e661–6.
- 32 Terracciano D, Ferro M, Terreri S, Lucarelli G, D’Elia C, Musi G, et al. Urinary long noncoding RNAs in nonmuscle-invasive bladder cancer: new architects in cancer prognostic biomarkers. *Transl Res J Lab Clin Med*. 2017 Jun;184:108–17.
- 33 Vartolomei MD, Ferro M, Cantiello F, Lucarelli G, Di Stasi S, Hurler R, et al. Validation of Neutrophil-to-lymphocyte Ratio in a Multi-institutional Cohort of Patients With T1G3 Non-muscle-invasive Bladder Cancer. *Clin Genitourin Cancer*. 2018 Dec;16(6):445–52.
- 34 Cantiello F, Russo GI, Vartolomei MD, Farhan ARA, Terracciano D, Musi G, et al. Systemic Inflammatory Markers and Oncologic Outcomes in Patients with High-risk Non-muscle-invasive Urothelial Bladder Cancer. *Eur Urol Oncol*. 2018 Oct;1(5):403–10.
- 35 Li S, Li L, Zeng Q, Zhang Y, Guo Z, Liu Z, et al. Characterization and noninvasive diagnosis of bladder cancer with serum surface enhanced Raman spectroscopy and genetic algorithms. *Sci Rep*. 2015 May;5:9582.
- 36 Chen S, Zhu S, Cui X, Xu W, Kong C, Zhang Z, et al. Identifying non-muscle-invasive and muscle-invasive bladder cancer based on blood serum surface-enhanced Raman spectroscopy. *Biomed Opt Express*. 2019 Jul;10(7):3533–44.
- 37 Hinsenveld FJ, Boormans JL, van der Poel HG, van der Schoot DKE, Vis AN, Aben KKH, et al. Intermediate-term survival of robot-assisted versus open radical cystectomy for muscle-invasive and high-risk non-muscle invasive bladder cancer in The Netherlands. *Urol Oncol Semin Orig Investig*. 2022 Feb;40(2):60.e1–60.e9.
- 38 Giacalone NJ, Shipley WU, Clayman RH, Niemierko A, Drumm M, Heney NM, et al. Long-term Outcomes After Bladder-preserving Tri-modality Therapy for Patients with Muscle-invasive Bladder Cancer: An Updated Analysis of the Massachusetts General Hospital Experience. *Eur Urol*. 2017 Jun;71(6):952–60.
- 39 Mandair GS, Han AL, Keller ET, Morris MD. Raman microscopy of bladder cancer cells expressing green fluorescent protein. *J Biomed Opt*. 2016 Nov;21(11):115001.
- 40 Li S, Li P, Ge M, Wang H, Cheng Y, Li G, et al. Elucidation of leak-resistance DNA hybridization chain reaction with universality and extensibility. *Nucleic Acids Res*. 2020 Mar;48(5):2220–31.
- 41 Davis RM, Kiss B, Trivedi DR, Metzner TJ, Liao JC, Gambhir SS. Surface-Enhanced Raman Scattering Nanoparticles for Multiplexed Imaging of Bladder Cancer Tissue Permeability and Molecular Phenotype. *ACS Nano*. 2018 Oct;12(10):9669–79.
- 42 Lamprecht C, Gierlinger N, Heister E, Unterauer B, Plochberger B, Brameshuber M, et al. Mapping the intracellular distribution of carbon nanotubes after targeted delivery to carcinoma cells using confocal Raman imaging as a label-free technique. *J Phys Condens Matter Inst Phys J*. 2012 Apr;24(16):164206.



APPENDICES

LIST OF ABBREVIATIONS

LIST OF PUBLICATIONS

DANKWOORD

CURRICULUM VITAE

LIST OF ABBREVIATIONS

ALA	5-AminoLevulinic Acid
AUC	Area Under the Curve
AUROC	Area Under the Receiver Operating Characteristic Curve
BCG	Bacillus Calmette-Guerin
CARS	Coherent Anti-stokes Raman Spectroscopy
CIS	Carcinoma In Situ
EMSC	Extended Multiplicative Scatter Correction
HAL	HexAminoLevulinic acid
HG	High Grade
IGZ	Dutch Health Care Inspectorate
LG	Low Grade
MDD	Medical Device Directive
MIBC	Muscle Invasive Bladder Carcinoma
MRS	Modulated Raman Spectroscopy
NA	Not Available
NAC	Neo Adjuvant Chemotherapy
NBI	Narrow Band Imaging
NMIBC	Non-Muscle-Invasive Bladder Carcinoma
OCT	Optical Coherence Tomography
PDD	Photodynamic Diagnostic
PC	Prostate Cancer
PCA/LDA	Principal Component fed Linear Discriminant Analysis
PET	Polyethylene Terephthalate
RM	Raman Microspectroscopy
RMI	Raman Molecular Imaging
SD	Standard Deviation
SERS	Surface Enhanced Raman Spectroscopy
SMOTe	Synthetic Minority Oversampling
SNR	Signal-to-Noise Ratio
SNR _{msr}	The mean SNR over the spectral range
TURBT	Transurethral Resection of a Bladder Tumor
UC	Urothelial Carcinoma
WLC	White Light Cystoscopy

LIST OF PUBLICATIONS

Papers in journals

M. Stomp-Agenant, T. van Dijk, A. Onur, M. Grimbergen, H. van Melick, G. Jonges, R. Bosch, C. van Swol. In vivo Raman spectroscopy for bladder cancer detection using a superficial Raman probe compared to a non-superficial Raman probe. *Journal Biophotonics*. Epub March 2022

M. Agenant, M. Grimbergen, R. Draga, E. Marple, R. Bosch, C. van Swol. Clinical superficial Raman probe aimed for epithelial tumor detection: Phantom model results. *Biomedical optics express*. 4;1203-1216, March 2014.

M. Agenant, H.J. Noordmans, W. Koomen, J.L. Bosch. Real-time bladder lesion registration and navigation: a phantom study. *PlosOne*. 10; August 2013.

M. Stomp-Agenant*, A. ten Dam*, T. van Dijk, A. Onur, C. van Swol, R. Bosch. Raman spectroscopy in the evaluation of tissue heterogeneity surrounding areas with urothelial carcinoma in radical cystectomy specimens. (Submitted: *Journal of Biomedical Optics Express*)

*Both authors contributed equally

S.G. Kroeze, M. Agenant, G.N. Jonges, T. Stein, J.L. Bosch. Clinical efficacy of bipolar radiofrequency ablation of small renal masses. *World journal of Urology*. 33;1535-1540, October 2015

M. de Haas*, M. Agenant*, L. Gijs, G. Eeckhout, S. Visser, E. Meuleman. Stoornis van lichaamsbeleving bij mannen. Ontwikkeling van een vragenlijst. *Tijdschrift voor Seksuologie*. 35;219-231, december 2011.

*Beide auteurs droegen in gelijke mate bij aan het artikel

M. Agenant, R.L. ten Berghe, H. Roshani. Urethratumoren bij de man: mis ze niet. *Nederlands Tijdschrift voor Urologie*. 1(1);7-11, februari 2011



Oral/Poster Presentations:

Oral presentation: Enable accurate resection by spatial analysis of urothelial carcinoma using Raman spectroscopy. A. Ten Dam, M. Stomp-Agenant, S. Onur, T. van Dijk, G. Jonges, R. Bosch. UROtech22, Istanbul, May 2022

Oral presentation: Real-Time Bladder navigation: the first laboratory tests. M. Agenant, A. van Rhijn, W. Koomen, F.E. Euwe, H.J. Noordmans, S.L. Been, J.L.H.R. Bosch. Real time navigation using an advanced stereotactic system. Spie Photonics West conference San Francisco, January 2012.

Poster presentation: Tissue heterogeneity in a cystectomy specimen: near infrared Raman spectroscopy compared to histopathologic findings. M. Agenant, M.C.M. Grimbergen, C.F.P. van Swol, J.H.R.L. Bosch. SPEC 2012 in Chang Mai, November 2012

Oral presentation: R.A. Korthorst, M. Agenant, B.P.M. Wijsman, J. de Vries, C.E.M. Blomjous, P.J.M. Kil. Sneldiagnostiek bij patiënten met een verhoogd PSA, een studie naar angstreductie en kwaliteit van leven. NVU najaarsvergadering 2010.

DANKWOORD

Mijn onderzoek zou onmogelijk zijn geweest zonder hulp en steun van anderen. Allereerst wil ik de geïnccludeerde patiënten hartelijk danken voor hun bijdrage aan dit onderzoek.

Collega's die bijgedragen hebben aan de totstandkoming van dit proefschrift van de afdelingen urologie in het UMCU, Antonius ziekenhuis en LUMC en de afdelingen klinische fysica van het Antonius ziekenhuis en UMCU, wil ik ook hartelijk bedanken.

Een aantal mensen noem ik in het bijzonder;

Beste Rob, dank je dat je me verwelkomde in dit warme nest en mij de mogelijkheid gaf om dit proefschrift af te ronden. Christiaan, bedankt dat je er altijd was om mijn onderzoek te stimuleren, als enige begeleider gedurende de hele periode (die dan ook meer dan 12 jaar was). Als er iets was kon ik altijd bij jou terecht. Thomas, dank je voor al je input en discussies die je met me deelde, zonder jouw hulp was dit proefschrift niet afgekomen. Beste Ruud, heel erg bedankt voor het vertrouwen voor de doorstart van dit onderzoek met mij en alle mogelijkheden die je me hebt gegeven. Matthijs, jij ook heel erg bedankt voor het vertrouwen in mij als niet-technisch onderlegde onderzoekster. Urenlang heb je me alles uitgelegd en hebben we gebrainstormd en discussies gehad. Graag wil ik alle medeauteurs bedanken voor de fijne samenwerking en hun input.

Bedankt collega-onderzoekers, Pauline, Paul, Boris en Katja voor de gezelligheid en steun op onze onderzoekskamer hoog en droog. Vrienden, vriendinnen, collega's en familie, bedankt voor het vertrouwen in mij en het plezier dat we deelden, waarvan ik de energie kreeg om dit proefschrift af te schrijven. Lieve papa, mama en Yvon, dank jullie wel dat jullie er altijd voor mij zijn, voor de eindeloze steun en de onvoorwaardelijke liefde die ik van jullie krijg. Lieve Wouter, ik wil je bedanken voor alle steun en liefde maar ook de mogelijkheid om dit proefschrift af te kunnen maken, je bent mijn rots in de branding, mijn grote liefde. En ten slotte, onze allerliefste kinderen Emma en Quinten, jullie zijn mijn alles! Op naar nieuwe avonturen samen!



CURRICULUM VITAE

Michelle Stomp-Agenant is geboren op 14 november 1982 in Colombo (Sri Lanka). Op een leeftijd van drie maanden is zij geadopteerd en groeide ze op in Leusden. Op basisschool Kinderland heeft ze leren lezen en schrijven. In 2001 heeft zij haar VWO diploma behaald in Amersfoort aan het Nieuwe Eemland College en begon zij met de studie Biomedisch Wetenschappen aan de Universiteit Leiden. In 2005 behaalde ze haar bachelor examen van Biomedische Wetenschappen en begon ze naast de Master van Biomedische Wetenschappen aan de studie Geneeskunde via de zij-instroom bij het Leids Universitair Medisch Centrum. Tijdens de co-schappen groeide haar interesse voor de urologie waarbij ze het afsloot met een Semi-Arts stage urologie in het HAGA ziekenhuis. In het kader van haar studies is ze driemaal een aantal maanden in het buitenland geweest: voor een stage in Tanzania, een co-schap in Suriname en een cursus in Stockholm. Na het behalen van haar artsenbul in 2009 heeft ze negen maanden als ANIOS urologie in het Rijnland ziekenhuis te Leiderdorp gewerkt en nadien vijf maanden in het St Elisabeth ziekenhuis te Tilburg. In 2011 startte zij haar promotietraject in het Universitair Medisch Centrum Utrecht en het St Antonius ziekenhuis te Nieuwegein. In 2012 haalde ze, met een publicatie welke in dit proefschrift is beschreven, haar Masters examen van Biomedische Wetenschappen. In 2014 begon zij haar vooropleiding voor de urologie bij de chirurgie in het Rijnland ziekenhuis. De opleiding urologie vervolgde ze in het Elisabeth-Tweesteden Ziekenhuis van 2016-2019 en het Universitair Medisch Centrum Utrecht van 2019-2021. Ze heeft haar opleiding afgerond in het Leids Universitair Medisch Centrum gedurende 2021-2022 waarbij ze ook stages in het Alrijne ziekenhuis en het Haaglanden Medisch Centrum deed. Per 1-5-2022 is ze uroloog en werkt ze in het Reinier De Graaf Gasthuis, als Chef-de-Clinique. Ze woont samen met haar man Wouter en twee kinderen Emma en Quinten.



